OXIDATIVE DEHYDROGENATION OF PROPANE OVER POTASSIUM HEXATITANATE-BASED CATALYSTS

MONCHANOK CHANTHAWONG

A THESIS SUBMITTED IN PARTIAL FULFILLMENT OF THE REQUIREMENT FOR THE DEGREE OF MASTER OF SCIENCE IN PETROCHEMICALS AND HYDROCARBON CHEMISTRY

DEPARTMENT OF CHEMISTRY

FACULTY OF SCIENCE

KING MONGKUT'S INSTITUTE OF TECHNOLOGY LADKRABANG

2018

KMITL-2018-SC-M-015-024

Thesis Title	Oxidative dehydrogenation of propane over potassium hexatitanate-based catalysts
Student Name	Monchanok Chanthawong
Student ID	58605039
Degree	Master of Science (Petrochemicals and hydrocarbon chemistry)
Department	Chemistry
Year	2018
Thesis Advisor	Assoc. Prof. Dr. Tawan Sooknoi
Thesis Co-advisor	Asst. Prof. Dr. Tosapol Maluangnont

Abstract

The oxidative dehydrogenation of propane was investigated using potassium hexatitanate-based catalysts, where Ti(IV) was substituted $K_2Ti_{5.9}M_{0.1}O_{13}$ by M = Mg(II), Co(II), Ni(II), Al(III), Cr(III), Mn(III), and Fe(III). The catalysts will be prepared by a traditional solid state synthesis method, and were characterized by powder X-ray diffraction (XRD), X-ray fluorescence (XRF), Temperature-Programmed Reduction (H_2-TPR) and Electron Spin Resonance (ESR). The metals (M = Co(II), Ni(II), Al(III), and Mn(III)) was successfully incorporated into the Ti sites of the hexatitanate structure. The metal incorporated can be dislodged from the hexatitanate framework, forming metallic phase and oxygen vacancy (for metal substituted hexatitanate) upon H_2 reduction. The reduced hexatitanate can be readily reoxidized and more reducible lattice oxygen was generated, as compared to TiO_2 (P-25). The catalytic activity testing will be performed in a fixed-bed flow reactor at 550 - 625 °C. A higher yield of light olefin containing ethylene and propylene is observed for $K_2Ti_{5.9}Ni_{0.1}O_{13}$ upon H_2 reduction (400 °C) at 600 °C. $K_2Ti_{5.9}Ni_{0.1}O_{13}$ provides the higher reducible lattice oxygen, while the dislodged metals are partially oxidized to metal oxide and promote total oxidation to CO and CO_2 as major products. Accordingly, ethylene and propylene can be predominated at relatively low metal loading (1 wt.%), reaction temperature (600 °C), concentration of O_2 gas in feed (20 %) and reduction temperature (400 °C). The reaction pathway proceeds via C-H activation by reducible lattice oxygen, forming propyl radical

followed by oxidative dehydrogenation to propylene. The parallel reaction include the cracking of propyl radical to methane and ethylene.

Keywords : alkali hexatitanate, oxidative dehydrogenation, oxygen vacancy, propane

ACKNOWLEDGEMENTS

The authors take this opportunity to acknowledge advisors my Assoc. Prof. Dr. Tawan Sooknoi and my co-advisor Asst. Prof. Dr. Tosapol Maluangnont, for the suggestion, inspiration, experimental instrument, useful discussion, and knowledge in catalysis throughout this research.

I would like to gratefully acknowledge chairperson and committee, Asst. Prof. Dr. Montree Thongkam, Dr. Amnat Permsubscul, and Prof. Dr. Sirirat Jitkarnka for judgment and valuable comments.

I would like to acknowledge the financial support from the Faculty of Science, King Mongkut's Institute of Technology Ladkrabang for the laboratory instruments, equipment, chemicals, and facilities.

Furthermore, I would like to grateful to my friends, members in this research group (Catalytic Chemistry Research Unit ; CCR) for their help, advice, support, and encouragement.

Finally, I deeply appreciate and thank the parents and family, who give love and support,

Monchanok Chanthawong

CONTENTS

CONTENTS (Continued)

LIST OF TABLES

CONTENTS (Continued)

LIST OF FIGURES

LIST OF FIGURES(Continued)

CHAPTER 1
INTRODUCTION

1.1 Motivation

Nowadays, the demand for light olefins containing ethylene and propylene has been increasing because it is the starting material for the production of polypropylene for propylene and polyethylene for ethylene. The catalytic (nonoxidative) dehydrogenation of propane is the most direct and selective route for production of light olefins [1]. However, it is a highly endothermic reaction requiring high reaction temperature. Alternatively, the oxidative dehydrogenation (ODH) is exothermic, converting propane to light olefin at relatively low temperatures. Consequently, ODH become more energy-economical.

The production of light olefins from propane over a metal oxide catalyst typically follows the Mars–van Krevelen redox cycle. First, propane is chemisorbed at the metal site. As a result of that, the C–H bond is activated by the lattice oxygen on the surfaces of the catalyst [2]. Then, the hydrogen of propane is abstracted by the oxygen atom, leaving H_2O as the product bearing the oxygen vacancy site on the surface [3]. It is important that such oxygen vacancy sites can be refilled by gaseous O_2 (i.e., become reoxidized) by an external oxygen source. Thus, the redox property of metal oxide is a crucial factor determining the catalytic performance [4].

Previous report in our group has found that several titanate-based oxides including $K_2Ti_6O_{13}$ can be reduced readily, producing oxygen vacancy sites. Structurally, the alkali hexatitanate structure is made of a ribbon of three edge-shared TiO_6 (or MO_6) octahedra linked via the edges to form the tunnel, with the alkali cations (K^+) located inside [5]. It is postulated that the tunnel structure, with coordinatively unsaturated sites (cus) of oxygen atoms, can easily promote the formation of the active oxygen vacancy sites. So, we extend this previous finding further by studying the effect of the type and amount of some metal cations [Mg(II), Co(II), Ni(II), Al(III), Cr(III), Mn(III), and Fe(III)] substituted for Ti(IV) in $K_2Ti_6O_{13}$. The catalysts will be synthesized via a solid state reaction and were characterized by XRD, XRF, H_2-TPR and ESR. The valence of the substituted metal (which is not equal to 4) [6] and a slight size (cationic radii) mismatch might allow the production of a larger concentration of oxygen vacancy at

lower temperature. If so, the modified catalysts might potentially boost up the selectivity and yield of light olefins.

1.2 Objectives

1.2.1 To obtain potassium hexatitanate-based catalysts ($K_2Ti_6O_{13}$) where Ti(IV) cations are partially substituted by Mg(II), Co(II), Ni(II), Al(III), Cr(III), Mn(III), and Fe(III) via a solid state reaction.

1.2.2. To understand structure-activity relationship of the potassium hexatitanate-based catalysts for oxidative dehydrogenation.

1.2.3. To obtain optimum conditions for ODH of propane to light olefins over potassium hexatitanate-based catalysts.

1.3 Scope of the study

1.3.1. Catalyst preparation ($K_2Ti_6O_{13}$) by solid state synthesis, including the partial substitution of Ti(IV) by Mg(II), Co(II), Ni(II), Al(III), Cr(III), Mn(III), and Fe(III).

1.3.2. Characterization of catalysts by powder X-ray powder diffraction (XRD), X-Ray Fluorescence (XRF), Temperature-programmed reduction (TPR) by H_2 gas and Electron Spin Resonance (ESR).

1.3.3. Study on the catalytic activity for the effect of the reaction temperature and type of the metal substitution and ratio of the metal substituted into hexatitanate.

1.3.4. Analysis and quantification of gas products by online gas chromatography with flame ionization detector (GC-FID).

1.4 Expected results

It is expected that the selective production of light olefins from propane at relatively low reaction temperature over potassium hexatitanate-based catalyst will be obtained. Moreover, the low coke formation leads to high process stability that can be applicable for industrial scale.

CHAPTER 2

THEORY AND LITERATURE REVIEWS

2.1 Propane

Propane is a three-carbon alkane gas (C_3H_8) (Figure 2.1). Typically, raw natural gas (which can be directly obtained from natural resources without going through any process) consists of 90% of methane, 5% of propane and 5% of other gases [7]. Propane can be separated from raw natural gas at the processing plant of natural gas, and is accounted for 55% of propane. The remaining 45% of propane is separated from petroleum by a typical processing plant called a refinery [8]. A major use of propane is for liquefied petroleum gas (LPG). Propane is a clean-burning, high-energy alternative fuel that finds uses to power light-, medium- and heavy-duty propane vehicles [9]. The chemical industry also uses propane as a raw material for making plastics and other compounds [10].

Figure 2.1 Molecular structure of propane.

Moreover, propane is also used by domestics, farms, business, and other industries, mostly for heating. Propane appliances include ranges, ovens, space heaters, furnaces, water heaters, clothes dryers, and air conditioners. Since propane is a very low-pollution fuel, fork-lift trucks powered by propane can operate safely inside factories and warehouses [11].

2.2 Ethylene

Ethylene is one of the most important petrochemical intermediates and is a feedstock for many products [12].

Figure 2.2 Molecular structure of Ethylene.

Global demand for ethylene is forecast to grow faster than average world GDP growth rates over the next five years. The most important regions in terms of growth are India (about 11% average annual growth), the CIS and Baltic States (about 8% average annual growth), the United States (about 5.8% average annual growth), China (about 5.6% average annual growth), and the Middle East (2.5% average annual growth). These five regions account for 89% of the volume growth between 2016 and 2021 [13]. Ethylene reacts by addition to many inexpensive reagents such as water, chlorine, hydrogen chloride, and oxygen to produce valuable chemicals. It can be initiated by free radicals or by coordination catalysts to produce polyethylene, the largest-volume thermoplastic polymer [10]. Ethylene is widely used in making containers, drums, pipes, and films. The burgeoning packaging industry in various developing and developed regions is expected to catalyze the market. There is a growing worldwide demand for ethylene oxide derivatives such as ethylene glycols and polyester fibers in the manufacturing of plastic products, particularly bottle [14].

Ethylene is the raw material used in the manufacture of polymers such as polyethylene (PE), polyethylene terephthalate (PET), polyvinyl chloride (PVC) and polystyrene (PS) as well as fibres and other organic chemicals. These products are used in a wide variety of industrial and consumer markets such as the packaging, transportation, electrical/electronic, textile and construction industries as well as consumer chemicals, coatings and adhesives [15].

2.3 Propylene

Propylene is second to ethylene as the largest-volume hydrocarbon intermediate for the production of chemicals [10]. Propylene is manufactured by 3 processes including: (i) steam cracking of propane and butane (from natural gas and oil), (ii) steam cracking of naphtha (from oil), and (iii) catalytic cracking of gas oil (from oil) and propane [16]. Steam cracking accounts for 56% and catalytic cracking for 33% of the global production of propylene. The rest of propylene is made from the production of oil from coal and from the cracking of gas oil under vacuum. Increasingly, propane is being catalytically cracked to form propene, using the same catalytic cracker that is used to crack gas oil [17].

Propylene (often known as propene) (Figure 2.3) is a very important building block for a large number of chemicals. The dominant use of propylene is polypropylene (PP), which accounts for nearly two-thirds of global propylene consumption [18]. Propylene is also used to produce acrylonitrile (ACN), propylene oxide (PO) [19], several alcohols, cumene and acrylic acid.

Figure 2.3 Molecular structure of propylene.

Polypropylene (Figure 2.4 (a)) is one of the most versatile polymers since it possesses not only good mechanical but also good chemical properties. Polypropylene is used in a wide range of consumer and industrial products [20]. It is manufactured by several high-volume forming methods. In the automotive sector, polypropylene and its alloys have become the polymer of choice accounting for over a third of plastics used in automobiles [21].

The second largest derivative, acrylonitrile (Figure 2.4 (b)) is used in a variety of elastomeric polymers and fibre applications [22]. The largest outlet for acrylonitrile is acrylic fibres, which are used in clothing, home furnishings, and bedding. Other uses for acrylonitrile include nitrile rubber, acrylonitrile-butadiene-styrene (ABS)/styrene acrylonitrile (SAN) resins, acrylamide and adiponitrile [23].

The next largest outlet for propylene is propylene oxide (Figure 2.4 (c)). Propylene oxide is used to make polyether polyols, which are reacted with an isocyanate to form polyurethanes. Polyurethane end uses include flexible foams for

the furniture and automotive industries, and rigid foams for appliance and building insulation [24]. Propylene oxide is also used to make propylene glycol [25], which is used in unsaturated polyester resins, antifreeze and aircraft de-icing fluids, and propylene glycol ethers (for e.g., paints, coatings, inks, resins and cleaners) [26].

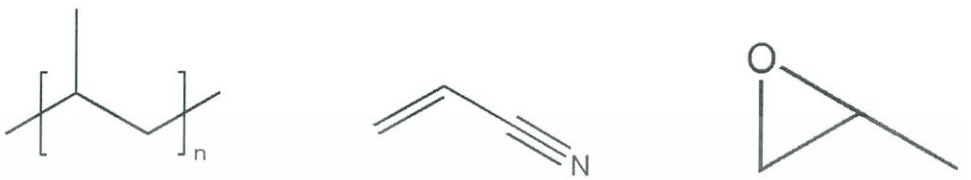

(a) (b) (c)

Figure 2.4 Major use of propylene to form: (a) polypropylene (b) acrylonitrile and (c) propylene oxide.

Propylene is an important chemical intermediate as shown in the diagram (Figure 2.5). As the industrial demand for propylene is increasing [27], the alternative method of propylene production is being sought and is of great commercial interest.

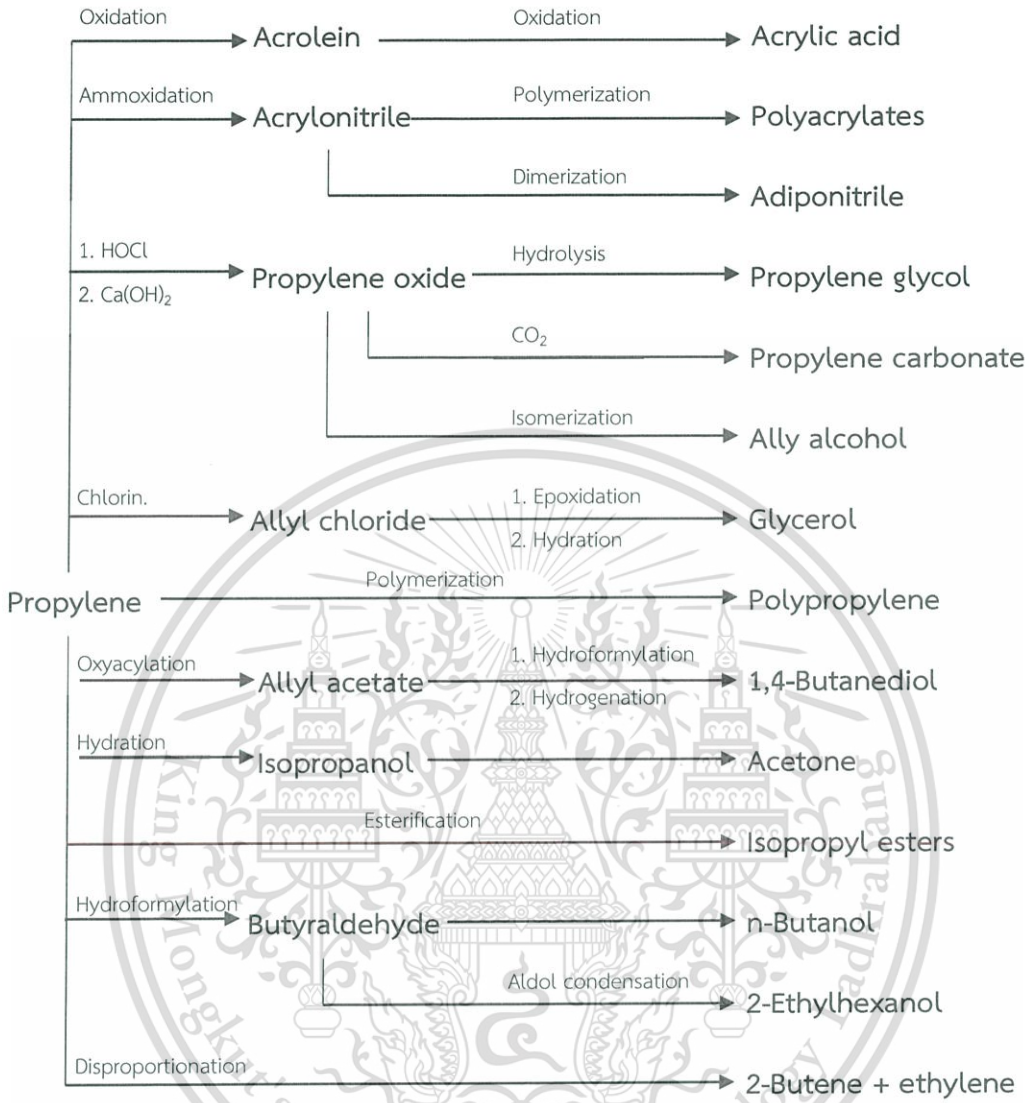

Figure 2.5 Important chemicals based on propylene [10].

2.4 Oxidative dehydrogenation of propane

Traditionally, propane dehydrogenation is an endothermic process [28], implying that high temperatures are needed to achieve a high yield of propylene (C_3H_6) at 1 atm. The propane dehydrogenation is shown in equation (2.1).

$$C_3H_8 \longleftrightarrow C_3H_6 + H_2 \qquad (2.1)$$

A major issue with propane dehydrogenation is the equilibrium limitation [29]. As a result, oxidative dehydrogenation (ODH) is utilized to overcome this problem. Unlike the nonoxidative dehydrogenation of propane, oxidative dehydrogenation where O_2 gas is co-fed into the system, equation (2.2) is exothermic and irreversible [30]. Here, hydrogen atoms in propane are removed by O_2 gas in the form of water which serves as a driving force for the reaction.

$$C_3H_8 + 0.5O_2 \longrightarrow C_3H_6 + H_2O \qquad (2.2)$$

Thermodynamic calculations associated with the main oxidative and nonoxidative dehydrogenation of propane reactions are reported in Table 2.1 [30]. Clearly, traditional (non-oxidative) dehydrogenation is endothermic, while the ODH of propane is exothermic [31]. Additionally, the nonoxidative dehydrogenation of propane reaction is feasible (i.e., negative ΔG) only at temperatures above 650 °C. On the other hand, the oxidative dehydrogenation of propane reaction can be accomplished at all temperature. (ΔG for oxidative dehydrogenation of propane is negative over the whole range.). At high temperature, cracking side reaction cannot be controlled that hydrocarbon products can be cracked to methane and ethylene [32].

Table 2.1 Thermodynamic Calculations As a Function of T(°C)

Reactions	$\Delta H_{20}°$ (kJ mol^{-1})	$\Delta G(T)$ (kJ mol^{-1})
$C_3H_8 \leftrightarrow C_3H_6 + H_2$	124.87	129.3-0.14T
$C_3H_8 + 0.5O_2 \rightarrow C_3H_6 + H_2O$	-117.43	-116.9-0.086T

2.5 Mechanism of oxidative dehydrogenation of propane

The mechanism of ODH of propane is via the Mars-van Krevelen redox mechanism [33]. Firstly, the lattice oxygen atoms abstract hydrogen atoms from C_3H_8 in an irreversible C-H bond activation step. The reactive species, i.e., the weak associative adsorption of propane on lattice oxygen (O*), was formed. Next, such reactive species then loses its hydrogen atom to the neighbouring lattice oxygen resulting in the adsorbed alkoxy species. Then, the desorption of propylene via hydride elimination from the adsorbed alkoxide species. Meanwhile, the hydrogenated lattice oxygen sites can be recombined, thereby regenerating the active sites. So, one can

envisage that the reducibility of the material will play some role in ODH. The reduced metal center will be converted to the (oxidised) original center upon the uptake of oxygen into the vacancy sites [34].

2.6 Titania (TiO_2)

TiO_2 has three crystal phases: anatase (tetragonal), rutile (tetragonal) and brookite (orthorhombic) (Figure 2.6). However, anatase and brookite phases may be transformed to rutile phase with heat treatment [35].

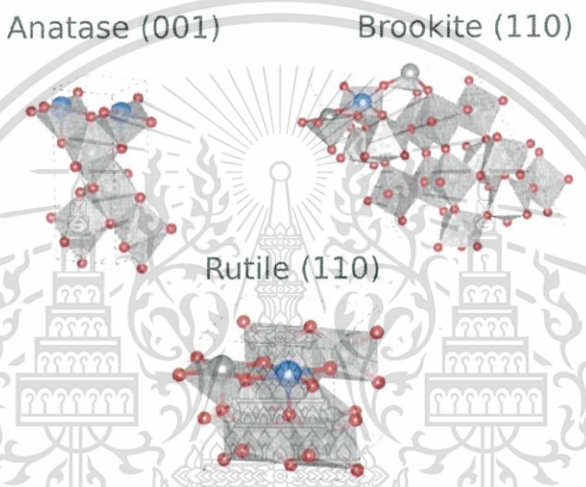

Figure 2.6 The crystal structure of anatase, rutile, and brookite phase TiO_2 [36]

The main use of titanium dioxide (TiO_2) is as a white powder pigment because of its brightness and very high refractive index. One of the major advantages for titanium dioxide is its resistance to discolouration under ultraviolet (UV) light in exposed applications [37,38]. It is used in products such as paints and coatings. In particular, high performance grades of TiO_2 are finding a growing market in the cosmetics sector and most toothpastes use TiO_2 [39].

The catalytic activity of TiO_2 is dependent on the nature and the composition of the surface defect sites. Formation of an oxygen vacancy and Ti^{3+} defects by the treatment of TiO_2 with H_2 gas is as an example. Firstly, hydrogen gas was adsorbed on the surface of TiO_2 at high temperature. Then, an electron from hydrogen atom was transferred to the lattice oxygen of TiO_2. Next, the lattice oxygen reacts with hydrogen gas, forming water molecules. Water molecules desorbs form the surface, resulting in

an oxygen vacancy site. Finally, the electron remaining there at the oxygen vacancy site could transfer to an adjacent Ti^{4+}, thereby forming the Ti^{3+} defect [40].

2.7 Titanate-based materials

2.7.1 Potassium hexatitanate

The crystal structure and properties of potassium titanates, $K_2O{\cdot}nTiO_2$ (n = 2–8) are dependent on the value of n. In the case of potassium titanates with a low potassium content (n = 6, 8), they have a tunnel structure and exhibit good thermo-insulation properties and good chemical stability [41]. Many methods have been developed to synthesize potassium titanate fibres and whiskers, including calcination, slow-cooling calcinations, hydrothermal reactions, flux growth (melting), flux evaporation and the combinative route of flux evaporation and the slow-cooling process [42]. Among many methods of synthesis, the calcination method has advantages in that it uses no flux; therefore, production costs could be reduced.

Potassium hexatitanate ($K_2Ti_6O_{13}$) is a relatively cheap, fibrous material possessing good thermal durability, chemical resistivity and dispersibility [43]. It has been found to be useful as a reinforcement material for plastic and ceramics, heat-insulating paints and automotive brake linings [44]. The structure of this material consists of three TiO_6 octahedra forming the tunnels with sharing edges and joining through the corners [45,46] as shown in (Figure 2.7). Because potassium ions in $K_2Ti_6O_{13}$ are enclosed by the tunnelling structure and isolated from the environment, potassium ions cannot escape from the tunnelling structure in the solution. This tunnel structure has also attracted additional interest because of its possible application as a photocatalytic material.

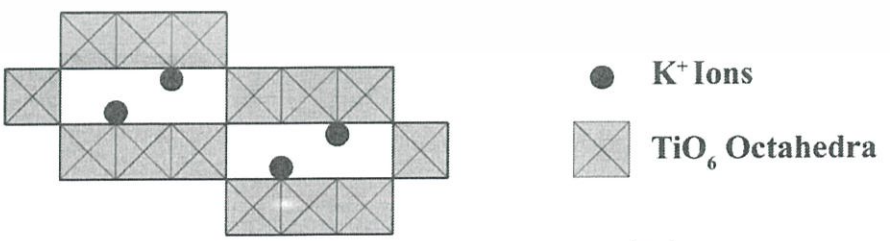

Figure 2.7 $K_2Ti_6O_{13}$ structure [47]

$K_2Ti_6O_{13}$ can be easily synthesized by a traditional solid-state route taking stoichiometric amounts of the grinded AR grade K_2CO_3 and TiO_2 powders (Purity～99.9%), under acetone and calcined at 1000 °C for 24 h followed by furnace cooling [6].

2.7.2 Reducibility of Potassium hexatitanate

Recently, our group has reported that $K_2Ti_6O_{13}$ readily loses its lattice oxygen as it gets reduced by H_2 [48]. Interestingly, the generation of the oxygen vacancy sites in $K_2Ti_6O_{13}$ is much more facile than other titanium-based oxides. It can be reoxidized by air zero gas even at room temperature. Considering the ODH mechanism mentioned above, the oxygen vacancy sites will be regenerated, ready for the abstraction of hydrogen atoms from propane to produce propylene. The substitution of Ti(IV) by other metals M which differs in the valency (i.e., not equal to 4) could generate a charge imbalance which acts as a driving force for the elimination of oxygen atoms on the surfaces. In addition, the substitution of Ti(IV) by other tetravalent cations (e.g., Sn(IV)) which is different cationic radius could generate a size mismatch. This size difference could in turn drives the formation of oxygen vacancy sites. These two approaches of substitution of Ti(IV), however, have not been conducted in $K_2Ti_6O_{13}$, especially regarding their effect on the facile formation of oxygen vacancy sites.

2.8 Literature review

Mohd Asim Siddiqui *et al.* [49] compared the synthesis of polycrystalline potassium hexatitanate by a conventional solid state reaction vs sol–gel method. In sol–gel process, $K_2Ti_6O_{13}$ was prepared by dissolving potassium acetate in distilled water and ethanol. The solution was added dropwise into the flask containing titanium isopropoxide. The mixture was heated under reflux at 70 °C for 72 h under constant stirring. Then, the pH of solution was adjusted into a basic one using a small amount of ammonium hydroxide. After heating, the solution was aged at 25 °C for 24 h until the gel forms. The gel was heat-treated at 800 °C for 8 h. The sol-gel-prepared $K_2Ti_6O_{13}$ was in the form of nanorods with the width less than 100 nm. The microrods sample prepared by a conventional solid state synthesis was observed an average cross section of approximately 1 μm and the length of 5 μm.

Mohd Asim Siddiqui *et al.* [50] studied of potassium hexatitanate whiskers synthesized by hydrothermal method. The conditions for synthesis are as follows: 10 wt.% concentration of KOH and K_2O/TiO_2 molar ratio of 5. There are several factors affecting the synthesis of high quality $K_2Ti_6O_{13}$. Firstly for the effect of titanium source, it was found that hydrated titania is more reactive with KOH, leading to a high supersaturation and a high nucleation rate compared to anatase TiO_2 and rutile TiO_2. In contrast to anatase TiO_2 and rutile TiO_2, high quality $K_2Ti_6O_{13}$ whiskers were obtained when hydrated titania were used. Additionally, annealing time also has some effect. It was found that annealing time for 2 h resulted unshaped morphology. Particles with more well-defined shape were observed at 5 h. Increasing the annealing time up to 12 and 24 h resulted in whisker morphology. In conclusion, the following optimized conditions were recommended: anatase as a titanium source; 10 wt.% KOH solution; annealing temperature and time of 300 °C and 5 h.

In the work of Jing Li *et al.* [51], $K_2Ti_6O_{13}$ crystallites were prepared at relatively low temperature via the reaction between low-melting-point KNO_3 and high-reactive-activity P-25 TiO_2 in air at 700 °C for 10 h. This method was simple. The powders of 3 mmol KNO_3 and 8.64 mmol P-25 TiO_2 were mixed and ground in mortar for 10 min, then transferred to a corundum crucible. The crucible was heated in a Muffle furnace at 700°C for 10 h, then cooled down to room temperature.

Lianqiang Xu et al. [52] studied single-crystalline $K_2Ti_6O_{13}$ nanoribbons which were prepared by a molten salt synthesis method. In this method, 1 mmol of K_2CO_3, 6 mmol of TiO_2 nanoparticles (pure anatase phase), and 10.0 g KCl were ground homogeneously in a mortar for 30 min. Then, the mixture was placed in an alumina crucible and was annealed at 850 °C for 3 h in a furnace before the natural cool down to room temperature. The resulted products were washed several times with distilled water to remove the residual KCl, and then dried at 100°C in an oven.

M.A. Chaar *et al.* [53] studied the selective oxidative dehydrogenation of propane over V-Mg-O catalysts. The condition are allows: propane/oxygen ratio of 2 at temperature 540 °C. Adding 24 and 40 wt.% vanadium into MgO gave a same activity in this reaction. The results showed that vanadium-magnesium oxides is an active and selective catalyst for the oxidative dehydrogenation of propane to propylene. At 10% of conversion, 65% of selectivity was obtained. However, the selectivity to propylene decrease with increasing conversion of propane. It has been suggested that

there was a breaking of a methylene C-H bond to form an adsorbed alkyl radical species.

Xiao-Zhang Lin et al. [54] studied a novel and effective catalyst for the oxidative dehydrogenation of propane, namely P-modified cobalt oxide. A series of nanosized cobalt oxide catalysts modified with phosphorus has been synthesized by the sol–gel method. Addition of phosphorus was done in the P/Co atomic ratio of 0, 0.05 and 0.1. By doing so, the cystallite size of P-modified cobalt oxide was largely decreased. Meanwhile, the highly dispersed P species in the catalyst acts as an agent for the isolation of active sites. P-modified samples where shown to exhibit a higher propane conversion and enhanced propylene selectivity compared to pure cobalt oxide. This finding can be explained considering that the P-modified samples had much smaller crystallite sizes. The optimum P/Co atomic ratio of 0.05 resulted in the maximum propylene yields of 15.7% with a propane conversion of 28.3% at 520 °C.

B.Y. Jibril *et al.* [55] studied the oxidative dehydrogenation of propane over chromium oxide-based catalysts. The effects of supports (γ-Al_2O_3, TiO_2, SiO_2, and MgO) was studied by impregnation with 10 wt.% Cr. The difference in the type of supports leads to different ability of a catalyst to donate oxygen and to desorb product, which related to the activity in this reaction. H_2-TPR result showed that the peak of reduction at lower temperature are in the order: TiO_2 > γ-Al_2O_3 > SiO_2 > MgO. On the 10 wt.% chromium oxide on alumina, the conversion of propane was 16.7% and the selectivity to C_3H_6 was 54.1% at 450 °C. In conclusion, the reaction follows a different reaction network depending on the degree of conversion and/or the reaction temperature. Moreover, rates of propane consumption and propylene productions were found to depend strongly on the oxygen partial pressures.

J.B. Stelzer *et al.* [56] studied the oxidative dehydrogenation of propane on TiO_2 supported antimony oxide/vanadia catalysts. The catalysts were prepared by depositing antimony oxide particles of a few nanometers on top of the TiO_2 crystallites, followed by the impregnation with different VO_x precursors including VO-(C_2O_4) • $2H_2O$ for VO_{oxa}, $(C_5H_5NH)_4H_2V_{10}O_{28}$ • $4H_2O$ for VO_{py} and NH_4VO_3 for VO_{meta}. After impregnation, the catalysts were calcined in air or nitrogen at 500 °C. The catalytic activity testing was performed at 500 °C under atmospheric pressure. Calcination in N_2 gave a high conversion but low propene selectivity for 5 wt.% V. On the contrary, the sample with

10 wt.% V has a higher propene selectivity compared to that calcined in air. Deposition of SbO_y on top of the TiO_2 supports enhance the conversion and propene yield, resulting in the value of 25% and 11% respectively compared to that without SbO_y-modification.

CHAPTER 3

EXPERIMENTAL DETAILS

3.1 Reagents

Chemicals	Grade of purity	Manufacturers
1. Titanium dioxide (P-25)	≥ 99.5%	Aerosil
2. Potassium nitrate	99.5%	CARLO ERBA
4. Magnesium(II) oxide (MgO)	-	Fluka
5. Cobalt(II,III) oxide (Co_3O_4)	-	SDFCL
6. Nickel(II) oxide (NiO)	97%	ACROS
9. Aluminum(III) oxide (Al_2O_3)	-	J.T. Baker
10. Chromium(III) oxide (Cr_2O_3)	-	CARLO ERBA
11. Manganese(III) oxide (Mn_2O_3)	99%	SIGMA-ALDRICH
12. Iron(III) oxide (Fe_2O_3)	99%	SIGMA-ALDRICH
14. Nitrogen gas	High purity (99.99%)	PRAXAIR
15. Hydrogen gas	High purity (99.99%)	PRAXAIR
16. Air zero gas	High purity (99.99%)	PRAXAIR
17. Propane gas	99.5%	LINDE

3.2 Apparatus

1. Laboratory glassware and plastic ware
2. Quartz tube (OD 8mm) and quartz bead
3. Quartz wool
4. Sieve
5. Alumina crucible
6. Mortar and pestle
7. Digital weighing balance (Sartorius)
8. Oven (Memmert)
9. Muffle furnace (WiseTherm)
10. Mass flow controller (Brooks)
11. Mass flow controller (AALBORG)
12. Catalytic testing rig

13. Heating tape
14. Gas Chromatography (Agilent 6890) with Flame Ionization Detector (GC-FID)
15. Temperature programmed reduction (H_2-TPR) system
16. Gas adsorption analyzer (Autosorb-1C, Quantachrome)
17. X-ray powder diffractometer (Rigaku, DMAX 2200/Ultima+, Faculty of Science, Chulalongkorn University)
19. X-ray powder diffractometer (Rigaku, DMAX 2200/Ultima+, Scientific and Technological Research Equipment Centre, Chulalongkorn University)
20. Electron Spin Resonance (ESR) (Department of Chemistry, Faculty of Science, Mahidol University)

3.3 Experimental procedure

3.3.1 Catalyst preparation

3.3.1.1 $K_2Ti_6O_{13}$

$$2KNO_3 + 6TiO_2 \longrightarrow K_2Ti_6O_{13}$$

The starting materials were titanium dioxide (P-25) nanocrystals and analytically pure KNO_3 powder [51]. A stoichiometric amount of KNO_3 and P-25 was mixed and ground by a mortar and pestle, then transferred to an alumina crucible and heated in a muffle furnace at 700 °C with heating rate 10 °C/min for 10 h, then cooled naturally to ambient temperature. KNO_3 was dried in an oven at 70 °C overnight prior to use. Other chemicals were used as received.

3.3.1.2 $K_2Ti_{6-n}M_nO_{13}$ (n= 0.05, 0.1, 0.2 and 0.5; M = Mg, Co, Ni, Al, Cr, Mn and Fe)

$$2KNO_3 + (6-n)TiO_2 + (n/x)M_xO_y \longrightarrow K_2Ti_{6-n}M_nO_{13}$$

The synthesis was similarly performed as described above, with the addition of MO (M = Fe, Mg, Ni), M_2O_3 (M = Al, Cr, Mn), M_3O_4 (M = Co).

3.3.2 Catalyst characterization

3.3.2.1 Structural analysis by powder X-ray Diffraction (XRD)

The crystalline phase of the prepared materials can be identified using XRD measurement. The sample was ground before it was packed on the sample holder. Analysis was done employing Bruker diffractometer (Cu K α radiation, 40kV, 30mA), covering the range 2θ = 5-65° and scanning rate 3 degree/min.

3.3.2.3 Determination of elemental composition analysis of the catalysts by X-ray Fluorescence (XRF)

X-ray fluorescence is a surface composition determination that is results from bombarding the sample with high-energy X-rays to releases characteristic secondary X-ray. This technique can be performed according to the procedure: the 0.5 g of catalyst sample and 4.5 g of boric acid were mixed and grinded together and compressed into alumina pan before bring into the X-ray fluorescence sample holder in X-ray fluorescence instrument.

3.3.2.3 Determination of reducibility of the catalysts by Temperature Programmed Reduction (TPR)

The sample weighed 0.3 g was placed into a quartz tube reactor. It was heated to 700 °C in air zero (30 mL/min) for 2 h at the heating rate 10 °C/min, followed by a cooling down to below 35 °C. Then, the sample was heated with a heating rate of 10 °C/min from 50 to 700 °C under 20 mL/min of 10% H_2/Ar, so as to generate the oxygen vacancy. The reducibility of a catalyst is expressed as μmol H_2/g of a catalyst. The conversion of peak area to μmol of H_2 was done using a known amount of CuO, which will be reduced completely and stoichiometrically in Cu and H_2O.

3.3.2.4 Determination of specific Surface area by nitrogen adsorption

Surface area of the catalysts can be determined by a gas adsorption analyzer (Autosorb-1C, Quantachrome). Approximately 0.06 - 0.1 g of the sample was loaded into the cell, which is attached to the outgassing station equipped with a heating mantle. The temperature was raised to 350 °C during outgassing process. After that, nitrogen gas was introduced to the sample cell where the adsorption can be measured at the range of the partial pressure (P/P_0) from 10^{-6} to 1.0. The adsorption

isotherm and the corresponding surface area was analyzed using ***BET equation*** as shown in **Equation 3.1**.

$$\frac{1}{\upsilon\,[(p_0/p)-1]} = \frac{c-1}{\upsilon_m c}\left(\frac{p}{p_0}\right) + \frac{1}{\upsilon_m c} \qquad \text{Equation 3.1}$$

where p and p_0 are the equilibrium and the saturation pressure of adsorbent at the temperature of adsorption, υ is the adsorbed gas quantity (for example, in volume units), υ_m is the monolayer adsorbed gas quantity, and C is the *BET constant*. The concept of the theory is an extension of the Langmuir theory, which is a theory for monolayer molecular adsorption to multilayer adsorption with the following hypotheses: (a) gas molecules physically adsorb on a solid in layers infinitely; (b) there is no interaction between each adsorption layer; and (c) the Langmuir theory can be applied to each layer.

3.3.2.5 Determination of an unpaired electron by Electron Spin Resonance (ESR)

Electron Spin Resonance (ESR), referred to as Electron Paramagnetic Resonance (EPR). This technique was study paramagnetic of heterogeneous catalysts [57]. ESR spectra were recorded on Bruker Elexys 500 using frequency 9.84 GHz, Power 0.63 mW and modulation amplitude 2 G. The DDPH (2,2-Diphenyl-1-Picrylhydrazyl) is a standard of the position and intensity of electron spin resonance signals.

3.3.3 Catalytic activity testing

The catalytic propane ODH reaction was carried out using a fixed bed flow reactor operating at atmospheric pressure. The catalyst was pressed, crushed, and sieved into particle size of 600-850 μm. After that, it was packed into a quartz tube reactor and covered by quartz bead and quartz wool as the support. This tube was then loaded at the center of a vertical tube furnace. Nitrogen was used as carrier gas throughout. Before activity testing, the catalyst was activated by heating from room temperature to 600 °C with heating rate 10 °C/min, held at 600 °C for 2 hours under air zero (30 mL/min), then cooled down to room temperature under nitrogen (30 mL/min). The flow rate of the gases was controlled by a mass flow controller and

checked by a bubble flow meter. Next, following TPR results, the catalyst was reduced by heating from room temperature to the chosen reduction temperature (10 °C/min, held at the final temperature for 2 hours) under 99.99% H_2 (60 mL/min). The catalyst after being activated and reduced, was heated from room temperature to the reaction temperature (600 °C). Then, the gases containing 99.95% propane with flow rate 10 mL/min, air zero at 10 mL/min and nitrogen (as a carrier gas) at 40 mL/min were separately fed into the reactor. The catalytic testing was conducted for a total time on stream (TOS) of 5 hours and gas products were analyzed and quantified by online gas chromatography with flame ionization detector (GC-FID). Schematic of the catalytic activity testing is shown in Figure 3.1.

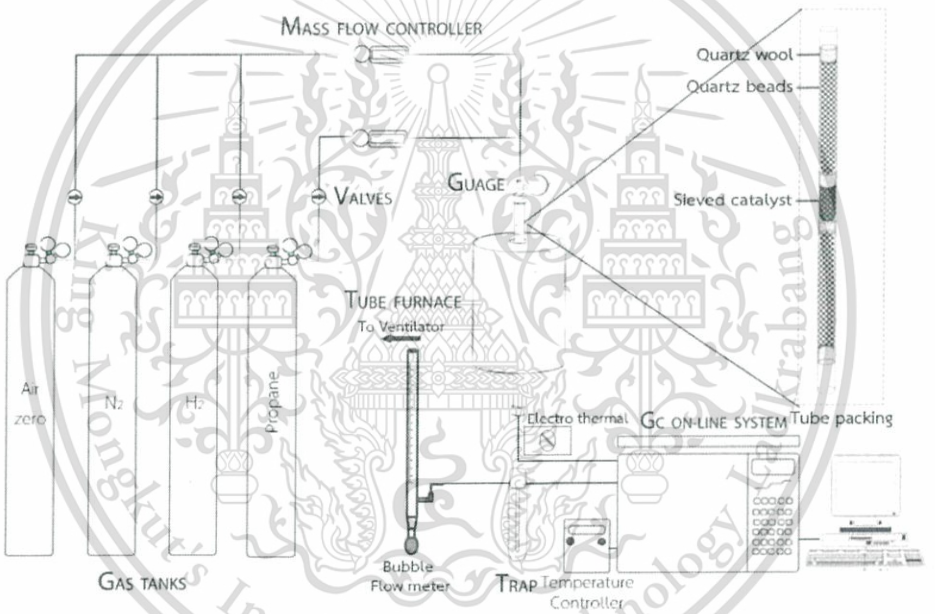

Figure 3.1 Catalytic activity testing rig

3.3.4 Analysis of products

The products were analyzed using an online gas chromatograph (HP 6890) equipped with a flame ionized detector (GC-FID). The products were collected in gas sampling loop. They were periodically injected into a GC column with a gas sampling loop and also with nitrogen as a carrier gas at every 30 minute. Conditions of the GC-FID used for products analysis are as follows: initial temperature at 80 °C, hold 3 minute, then ramping 10 °C/min to 150 °C followed by another hold for 10 minutes, with a total analytical time of 20 minutes. The temperature at the injector and FID detector was set at 100 and 250 °C, respectively. The gas products were recorded into

a chromatogram. The peak area of each product was measured and quantified using peak areas of the standard. A representative chromatogram, including the retention time and the identity of the product, can be found in Appendix B.

CHAPTER 4
RESULTS AND DISCUSSION

4.1 Catalyst Characterization

4.1.1 Pristine and metal-substituted hexatitanates

The XRD pattern of $K_2Ti_6O_{13}$ prepared by solid-state method is shown in Figure 4.1, with the hkl indexes shown on top of each peak. The hkl indexes are taken from the reports in the literature, and the similarity between current and reported XRD patterns [49] suggest the successful synthesis of $K_2Ti_6O_{13}$. The background found here was similarly observed in [51], which is ascribed to the use of relatively low temperature (700 °C) in the synthesis, and from the use of small crystallite size TiO_2 (P-25) as the starting material. The peak with the highest intensity is at 2θ = 11.46° (d = 0.6710 nm) corresponding the 200 reflection which is the repeating distance along the tunnel of $K_2Ti_6O_{13}$ with a monoclinic unit cell (Figure 2.6).

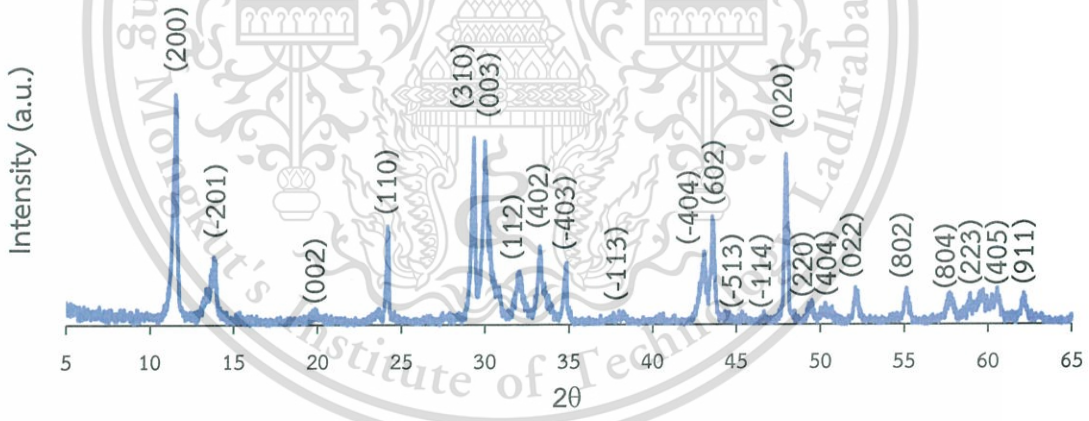

Figure 4.1 The XRD pattern of $K_2Ti_6O_{13}$.

The XRD patterns of $K_2Ti_{6-x}M_xO_{13}$ (x = 0.1) where the Ti(IV) atoms were partially substituted by divalent and trivalent cations (M = Mg(II), Co(II), Ni(II), Al(III), Cr(III), Mn(III), and Fe(III)) are illustrated in Figure 4.2. The pattern of $K_2Ti_6O_{13}$ is also shown for comparison. In all cases, the XRD patterns of $K_2Ti_{6-x}M_xO_{13}$ are similar to that of the parent $K_2Ti_6O_{13}$. So, the crystal structure of these products should be similar to that of $K_2Ti_6O_{13}$. It can be assumed that the metal cation M is statistically substituted for Ti at the nominal ratio of Ti/M = (6-x)/x = 5.9/0.1 = 59. $K_2Ti_{5.9}Mg_{0.1}O_{13}$, $K_2Ti_{5.9}Cr_{0.1}O_{13}$ and

$K_2Ti_{5.9}Fe_{0.1}O_{13}$ show additional peaks of impurity phase including MgO (2θ = 38.3° [58]), CrO_3 (2θ = 19.7° [59]), Cr_2O_3 (2θ = 33.8° [60]) and Fe_2O_3 (2θ = 35.8° [61]), respectively. So, the actual content of Mg, Cr and Fe incorporated into the $K_2Ti_6O_{13}$ framework should be lower than the nominal value. Nevertheless, the lack of extra peaks in other compositions studied suggests that $K_2Ti_{5.9}M_{0.1}O_{13}$ catalysts are free from crystalline impurity, or the amount of the impurity phase is lower than the detection limit.

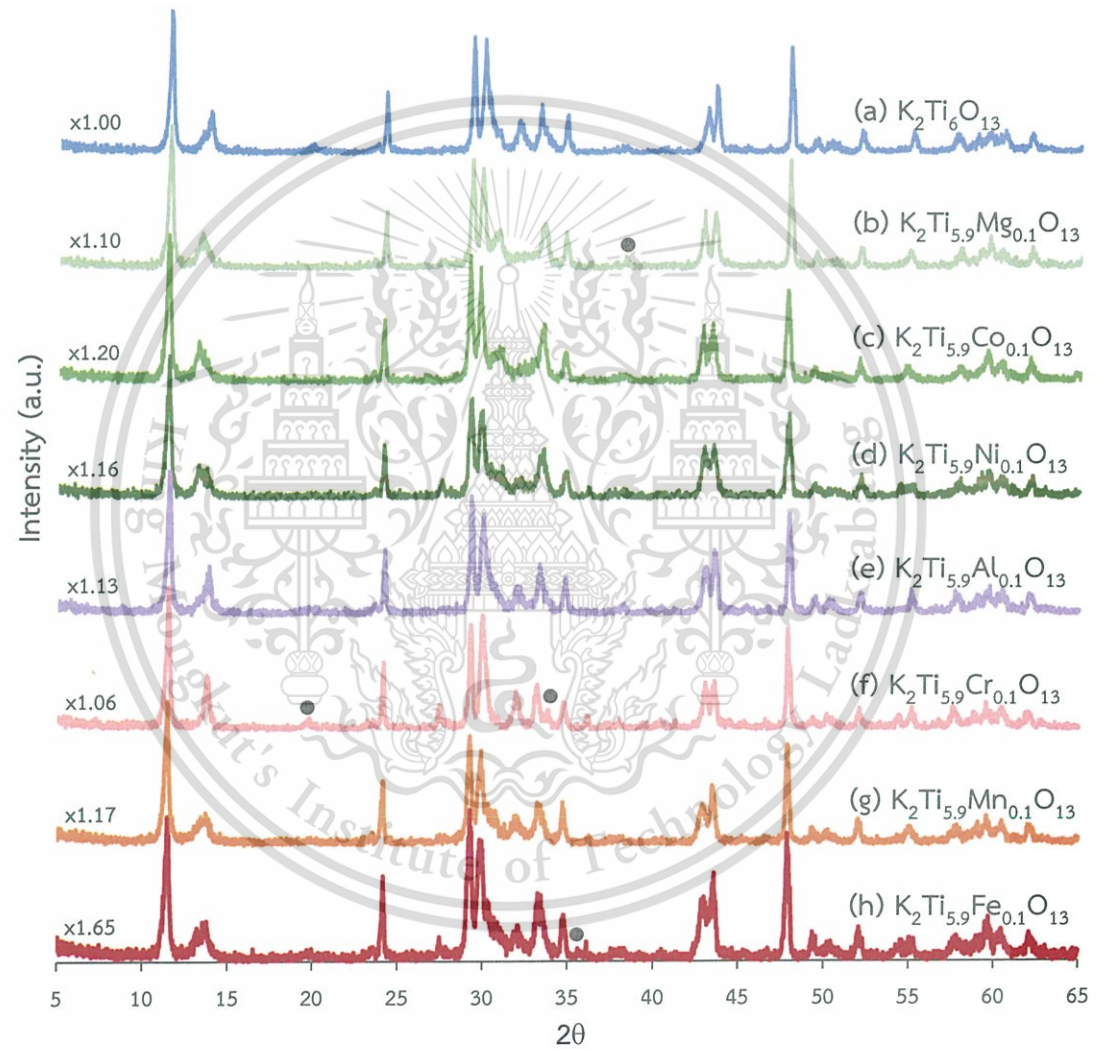

Figure 4.2 The XRD patterns of $K_2Ti_6O_{13}$ (a), $K_2Ti_{5.9}Mg_{0.1}O_{13}$ (b), $K_2Ti_{5.9}Co_{0.1}O_{13}$ (c), $K_2Ti_{5.9}Ni_{0.1}O_{13}$ (d), $K_2Ti_{5.9}Al_{0.1}O_{13}$ (e), $K_2Ti_{5.9}Cr_{0.1}O_{13}$ (f), $K_2Ti_{5.9}Mn_{0.1}O_{13}$ (g) and $K_2Ti_{5.9}Fe_{0.1}O_{13}$ (h). All patterns were normalized by a factor shown on the left such that the intensity of the first peak appears of the same height.

The d-spacing of the 200 peak for several compositions of the $K_2Ti_{5.9}M_{0.1}O_{13}$ is selected for further comparison, since this peak has the strongest intensity. Comparing to the parent one (Figure 4.3), the positions of the d(200) peak have shifted to lower 2θ, indicating the expansion along the inter-tunnel direction. A close up of the 200-peak is shown in Figure 4.3. Since the metals M substituted for Ti(IV) possess larger cationic radii, the expansion of the spacing is understandable and indeed expected. The shift of the 200 plane to the higher angular side in the sample substituted with Al(III) is not uncommon, since Al(III) is smaller than Ti(IV); such a shift nicely indicates the shrinking of the spacing as anticipated.

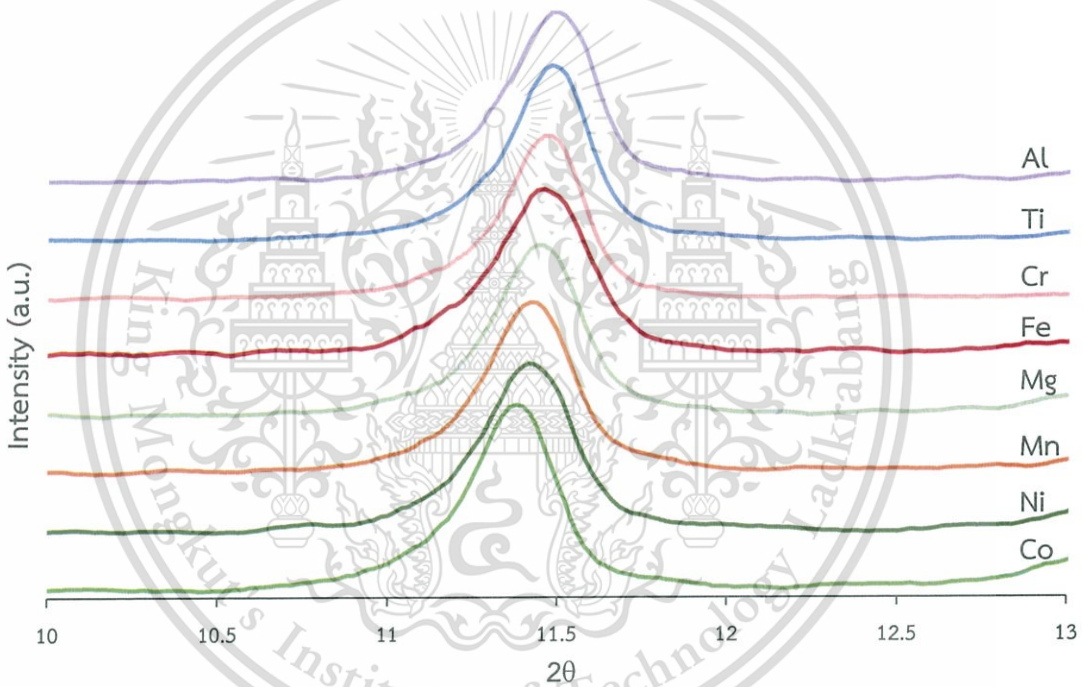

Figure 4.3 The zoomed-in, normalized XRD pattern of the $K_2Ti_{5.9}M_{0.1}O_{13}$ catalysts at the d(200) position.

The d-spacing of the 200 peak (the calculation shown in Appendix A) is plotted against the cationic radius of each M with the coordination number of 6 [62] as shown in Figure 4.4. The reasonably linear correlation can be observed, further confirming the successful incorporation of M into the Ti sites of the hexatitanate structure. It is noted that the extra framework metal oxide which forms another phase out of the hexatitanate framework was present in $K_2Ti_{5.9}Mg_{0.1}O_{13}$, $K_2Ti_{5.9}Cr_{0.1}O_{13}$, $K_2Ti_{5.9}Fe_{0.1}O_{13}$ as evidenced by XRD (Figure 4.2).

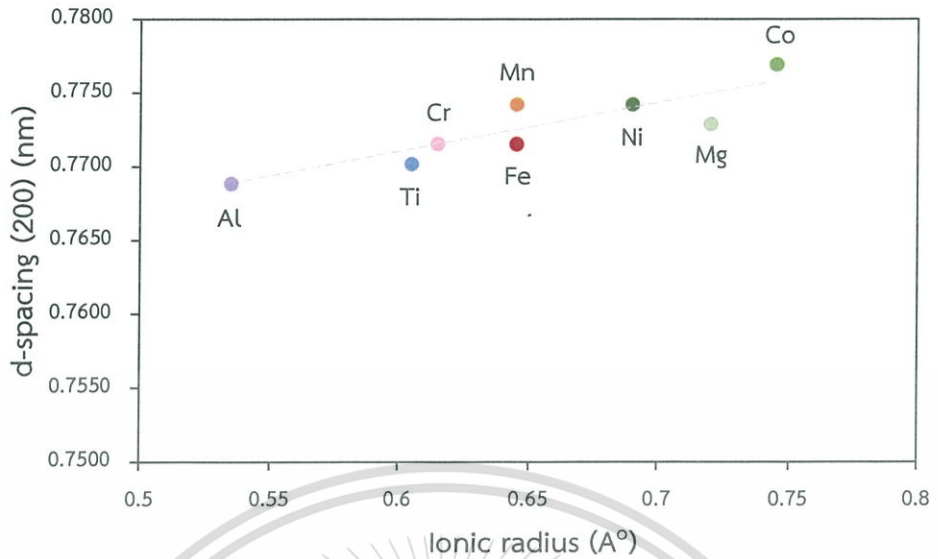

Figure 4.4 d-spacing (200) *vs* the ionic radius (A°) of the metal in $K_2Ti_{5.9}M_{0.1}O_{13}$.

The reducibility of all hexatitanate samples was investigated by H_2-temperature programmed reduction (H_2-TPR). The respective metal oxide precursors have been similarly investigated to aid in the assignment of reduction peaks. Figure 4.5 compares the H_2-TPR profiles of $K_2Ti_6O_{13}$ (a), and TiO_2 (P-25) (a'). The parent $K_2Ti_6O_{13}$ shows the reduction of Ti^{4+} to Ti^{3+} around 670-700 °C while TiO_2 (P-25) shows the similar reduction around 500-600 °C.

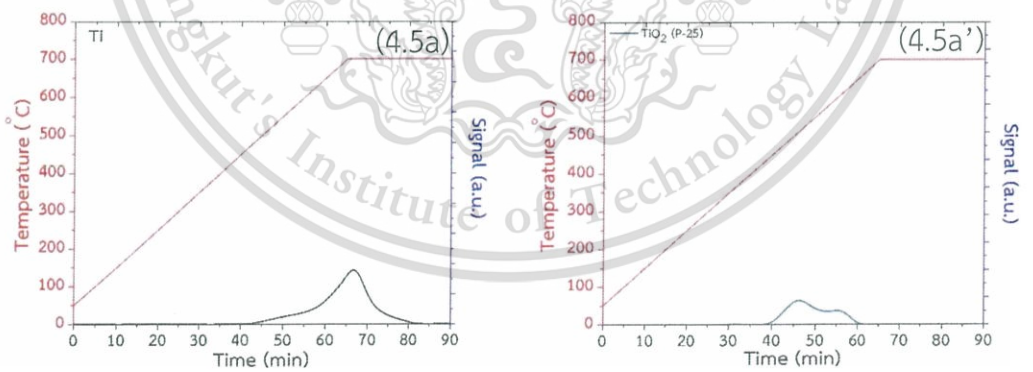

Figure 4.5 H_2-TPR profiles of $K_2Ti_6O_{13}$ (a), and TiO_2 (P-25) (a').

The $K_2Ti_6O_{13}$ structure, containing negatively charged $Ti_6O_{13}^{2-}$ framework, would possess relatively high electron density and hence its reduction would be more difficult, as compared to TiO_2 (P-25). In addition, the $K_2Ti_6O_{13}$ shows a higher H_2-consumption, as compared to TiO_2 (P-25), which indicates that a larger number of oxygen vacancies are generated. This is because the tunnel structure of $K_2Ti_6O_{13}$ is

arranged by sharing the corner lattice oxygen of a ribbon with another one (three TiO_6 octahedra forming a ribbon) as shown in Figure 2.6. Accordingly, relatively higher number of exposed lattice oxygens can be expected for $K_2Ti_6O_{13}$, as compared to the defect surface of TiO_2 (P-25). The oxygen vacancy of $K_2Ti_6O_{13}$ was generated upon H_2 reduction, as shown in Scheme 4.1.

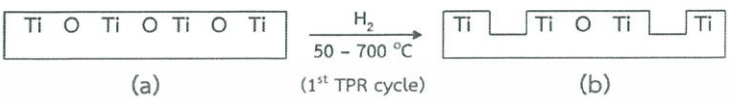

Scheme 4.1

The H_2-TPR profiles of the samples where Ti in the framework was substituted by non-reducible metals (M = Mg, Al) are compared in Figure 4.6. The H_2-TPR profile of $K_2Ti_{5.9}Mg_{0.1}O_{13}$ shows a higher H_2-consumption in both cycles, as compared to the parent $K_2Ti_6O_{13}$ as shown in Table 4.1. So, the higher oxygen vacancy generated when Mg was substituted in Ti framework suggests that the hexatitanate is relatively less stable (more reactive) when Mg is present. Since Ti(IV) was partially substituted by Mg(II), the resulting material becomes deficient in the positive charges. This lack of positive charges (i.e., the surplus of negative charges) could be the driving force for liberating lattice oxygen as anticipated. So, the higher H_2-consumption was observed in $K_2Ti_{5.9}Mg_{0.1}O_{13}$ compared to the pristine $K_2Ti_6O_{13}$. While substituting Al(III) for Ti(IV) has no critical effect on the reducibility, presumably due to higher stability of $K_2Ti_{5.9}Al_{0.1}O_{13}$, as compared to $K_2Ti_6O_{13}$.

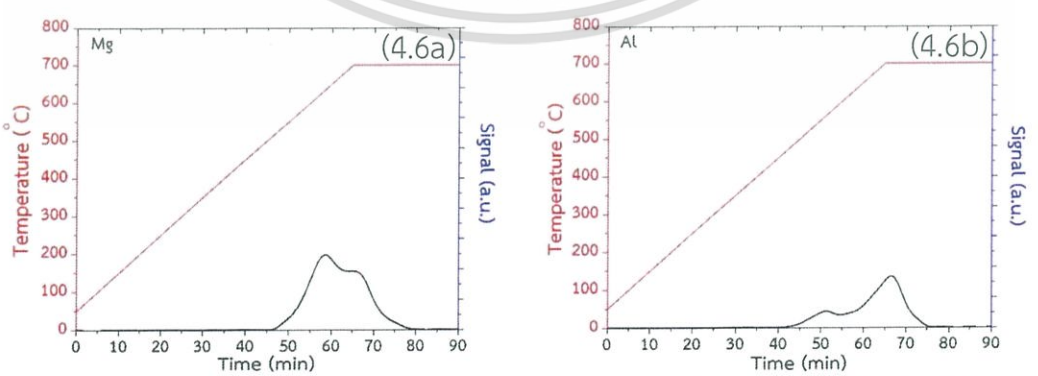

Figure 4.6 H_2-TPR profiles of $K_2Ti_{5.9}Mg_{0.1}O_{13}$ (a), and $K_2Ti_{5.9}Al_{0.1}O_{13}$ (b).

Table 4.1 H_2-consumption and metal loading (wt.%) of the $K_2Ti_{5.9}M_xO_{13}$ catalysts

Catalysts	H_2-consumption (μmol/g)		Metal loading (wt.%)
	Metal	TiO_2	Metal
$K_2Ti_6O_{13}$	-	36	-
$K_2Ti_{5.9}Mg_{0.1}O_{13}$	-	62	-
$K_2Ti_{5.9}Al_{0.1}O_{13}$	-	35	-
$K_2Ti_{5.9}Cr_{0.1}O_{13}$	216	10	0.37
$K_2Ti_{5.9}Co_{0.1}O_{13}$	7	45	0.04
$K_2Ti_{5.9}Ni_{0.1}O_{13}$	88	163	0.52
$K_2Ti_{5.9}Fe_{0.1}O_{13}$	89	32	0.50
$K_2Ti_{5.9}Mn_{0.1}O_{13}$	89	21	0.49

The H_2-TPR profiles of $K_2Ti_{5.9}M_{0.1}O_{13}$ with *reducible* metals (Ni, Mn, Fe, Cr and Co) are compared in Figure 4.7. Since these substituted metals are reducible, all of the H_2-TPR profiles show additional reduction peak(s) at lower temperature, ascribed to the reduction of M substituted in framework. The reduction temperature of substituted M species is typically higher than that of the corresponding bulk metal oxides, i.e., the reduction has become more difficult. This result can be similarly explained by the relatively high electron density of the metal as a result of the negatively-charged framework compared to the bulk metal oxides, as discussed previously. However, the reduction peak(s) at the temperature similar to bulk metal oxides can be observed after peak deconvolution, as shown in Appendix A indicating the reduction of trace metal oxide present in the sample as impured extra framework phase. While M = Co in hexatitanate framework cannot be reduced, only the reduction peak of extra framework cobalt oxide can be observed (Figure 4.7 (a)).

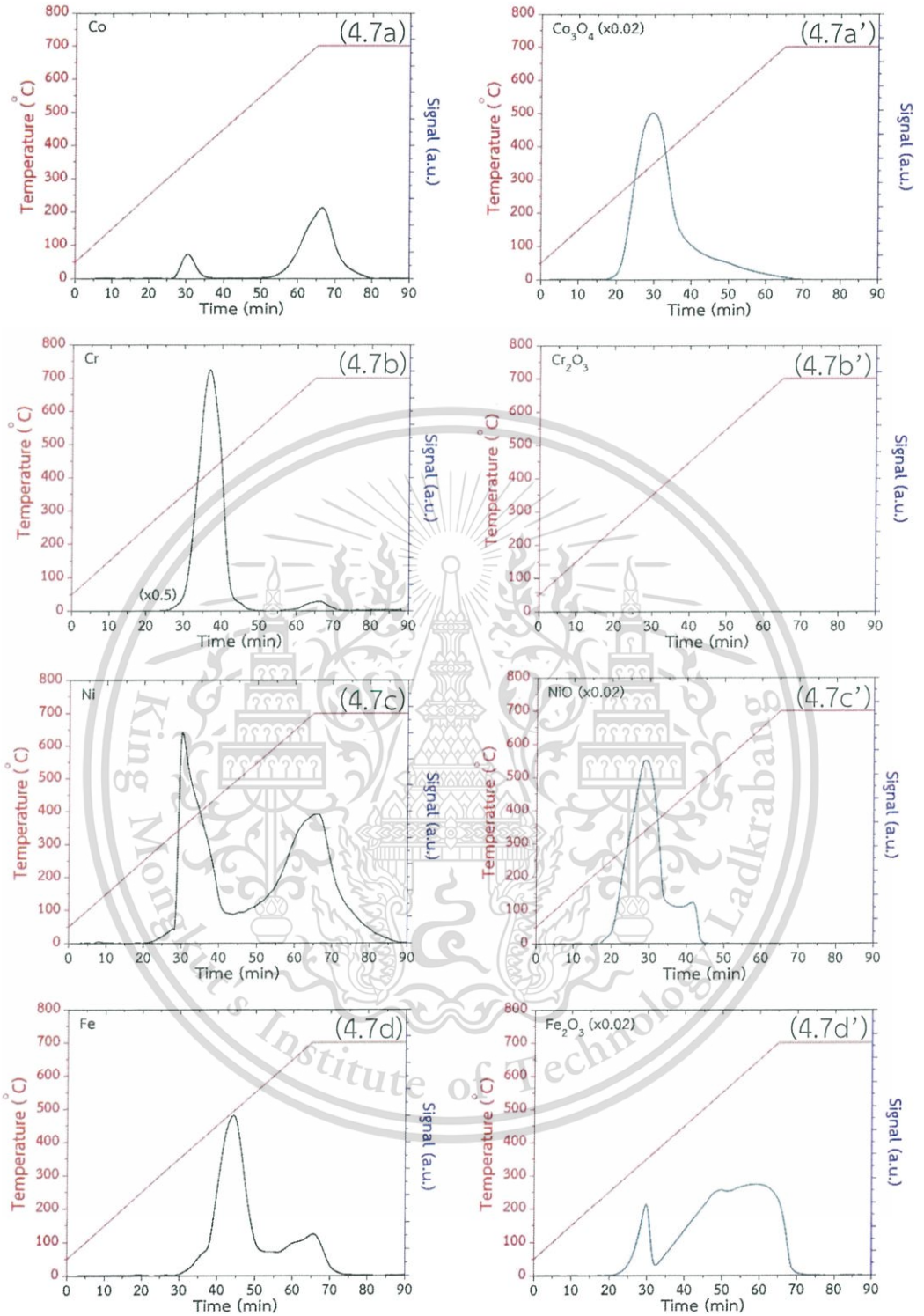

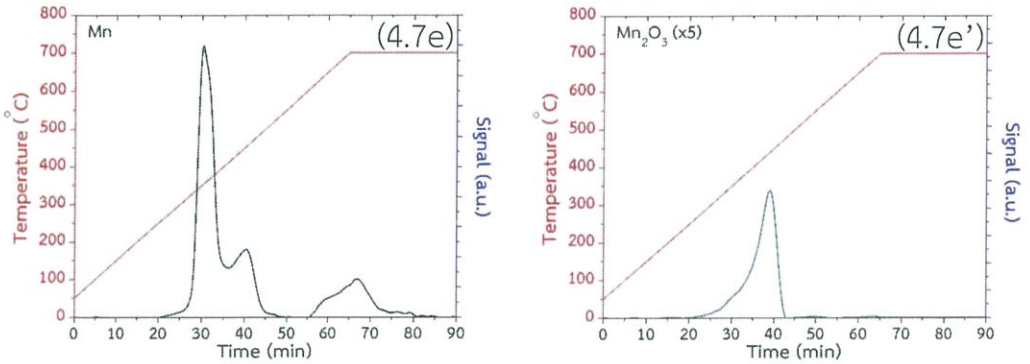

Figure 4.7 H_2-TPR profiles of $K_2Ti_{5.9}Co_{0.1}O_{13}$ (a), Co_3O_4 (a'), $K_2Ti_{5.9}Cr_{0.1}O_{13}$ (b), and Cr_2O_3 (b'), $K_2Ti_{5.9}Ni_{0.1}O_{13}$ (c), NiO (c'), $K_2Ti_{5.9}Fe_{0.1}O_{13}$ (d), Fe_2O_3 (d'), $K_2Ti_{5.9}Mn_{0.1}O_{13}$ (e), and Mn_2O_3 (e').

The relatively large H_2-consumption for $K_2Ti_{5.9}Cr_{0.1}O_{13}$ at low temperature can be explained by the reduction of impure phase of bulk chromium(VI) oxide to chromium(III) oxide [63]. (Recall from XRD results that not all Cr could be substituted for Ti at x = 0.1.).

For M = Co, the H_2-consumption (at the metal) is lower than the other $K_2Ti_{5.9}M_{0.1}O_{13}$ samples. This finding suggests that only a trace of cobalt oxide as impurity phase can be reduced. On the other hand, a relatively high fraction of Ni, Fe, and Mn can be reduced and dislodged from the framework as shown by their relatively high H_2-consumption at the low temperature (300 -500 °C) in Table 4.1. Accordingly, the reduction peak observed at 300 – 500 °C is attributed to those substituted framework and also of extra framework trace metal oxide, as shown in Scheme 4.2.

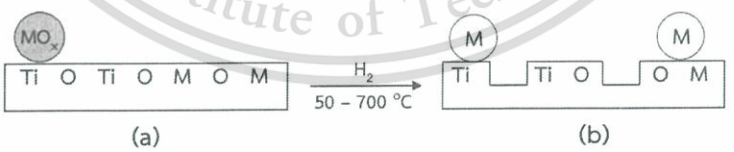

Scheme 4.2

In addition to the reduction of M, the hexatitanate framework could also be reduced, i.e., lattice oxygen could be removed. This event typically occurred at relatively high temperature, as demonstrated for $K_2Ti_6O_{13}$ in Figure 4.5(a). As M was dislodged from the framework as metallic phase during the TPR cycle (Scheme 4.2 (a) to (b)), the higher fraction of oxygen vacancy is generated. Especially, $K_2Ti_{5.9}Ni_{0.1}O_{13}$ gave higher H_2-consumption for *Ti reduction*, shown as the reduction peak at higher temperatures. For example, 36 μmol H_2/g were consumed to generate the oxygen vacancy in $K_2Ti_6O_{13}$ in the first TPR cycle. The corresponding number for $K_2Ti_{5.9}Ni_{0.1}O_{13}$ is as large as 163 μmol H_2/g. It can be seen that the Ti in framework of $K_2Ti_{5.9}Ni_{0.1}O_{13}$ can be easily reduced, as compared to the other reducible metal incorporated. So, one can deduce that the resulting hexatitanate structure (doped with Ni) is relatively unstable and could be very reactive.

4.1.2 Effect of Ni loading

The XRD patterns of $K_2Ti_{6-x}Ni_xO_{13}$ with different amounts of Ni(II) partially substituted for Ti(IV), including $K_2Ti_{5.95}Ni_{0.05}O_{13}$ (Ni0.05), $K_2Ti_{5.9}Ni_{0.1}O_{13}$ (Ni0.1), $K_2Ti_{5.8}Ni_{0.2}O_{13}$ (Ni0.2) and $K_2Ti_{5.5}Ni_{0.5}O_{13}$ (Ni0.5) are shown in Figure 4.8. The general patterns for x = 0.05 and 0.1 are similar to that of parent $K_2Ti_6O_{13}$. Meanwhile, the samples with x = 0.2 and 0.5 show additional peaks of impurity phase NiO at 37° and 63° [64].

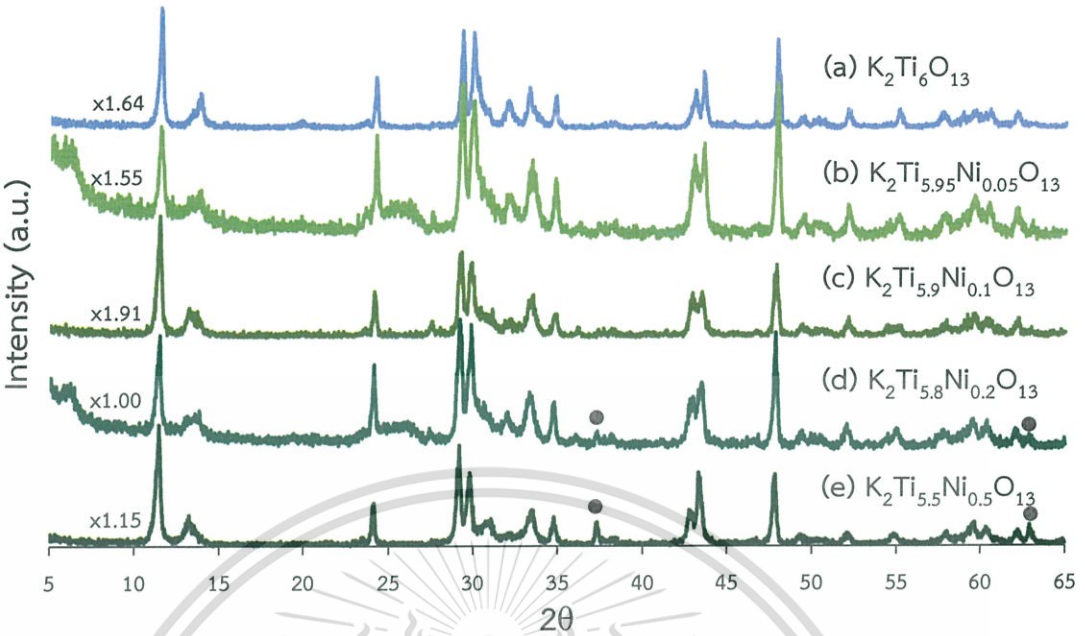

Figure 4.8 The XRD patterns of $K_2Ti_6O_{13}$ (a), $K_2Ti_{5.95}Ni_{0.05}O_{13}$ (b), $K_2Ti_{5.9}Ni_{0.1}O_{13}$ (c), $K_2Ti_{5.8}Ni_{0.2}O_{13}$ (d) and $K_2Ti_{5.5}Ni_{0.5}O_{13}$ (e). All patterns were normalized by a factor shown on the left such that the intensity of the first peak appears of the same height.

The d(200) positions of Ni substituted hexatitanate samples have shifted to lower 2θ as compared to the parent one (Figure 4.9). The d-spacing along the tunnel continuously expanded with Ni content up to x = 0.1 as seen from Figure 4.10. This is because the cationic radius of Ni(II) is larger than that of Ti(IV). This result strongly confirm the successful synthesis of the Ni-substituted $K_2Ti_{6-x}Ni_xO_{13}$ where Ni forms the solid solution with Ti. Beyond that, the excess Ni cannot be substituted into the hexatitanate structure, but instead formed NiO aggregate, as evidenced by XRD (Figure 4.8).

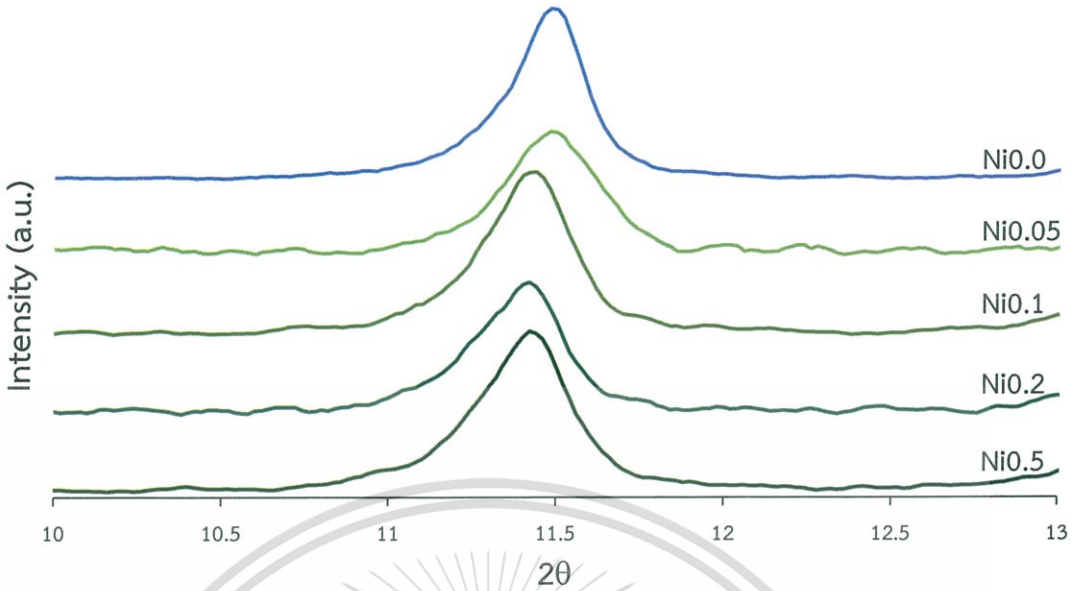

Figure 4.9 The XRD pattern of Ni-substituted hexatitanate $K_2Ti_{6-x}Ni_xO_{13}$ (x = 0-0.5) at the d(200) position.

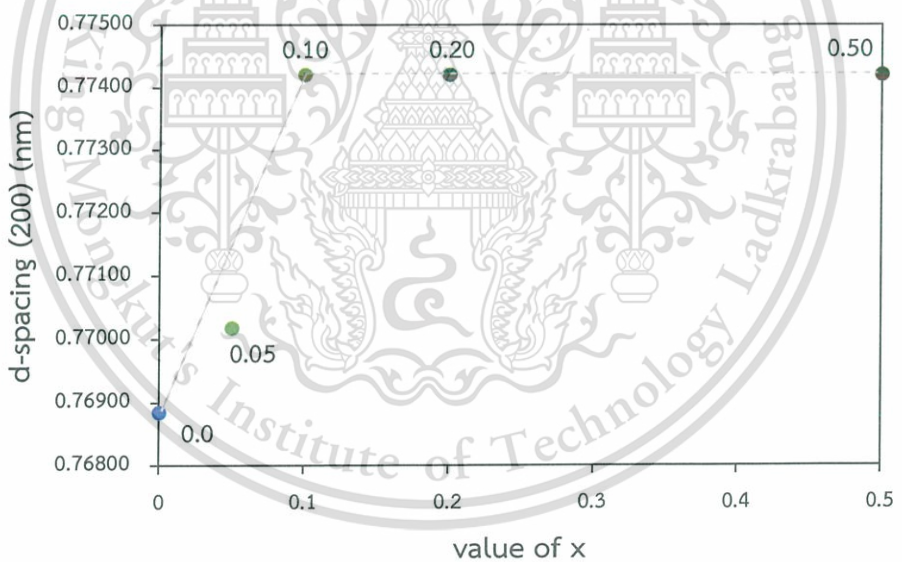

Figure 4.10 d-spacing (200) *vs* values of x (in the formula $K_2Ti_{6-x}Ni_xO_{13}$) in Ni-substituted potassium hexatitanate samples.

The elemental analysis of these $K_2Ti_{6-x}Ni_xO_{13}$ catalysts were determined by XRF. The results are shown in Table 4.2. The elemental analysis of K, Ti and Ni content is in reasonable agreement with the theoretical values (Appendix A) calculated from the ideal composition. The exception is for Ni0.2, where the Ni content (1.3 wt.%) is lower than the expected loading (2.0 wt.%).

Table 4.2 Elemental analysis of the Ni loading catalysts

Catalysts	Elemental composition (wt.%) by XRF			Theoretical composition (wt.%)		
	K	Ti	Ni	K	Ti	Ni
$K_2Ti_6O_{13}$ (Ni0.0)	11.6	51.6	-	13.63	49.27	-
$K_2Ti_{5.95}Ni_{0.05}O_{13}$ (Ni0.05)	14.2	48.4	0.5	13.62	49.22	0.51
$K_2Ti_{5.9}Ni_{0.1}O_{13}$ (Ni0.1)	13.6	48.2	1.0	13.61	49.18	1.02
$K_2Ti_{5.8}Ni_{0.2}O_{13}$ (Ni0.2)	14.3	47.4	1.3	13.58	49.08	2.04
$K_2Ti_{5.5}Ni_{0.5}O_{13}$ (Ni0.5)	14.3	44.8	5.3	13.51	48.81	5.07

The H_2-TPR profiles of $K_2Ti_{5.95}Ni_{0.05}O_{13}$ (a), $K_2Ti_{5.9}Ni_{0.1}O_{13}$ (b), $K_2Ti_{5.8}Ni_{0.2}O_{13}$ (c), and $K_2Ti_{5.5}Ni_{0.5}O_{13}$ (d) are shown in Figure 4.11.

The H_2-consumption from Ni species (i.e., the reduction at low temperature 280-300 °C) is increased with amount of substituted Ni as shown in Table 4.3. This result suggests that higher Ni content can be dislodged from the hexatitanate framework as the Ni loading is increased, since the Ni-substituted hexatitanate structure has become progressively more active. Moreover, Ti in the framework can be easily reduced starting from 400 °C as the Ni content is increased, as seen from the higher H_2-consumption at the high temperature peak in Table 4.3 and Figure 4.12. Higher amount of Ni can be dislodged from Ni0.5 as extra framework NiO phase, as evidenced by XRD (Figure 4.8).

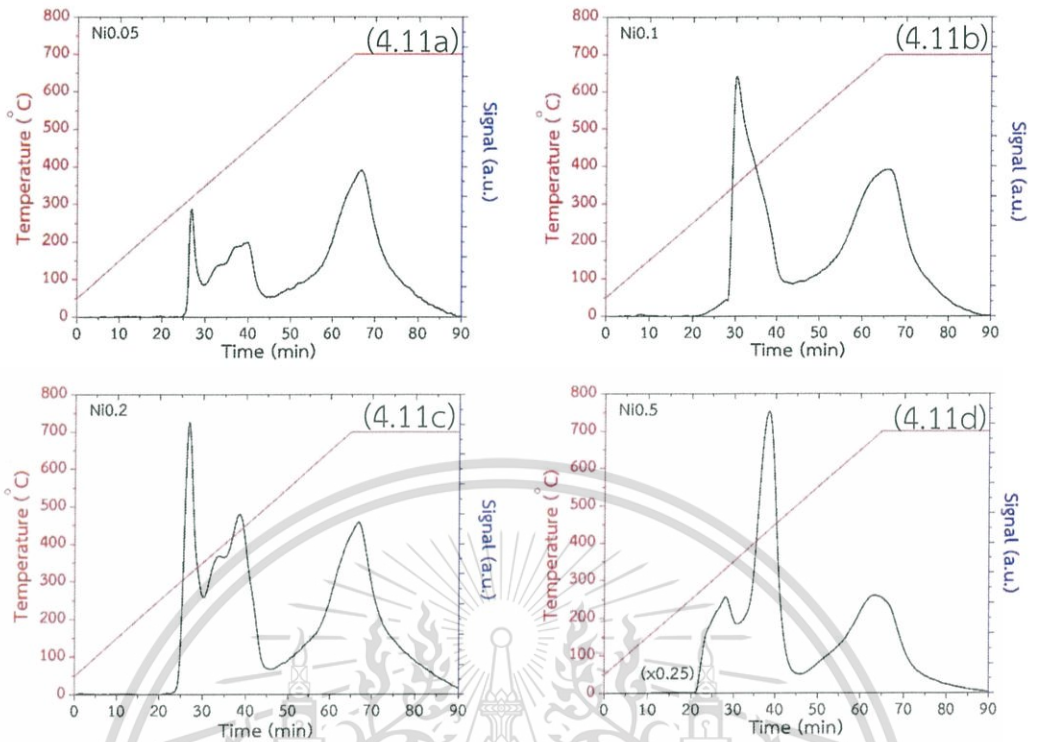

Figure 4.11 H_2-TPR profiles of $K_2Ti_{5.95}Ni_{0.05}O_{13}$ (a), $K_2Ti_{5.9}Ni_{0.1}O_{13}$ (b), $K_2Ti_{5.8}Ni_{0.2}O_{13}$ (c), and $K_2Ti_{5.5}Ni_{0.5}O_{13}$ (d).

Table 4.3 H_2-consumption and Ni loading (wt.%) of the $K_2Ti_{6-x}Ni_xO_{13}$ catalysts. The values for x = 0 are also shown for comparison

Catalysts	H_2-consumption (μmol/g)		Ni loading (wt.%)
	Ni	TiO_2	Ni
Ni0.0	-	36	-
Ni0.05	51	13	0.30
Ni0.1	88	163	0.52
Ni0.2	139	163	0.82
Ni0.5	520	386	3.05

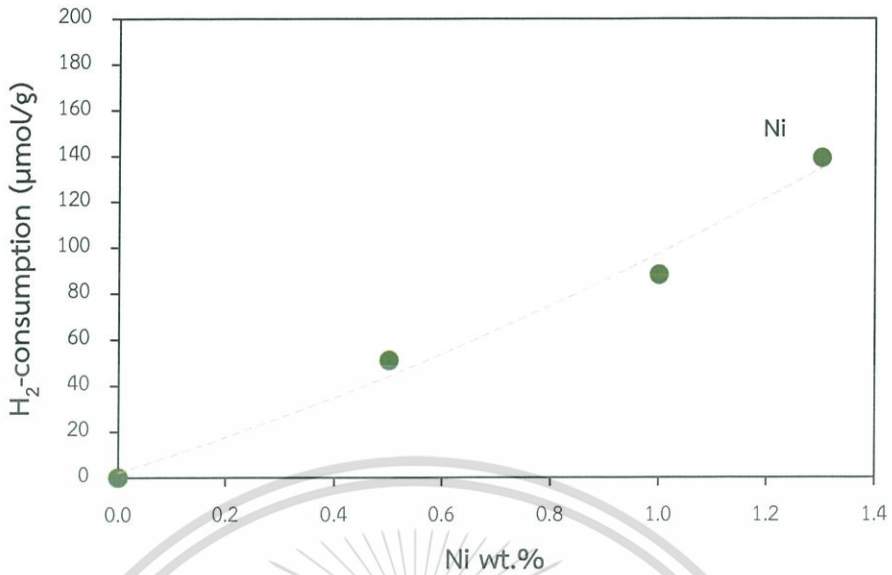

Figure 4.12 H_2-consumption for reduction/dislodgement of in Ni-substituted potassium hexatitanate vs Ni wt.% in Ni-substituted potassium hexatitanate samples.

In line with TPR results, the presence of oxygen vacancy after reduction was supported by ESR that is sensitive to the presence of an unpaired electron in the catalysts [65]. It can be seen in Figure 4.13 that both non-reduced $K_2Ti_6O_{13}$ and $K_2Ti_{5.9}Ni_{0.1}O_{13}$ (dash line) showed a single broad peak barely above the background. This result suggests a very small amount of paramagnetic species in these two samples prior to the reduction. However, upon reduction, the signal (full line) was enhanced by a factor of ~10^4 over reduced $K_2Ti_6O_{13}$, and of ~10^6 for $K_2Ti_{5.9}Ni_{0.1}O_{13}$. This result provides an evidence for Ti^{3+} where oxygen vacancy can be generated after the reduction, as suggested earlier by H_2-TPR. Particularly for Ni containing-sample, the higher amount of oxygen vacancy sites were generated due to Ni dislodgement from $K_2Ti_{5.9}Ni_{0.1}O_{13}$ surface which in turn leaving the empty sites at the framework. Accordingly, a significantly large signal of unpaired electron resonance was observed for $K_2Ti_{5.9}Ni_{0.1}O_{13}$ after reduction. Unfortunately, the broadness of the spectra did not allow us to extract a reliable *g*-factor, otherwise this will be helpful for identification of the ESR-active species.

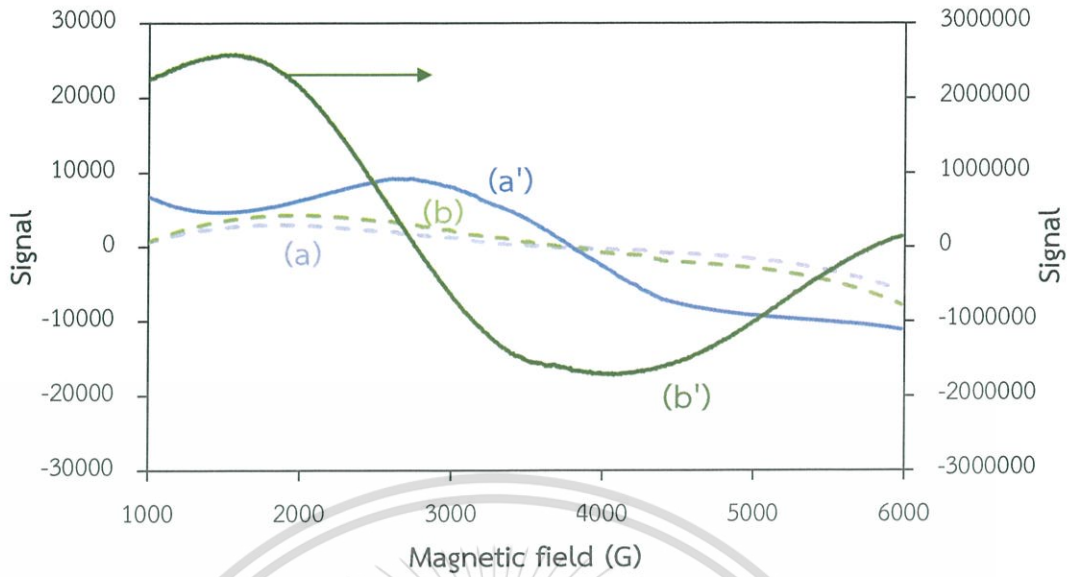

Figure 4.13 *Ex-situ* ESR spectra of $K_2Ti_6O_{13}$ as made (a) and after the reduction at 700 °C (a'); and of $K_2Ti_{5.9}Ni_{0.1}O_{13}$ as made (b), and after the reduction at 400 °C (b').

4.2 Oxidative dehydrogenation of propane

4.2.1 Comparison with common metal oxides

The activities of selected common metal oxides in the oxidative dehydrogenation of propane are summarized in Table 4.4. TiO_2 and NiO were selected for comparison with layer titanate catalysts. CeO_2 is well known to form oxygen vacancy so its catalytic activity was compared as well.

Table 4.4 Oxidative dehydrogenation of propane over $K_2Ti_6O_{13}$, and typical metal oxides catalysts

Catalysts	S_{BET} (m^2/g)	Conversion (%)	Yield (%)								Ratio of $C_2=+C_3=/CO+CO_2$ [a]
			Methane	Ethane	Ethylene	Propylene	Butane	iso-butane	C_5^+	CO, CO_2	
P-25	50	8.5	0.2	0.01	0.6	1.6	0.01	0.00	0.00	6.1	0.4
CeO_2	139	10.9	0.3	0.01	1.1	1.8	0.01	0.00	0.00	7.7	0.4
NiO	18	11.7	0.5	0.02	0.7	2.0	0.00	0.01	0.00	8.5	0.3
$K_2Ti_6O_{13}$	21	13.0	0.5	0.03	3.4	2.5	0.03	0.1	0.01	6.4	0.9

The data is collected at initial time on stream of 0.5 h.

[a] yield of ethylene+propylene/CO and CO_2

(Reaction condition: T_{react} = 600 °C, T_{red} = 700 °C, F = 10:10:40 mL/min (C_3H_8:Air:N_2), W/F = 23 g·h/mol, atmospheric pressure)

The non-substituted $K_2Ti_6O_{13}$ catalyst gave relatively high activity and yields of ethylene and propylene as compared to the other metal oxides (TiO_2, CeO_2 and NiO). This performance is rather impressive considering that its surface area of is 2-7 times lower than TiO_2 (P-25) and CeO_2, and is similar to NiO. It is suggested that the C-H activation of propane can be readily promoted by reducible lattice oxygen of the hexatitanate [66]. This active site was generated upon reduction of the catalyst. H_2-TPR results in Figure 4.5 indeed indicate that the content of oxygen vacancy in potassium hexatitanate is higher than that in TiO_2 (P-25). This is because the hexatitanate structure contains three TiO_6 octahedra forming the ribbon; the ribbons in turn share the corners with another ribbon and form the tunnel as shown in Figure 2.6. O atoms in the

hexatitanate structure are therefore *coordinatively unsaturated* (cus), compared to those of TiO_6 units in anatase (or rutile) with dense 3D structure. Therefore, a higher fraction of oxygen atoms in alkali hexatitanate can be removed, generating oxygen vacancy, upon reduction in H_2.

However, high content of CO and CO_2 was produced as a major product for all catalysts. It is suggested that propane and hydrocarbon products can be combusted with gas phase O_2. Nevertheless, the hexatitanate gave relatively higher ethylene and propylene yields, as compared to the other metal oxides investigated.

4.2.2 Effect of metals substituted in hexatitanate

The $K_2Ti_{5.9}M_{0.1}O_{13}$ samples where metal cations, M were successfully substituted for Ti(IV), were tested for the oxidative dehydrogenation of propane. Some of the samples with a trace of impurity phase including M = Mg, Cr and Fe (as evidenced by XRD results in Figure 4.2), were not studied. The results are summarized in Table 4.5.

Table 4.5 Oxidative dehydrogenation of propane over various metal substituted $K_2Ti_{5.9}M_{0.1}O_{13}$ catalysts

M	S_{BET} (m^2/g)	Conversion (%)	Yield (%)								Ratio of $C_2=+C_3=/CO+CO_2$ [a]
			Methane	Ethane	Ethylene	Propylene	Butane	iso-butane	C_5^+	CO, CO_2	
Ti	21	13.8	0.5	0.02	3.4	2.7	0.02	0.1	0.01	7.0	0.9
Al	36	11.5	0.4	0.01	2.6	2.4	0.03	0.03	0.01	6.0	0.8
Ni	35	14.6	0.7	0.02	2.3	5.3	0.1	0.1	0.04	6.0	1.3
Co	32	15.2	0.5	0.02	3.1	2.1	0.01	0.04	0.01	9.4	0.6
Mn	27	16.0	0.6	0.1	3.2	2.8	0.1	0.2	0.1	8.9	0.7

All data were averaged from the time on stream of 0.5-3.0 h.

[a] yield of ethylene+propylene/CO and CO_2

(Reaction condition: T_{react} = 600 °C, T_{red} = 700 °C (Ti), 600 °C (Al), 500 °C (Mn), 400 °C (Co and Ni), F = 10:10:40 mL/min (C_3H_8:Air:N_2), W/F = 23 g·h/mol, atmospheric pressure)

The conversion of propane over $K_2Ti_{5.9}M_{0.1}O_{13}$ catalysts decreased in the order M of Co > Mn > Ni > Al > Ti. This order (excluding M = Ti) is in parallel with the redox ability as indicated by the standard reduction potential (E^0) of the respective cations $M^{n+} + ne^- \longrightarrow M^0$ [67], with E^0 = 1.82 (Co), 1.21 (Mn), -0.23 (Ni) and -1.66 V (Al). Here, the positive value indicates that the reduction is thermodynamically favorable; and the larger E^0 indicates the strong driving force for reduction. The correlation with E^0 is understandable considering the redox nature of this reaction where M^{n+} (in the solid) must be reduced so as to induce a higher concentration of oxygen vacancy. The redox chemistry also involves in the oxidation of propane (and hydrocarbon products) to CO and CO_2, likely over bulk metal oxides. The metal oxides can be formed by partial oxidation of the metal dislodged from the hexatitanate framework after reduction. Because of this side reaction, ethylene and propylene was produced as minor products for all catalysts. Except for $K_2Ti_{5.9}Ni_{0.1}O_{13}$, the yields of ethylene and propylene are larger than those of CO and CO_2 at very similar propane conversion, as compared to other catalysts. This is because a higher content of oxygen vacancy can be generated over $K_2Ti_{5.9}Ni_{0.1}O_{13}$ as deduced from H_2-TPR (Table 4.1). As discussed previously the structure of $K_2Ti_{5.9}Ni_{0.1}O_{13}$ has become relatively unstable (i.e. more reactive) by Ni substitution, such that upon reduction Ni is dislodged from the framework, accompanying by the generation of the high content of oxygen vacancy. The oxygen vacancy can be replenished by O_2 gas, and the active sites are regenerated. These sites promoted C-H activation and oxidative dehydrogenation of propane to produce propylene (Scheme 4.3), while ethylene would be derived from cracking of propyl radical. Nevertheless, combustion of propane to CO and CO_2 can also be observed over $K_2Ti_{5.9}Ni_{0.1}O_{13}$. This is because NiO is partially formed during the reaction.

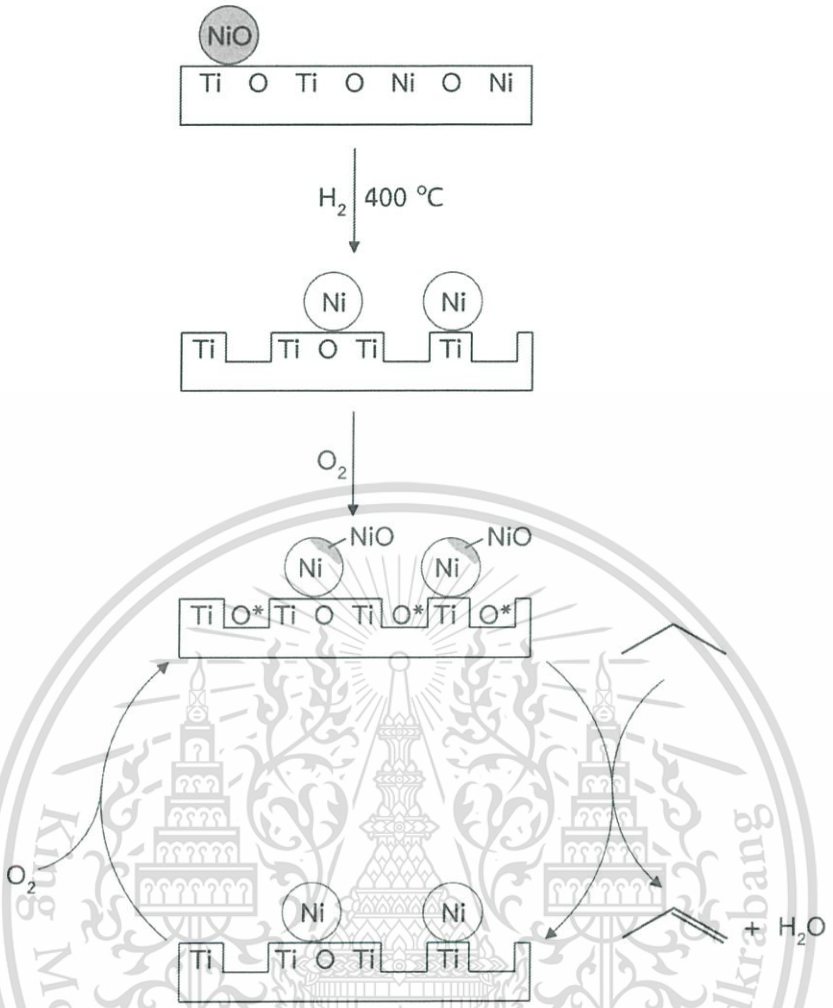

Scheme 4.3

The dislodged Ni is not active for the improve activity in oxidative dehydrogenation of propane as shown in Table 4.3.

The assumption that NiO phase is not active for the oxidative dehydrogenation of propane can be further validated by the reaction employing 1%Ni/P-25 as a catalyst. (The loading of 1 wt.% Ni corresponds to the Ni content in the x = 0.1 sample, Table 4.2.) This catalyst was reduced at 400 °C prior to the reaction. Results are shown in Figure 4.14.

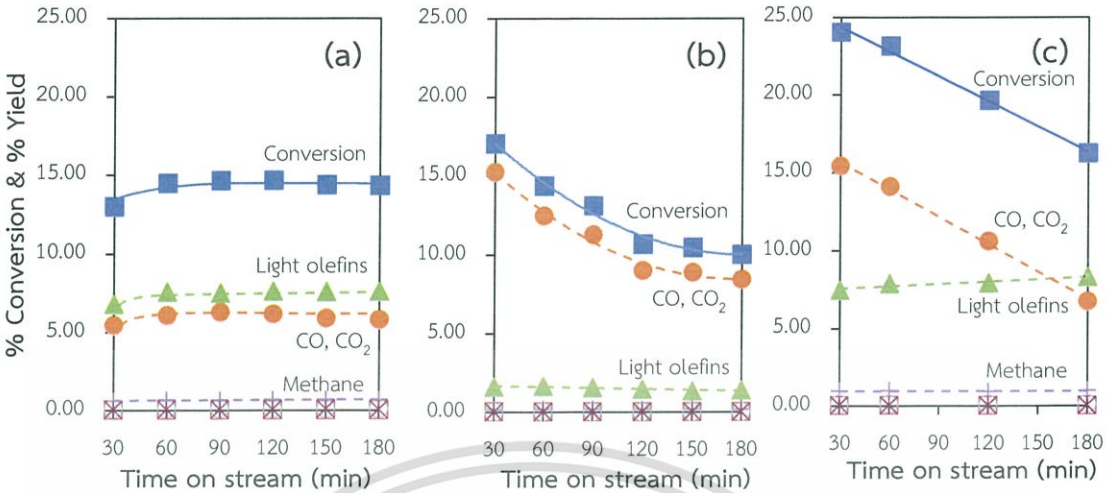

Figure 4.14 Oxidative dehydrogenation of propane at 600 °C over (a) reduced 400 °C $K_2Ti_{5.9}Ni_{0.1}O_{13}$, (b) reduced 400 °C $K_2Ti_{5.9}Ni_{0.1}O_{13}$, reduced 400 °C 1%Ni/P-25 and (c) reduced 400 °C and oxidized 400 – 600 °C $K_2Ti_{5.9}Ni_{0.1}O_{13}$ (heating rate 10 °C/min).

(Reaction condition: T_{react} = 600 °C, T_{red} = 400 °C, F = 10:10:40 mL/min (C_3H_8:Air:N_2), W/F = 23 g·h/mol, atmospheric pressure, Symbol = Conversion(■), Methane (+), Ethane (□), Light olefins (Ethylene, Propylene) (▲), Butane(×), iso-butane (◇), $C5^+$ (✳), CO and CO_2 (●))

It can be seen that the yield of ethylene and propylene over 1%Ni/P-25 (Figure 4.14 (b)) are lower than that achieved over reduced $K_2Ti_{5.9}Ni_{0.1}O_{13}$ (Figure 4.14 (a)), while the yield of combustion gases is relatively high. It is likely that all amount of Ni can be formed NiO over 1%Ni/P-25 surface (even though it was not detected by XRD, likely due to the small amount and the small size, see the XRD pattern in Appendix A). As shown previously, such NiO can promote the deep oxidation of propane and hydrocarbon products to CO and CO_2. In addition, catalyst deactivation is particularly pronounced over 1%Ni/P-25 (Figure 4.14 (b)) but not over $K_2Ti_{5.9}Ni_{0.1}O_{13}$ (Figure 4.14 (a)). This suggests that NiO present in 1%Ni/P-25 (Figure 4.14 (b)) can be reduced by hydrocarbon products to form metallic Ni and then sintering at high temperature. As metallic Ni is inactive for combustion, a decrease yield of CO and CO_2 is observed with time on stream. To verify this hypothesis, the $K_2Ti_{5.9}Ni_{0.1}O_{13}$ was reduced at 400 °C and then oxidized at 400 – 600 °C to ensure that NiO is present in the sample. As shown in Figure 4.14 (c), the higher amount of CO and CO_2 are observed, suggesting that the active site for combustion is NiO. Moreover, this catalyst is deactivated and yields of

CO and CO_2 are decreased with time on stream in a manner similar to that over 1%Ni/P-25 (Figure 4.14 (b)). This implies that, NiO (active site for combustion) can be reduced to metallic Ni during the reaction by hydrocarbon products. While the yields of light olefins over oxidized $K_2Ti_{5.9}Ni_{0.1}O_{13}$ catalyst (Figure 4.14 (c)) is similar to the reduced $K_2Ti_{5.9}Ni_{0.1}O_{13}$ (Figure 4.14 (a)). This is because oxygen vacancy remains similar, but small amount of NiO can be formed over reduced $K_2Ti_{5.9}Ni_{0.1}O_{13}$ (Figure 4.14 (a)), as compared to that in oxidized $K_2Ti_{5.9}Ni_{0.1}O_{13}$ (Figure 4.14 (c)).

4.2.3 Effect of reaction temperature

The activity of $K_2Ti_{5.9}Ni_{0.1}O_{13}$ was tested at the reaction temperatures of 550, 575, 600, and 625 °C. The results are shown in Figure 4.15.

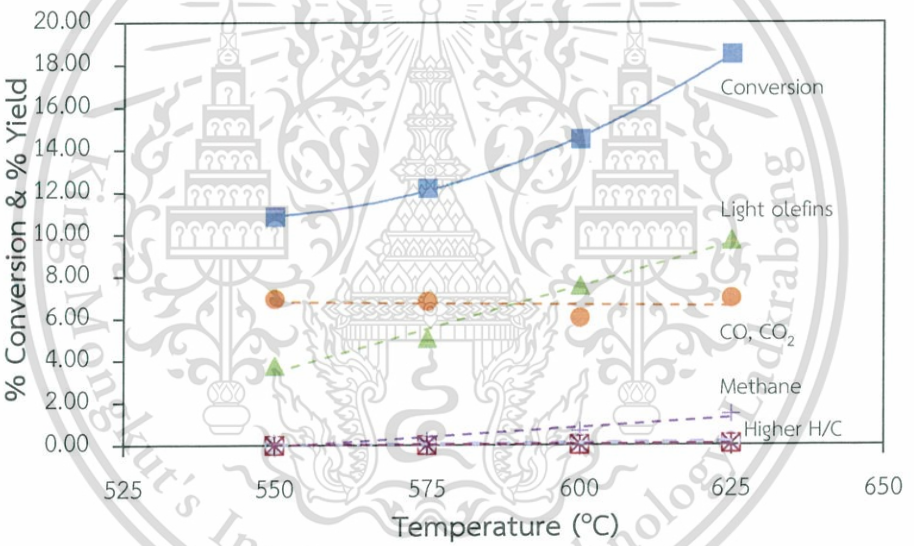

Figure 4.15 Activity of $K_2Ti_{5.9}Ni_{0.1}O_{13}$ catalyst at temperature 550, 575, 600, and 625 °C. *(Reaction condition: T_{react} = 550-625 °C, T_{red} = 400 °C, F = 10:10:40 mL/min (CH_3H_8:Air:N_2), W/F = 23 g·h/mol, atmospheric pressure, Symbol = Conversion(■), Methane (+), Ethane (□), Light olefins (Ethylene, Propylene) (▲), Butane(×), iso-butane (○), $C5^+$ (✳), CO and CO_2 (●))*

The conversion and yield of all products are increased with the reaction temperature. This is because the C-H activation is favored at high reaction temperature. The yield of the combustion gas products is somewhat independent with the temperature.

The higher ethylene and propylene yields were obtained at 625 °C, as compared to the other reaction temperatures. It is suggested that Ni is increasingly dislodged from hexatitanate at 625 °C resulting in a high amount of oxygen vacancy. However, the yield of CO and CO_2 is increased with time on stream at 625 °C as shown in Figure 4.16. This may be because the oxygen vacancy could be decreased with time due to the surface rearrangement at 625 °C. Accordingly, oxidative dehydrogenation activity is decreased (ethylene, propylene), while combustion is promoted with time. Therefore, the reaction temperature at 625 °C is not suitable for the oxidative dehydrogenation of propane over $K_2Ti_{5.9}Ni_{0.1}O_{13}$ further investigation were conducted at 600 °C.

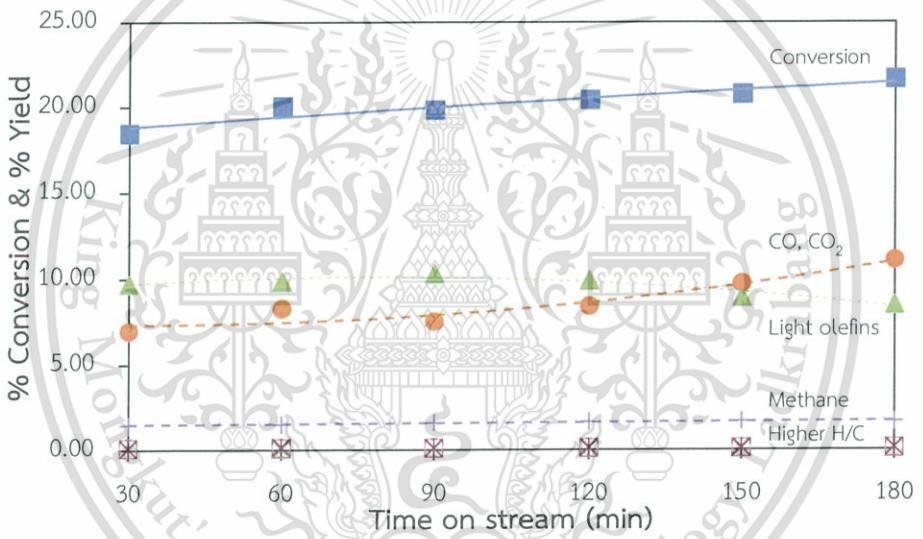

Figure 4.16 Activity of $K_2Ti_{5.9}Ni_{0.1}O_{13}$ catalyst at the reaction temperature of 625 °C. *(Reaction condition: T_{react} = 625 °C, T_{red} = 400 °C, F = 10:10:40 mL/min (C_3H_8:Air:N_2), W/F = 23 g·h/mol, atmospheric pressure, Symbol = Conversion(■), Methane (+), Ethane (□), Light olefins (Ethylene, Propylene) (▲), Butane(×), iso-butane (○), $C5^+$ (✳), CO and CO_2 (●))*

4.2.4 Effect of O_2 concentration in feed

Since oxygen vacancy of hexatitanate framework can be replenished by O_2 gas, as demonstrated in Section 4.1.1 (H_2-TPR). The reducible lattice oxygen was not totally used up but was regenerated to some extent. So, the influence of O_2 concentration during propane conversion was studied.

Figure 4.17 shows that the conversion and yields of all products increased with O_2 concentration in the feed. This result implies that with increasing O_2 concentration, the higher number of active lattice oxygen in $K_2Ti_{5.9}Ni_{0.1}O_{13}$ can be generated via such oxidation with O_2 gas. However, a significantly increased yield of CO, CO_2 at 30% O_2 concentration in feed was obtained. It is suggested that propane and hydrocarbon products can be oxidized with gas phase O_2. Therefore, the suitable concentration of O_2 gas is determined to be 20% for the oxidative dehydrogenation of propane over $K_2Ti_{5.9}Ni_{0.1}O_{13}$.

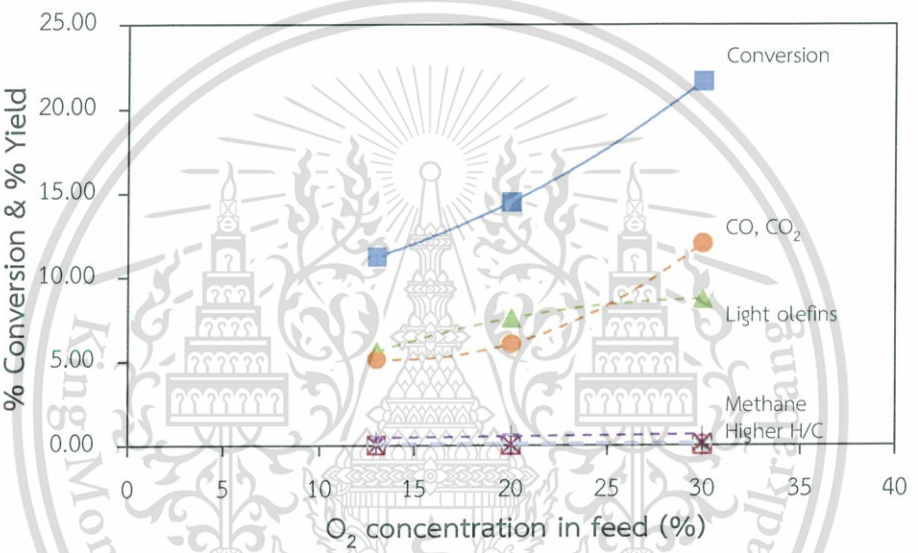

Figure 4.17 Conversion and yield of products over $K_2Ti_{5.9}Ni_{0.1}O_{13}$ catalyst at different O_2 concentrations.

(Reaction condition: T_{react} = 600 °C, T_{red} = 400 °C, F = 10:6.5:43.5, 10:10:40 and 10:16:34 mL/min (C_3H_8:Air:N_2), W/F = 23 g·h/mol, atmospheric pressure, Symbol = Conversion(■), Methane (+), Ethane (□), Light olefins (Ethylene, Propylene) (▲), Butane(×), iso-butane (○), $C5^+$ (✳), CO and CO_2 (●)). Data averaged from the time on stream of 0.5-3.0 h.

4.2.5 Effect of Ni loading

The activity of several $K_2Ti_{6-x}Ni_xO_{13}$ catalysts with various Ni loading (x = 0.05, 0.1, 0.2 and 0.5) for the oxidative dehydrogenation of propane is shown in Table 4.6.

Table 4.6 Activity of the Ni loading $K_2Ti_{6-x}Ni_xO_{13}$ catalysts (x= 0-0.5)

Catalysts	Ni loading (wt.%)[a]	S_{BET} (m^2/g)	Conversion (%)	Yield (%)								Ratio of $C_2=+C_3=/CO+CO_2$[c]
				Methane	Ethane	Ethylene	Propylene	Butane	iso-butane	C_5^+	CO, CO_2	
Ni0.0	-	21	13.8	0.5	0.02	3.4	2.7	0.02	0.1	0.01	7.0	0.9
Ni0.05	0.5	39	13.8	0.6	0.02	2.3	4.4	0.1	0.1	0.02	6.3	1.1
Ni0.1	1.0	35	14.6	0.7	0.02	2.3	5.3	0.1	0.1	0.04	6.0	1.3
Ni0.2	1.3	24	13.7	0.6	0.02	1.8	5.1	0.1	0.1	0.02	6.0	1.2
Ni0.5[b]	5.3	34	30.0	0.4	0.1	0.01	0.4	0.02	0.00	0.00	29.0	0.01

All data were averaged from the time on stream of 0.5-3.0 h.

[a] Determined by XRF

[b] The data is collected at initial point 0.5 h.

[c] yield of ethylene+propylene/CO and CO_2

(Reaction condition: T_{react} = 600 °C, T_{red} = 400 °C and 700 °C (Ni0.0), F = 10:10:40 mL/min (C_3H_8:Air:N_2), W/F = 23 g·h/mol, atmospheric pressure)

The conversion of propane are similar over for x = 0.05-0.2. However, a relatively higher conversion was observed for x = 0.5. It can also be seen that the significant yields of CO and CO_2 were obtained over x = 0.5. This is because the Ni0.5 catalyst contains a separated NiO phase, as evidenced by XRD (Figure 4.8). NiO can readily oxidize propane and hydrocarbon products to CO and CO_2. Meanwhile, Ni0.05, Ni0.1 and Ni0.2 produced light olefins containing ethylene and propylene as major products. This result can be explained by the reducible lattice oxygen formed by dislodgement of Ni after reduction, which is capable of C-H activation, as discussed earlier. However, the yield of light olefins containing ethylene and propylene over Ni0.2 is lower than that over Ni0.1. It is suggested that Ni0.2 possessed trace of NiO as impurity phase, and again this is evidenced by XRD (Figure 4.8). Accordingly, Ni0.1 contains appropriate Ni content that optimized the yield of the desirable products (ethylene and propylene) while minimizing CO and CO_2.

4.2.6 Effect of reduction temperature

Reduction is beneficial in the catalytic oxidative dehydrogenation of propane over $K_2Ti_{6-x}Ni_xO_{13}$-based catalysts, since it readily dislodges Ni from the framework and thereby generates the oxygen vacancy. So, it is interesting to comparatively study the effect of the reduction temperatures (400 and 700 °C) with respect to the non-reduced catalyst. Results are shown in Figure 4.18.

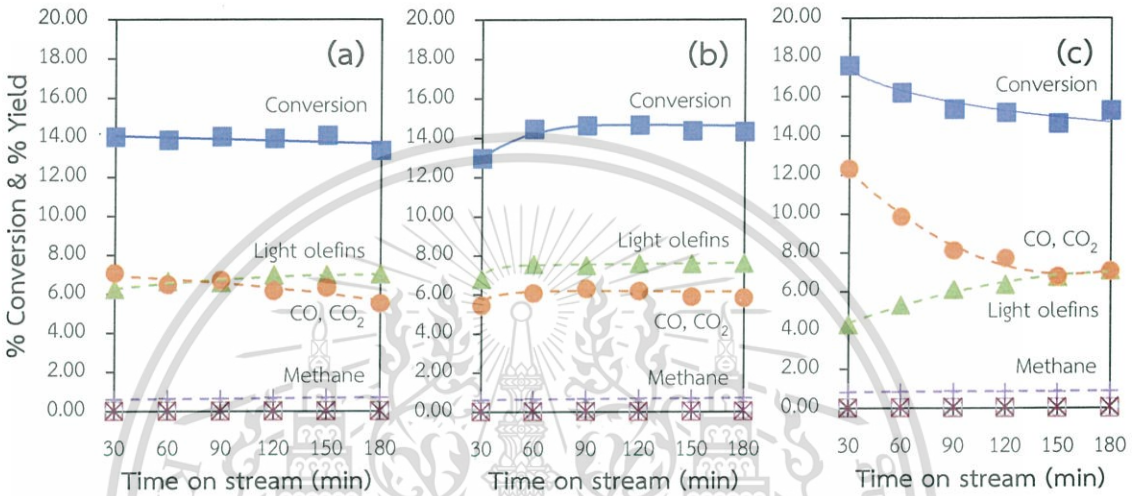

Figure 4.18 The catalytic activity of $K_2Ti_{5.9}Ni_{0.1}O_{13}$ catalyst varied reduction temperature: non-reduced (a), 400 °C (b), and 700 °C (c).

(Reaction condition: T_{react} = 600 °C, T_{red} = non-reduced, 400 and 700 °C, F = 10:10:40 mL/min (C_3H_8:Air:N_2), W/F = 23 g·h/mol, atmospheric pressure, Symbol = Conversion(■), Methane (+), Ethane (□), Light olefins (Ethylene, Propylene) (▲), Butane(×), iso-butane (○), $C5^+$ (✳), CO and CO_2(●))

Although the conversion of propane are similar, the combined yield of light olefins containing ethylene and propylene is slightly higher for the catalyst reduced at 400 °C, as compared to the non-reduced one. In addition, the reduction at 400 °C is beneficial since a decrease in yields of CO and CO_2 was obtained. The conversion for the catalyst reduced at 700 °C is increased due to the increase oxygen vacancy as shown in Figure 4.19. However, over-reduction at 700 °C results in a drop of the yield of light olefins. Moreover, the yields of CO and CO_2 from this catalyst is relatively high, as compared to those from the other two catalysts. It is suggested that the dislodged Ni that is increasing at reduction temperature (i.e, 700 °C), promoted total oxidation of propane and hydrocarbon products. Moreover, NiO can be reduced by hydrocarbon

products to metallic Ni that is also sintering as mentioned in Figure 4.14. Hence, the yields of CO and CO_2 are decreased with time on stream due to the reduction of NiO to metallic Ni. One may argue that the ESR intensity of $K_2Ti_{5.9}Ni_{0.1}O_{13}$ is gradually increased with reduction temperature (Figure 4.19), suggesting the higher oxygen vacancy sites at 700 °C, compared to 400 °C. Nevertheless, the increased proportion of NiO higher than that compensated for the increased oxygen vacancy would lead to deep oxidation to the undesirable CO and CO_2.

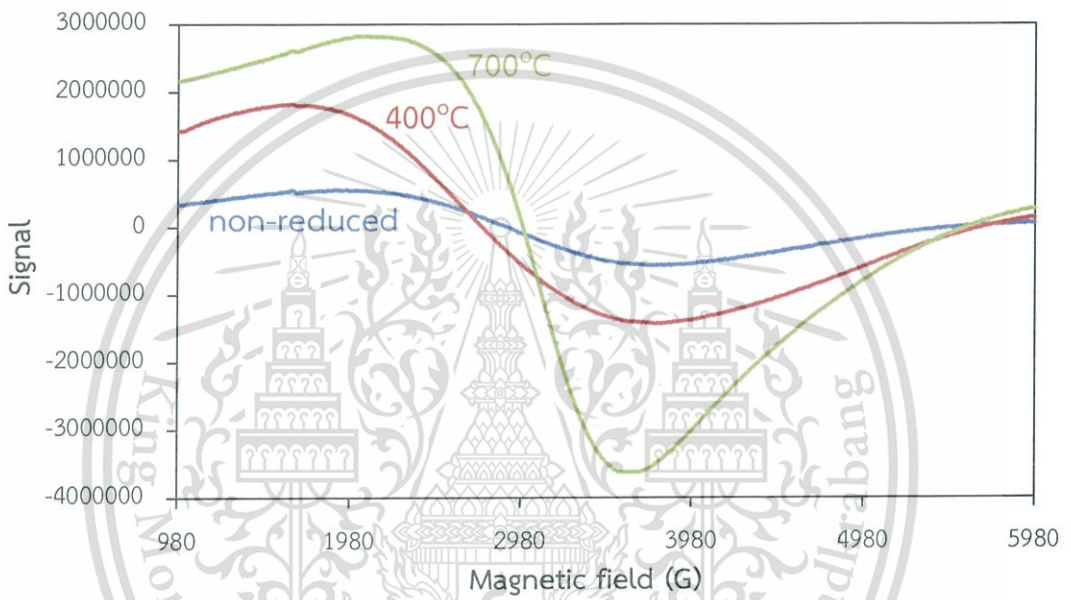

Figure 4.19 The ESR spectra of $K_2Ti_{5.9}Ni_{0.1}O_{13}$ non-reduced (—), or reduced at 400 °C (—) and 700 °C (—).

4.2.7 Effect of contact time

The effect of contact time is summarized in Figure 4.20. When contact time is increased, the conversion is increased, and reaches a plateau after contact time 23 g.h/mol presumably due to limits by O_2 partial pressure in the feed stream. The yields of all products increased with contact time. In all cases, light olefins containing ethylene and propylene are the major products.

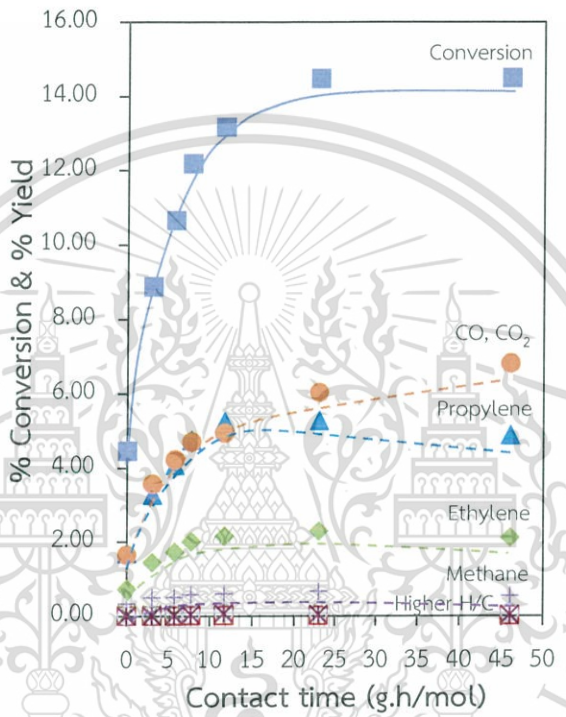

Figure 4.20 Contact time profile over the $K_2Ti_{5.9}Ni_{0.1}O_{13}$ catalyst.

(Reaction condition: T_{react} = 600 °C, T_{red} = 400 °C, F = 10:10:40 mL/min (C_3H_8:Air:N_2), W/F = 3.1, 5.8, 7.8, 11.5, 23 and 46 g·h/mol, atmospheric pressure, Symbol = Conversion(■), Methane (+), Ethane (□), Ethylene(◆), Propylene(▲), Butane(×), iso-butane (○), $C5^+$ (✳), CO and CO_2(●))

It is suggested that propylene can be produced via C-H activation forming propyl radical followed by oxidative dehydrogenation. Methane and ethylene can be also produced via cracking of such propyl radical. Small amount of propyl radical can be also coupled, then cracked to ethane and higher hydrocarbons (butane, iso-butane and C_5^+), as shown in Scheme 4.4. CO and CO_2 are observed initially with significant yield and increased substantially at higher contact time. This indicated that produced in parallel via the oxidation of propane over the NiO phase. Nevertheless, the yields

of light olefins containing ethylene and propylene are decreased while those of CO and CO_2 are increased at the contact time higher than 23 g.h/mol. It is suggested that hydrocarbon products (ethylene and propylene) are further oxidized to CO and CO_2. This indicates that the increased in a number of the NiO phase can promote non-desirable oxidation of hydrocarbon to CO and CO_2.

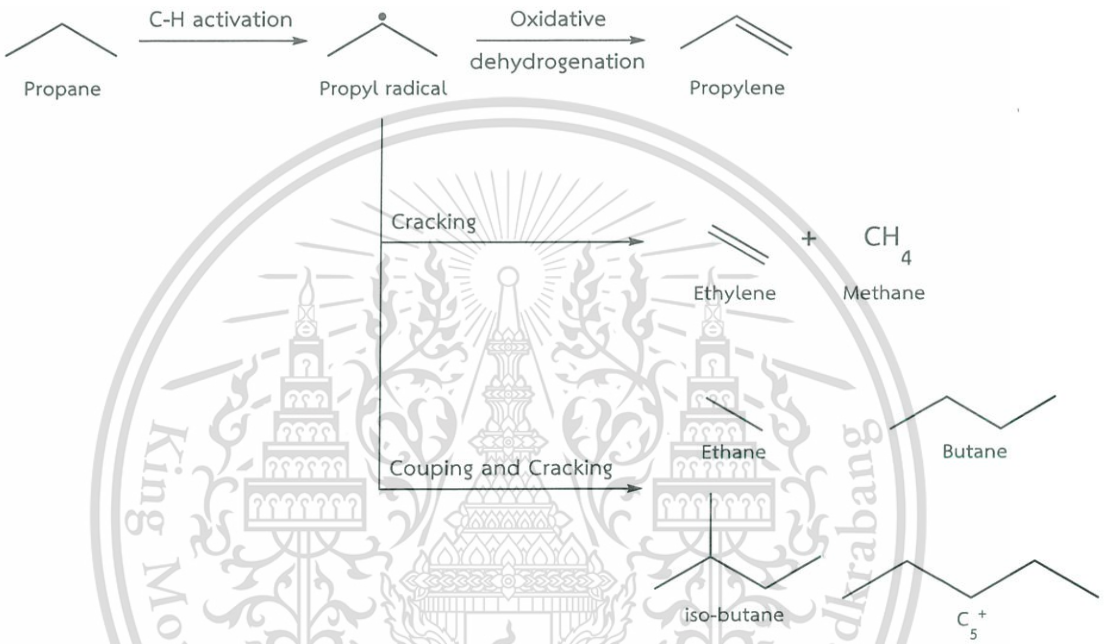

Scheme 4.4

CHAPTER 5
CONCLUSIONS AND SUGGESTIONS

5.1 Conclusions

Oxidative dehydrogenation of propane over potassium hexatitanate-based catalysts was investigated. All catalysts were modified with substitution of Ti ($K_2Ti_{5.9}M_{0.1}O_{13}$) by other metals (M = Mg(II), Co(II), Ni(II), Al(III), Cr(III), Mn(III), and Fe(III)) by solid-state synthesis. For M = Ni the metal content for $K_2Ti_{6-x}Ni_xO_{13}$ (x = 0.05, 0.1, 0.2 and 0.5) is in the range 0.5 - 5.3 wt.%, as evidenced by X-ray fluorescence (XRF). The XRD results confirm the successful incorporation of Co(II), Ni(II), Al(III) and Mn(III)) into the Ti sites of the hexatitanate structure with the inter-tunnel distance expansion, while the incorporation some of metals gave impurity phase (in parenthesis) including $K_2Ti_{5.9}Mg_{0.1}O_{13}$ (MgO), $K_2Ti_{5.9}Cr_{0.1}O_{13}$ (Cr_2O_3 and CrO_3) and $K_2Ti_{5.9}Fe_{0.1}O_{13}$ (Fe_2O_3). The H_2-TPR results show that the potassium hexatitanate-based catalyst can be reduced and the higher oxygen vacancy was generated, particularly for Ni substituted hexatitanate, as also confirmed by ESR results. It is noted that the higher dislodgement of Ni from the framework generated higher oxygen vacancy sites.

The activity of $K_2Ti_6O_{13}$ is higher than TiO_2 (P-25), NiO and CeO_2 because higher oxygen vacancy sites can be generated over $K_2Ti_6O_{13}$ upon reduction. This is likely due to the presence of coordinatively unsaturated sites (cus) of oxygen atoms in $K_2Ti_6O_{13}$ structure with corner-sharing of TiO_6 units. Among metals substituted hexatitanate, $K_2Ti_{5.9}Ni_{0.1}O_{13}$ gives higher ethylene and propylene yields, as compared to other metal substituted (Co, Al and Mn). This is because the structure of $K_2Ti_{5.9}Ni_{0.1}O_{13}$ is relatively unstable leading to the higher number of dislodged Ni from the hexatitanate framework upon reduction. This results in the generation of higher oxygen vacancy sites which can be reoxidized to form reducible lattice oxygen (163 μmol/g), while dislodged Ni is partially oxidized to form NiO phase under the reaction condition. Non-reduced and $K_2Ti_{5.9}Ni_{0.1}O_{13}$ reduced at 400 °C give similar conversion of propane. However, the yields of light olefins containing ethylene and propylene are higher for the catalyst reduced at 400 °C because higher reducible lattice oxygen are obtained from the reduced catalyst. Despite the fact that an even higher conversion was obtained over the catalyst reduced at 700 °C, the combined yield of light olefins

CHAPTER 5
CONCLUSIONS AND SUGGESTIONS

5.1 Conclusions

Oxidative dehydrogenation of propane over potassium hexatitanate-based catalysts was investigated. All catalysts were modified with substitution of Ti ($K_2Ti_{5.9}M_{0.1}O_{13}$) by other metals (M = Mg(II), Co(II), Ni(II), Al(III), Cr(III), Mn(III), and Fe(III)) by solid-state synthesis. For M = Ni the metal content for $K_2Ti_{6-x}Ni_xO_{13}$ (x = 0.05, 0.1, 0.2 and 0.5) is in the range 0.5 - 5.3 wt.%, as evidenced by X-ray fluorescence (XRF). The XRD results confirm the successful incorporation of Co(II), Ni(II), Al(III) and Mn(III)) into the Ti sites of the hexatitanate structure with the inter-tunnel distance expansion, while the incorporation some of metals gave impurity phase (in parenthesis) including $K_2Ti_{5.9}Mg_{0.1}O_{13}$ (MgO), $K_2Ti_{5.9}Cr_{0.1}O_{13}$ (Cr_2O_3 and CrO_3) and $K_2Ti_{5.9}Fe_{0.1}O_{13}$ (Fe_2O_3). The H_2-TPR results show that the potassium hexatitanate-based catalyst can be reduced and the higher oxygen vacancy was generated, particularly for Ni substituted hexatitanate, as also confirmed by ESR results. It is noted that the higher dislodgement of Ni from the framework generated higher oxygen vacancy sites.

The activity of $K_2Ti_6O_{13}$ is higher than TiO_2 (P-25), NiO and CeO_2 because higher oxygen vacancy sites can be generated over $K_2Ti_6O_{13}$ upon reduction. This is likely due to the presence of coordinatively unsaturated sites (cus) of oxygen atoms in $K_2Ti_6O_{13}$ structure with corner-sharing of TiO_6 units. Among metals substituted hexatitanate, $K_2Ti_{5.9}Ni_{0.1}O_{13}$ gives higher ethylene and propylene yields, as compared to other metal substituted (Co, Al and Mn). This is because the structure of $K_2Ti_{5.9}Ni_{0.1}O_{13}$ is relatively unstable leading to the higher number of dislodged Ni from the hexatitanate framework upon reduction. This results in the generation of higher oxygen vacancy sites which can be reoxidized to form reducible lattice oxygen (163 μmol/g), while dislodged Ni is partially oxidized to form NiO phase under the reaction condition. Non-reduced and $K_2Ti_{5.9}Ni_{0.1}O_{13}$ reduced at 400 °C give similar conversion of propane. However, the yields of light olefins containing ethylene and propylene are higher for the catalyst reduced at 400 °C because higher reducible lattice oxygen are obtained from the reduced catalyst. Despite the fact that an even higher conversion was obtained over the catalyst reduced at 700 °C, the combined yield of light olefins

containing ethylene and propylene is lower due to a higher amount of NiO that promoted total oxidation of propane to CO and CO_2. CO, CO_2 are decreased with time on stream due to NiO can be reduced by hydrocarbon products to metallic Ni that can be sintering at high temperature. The yield of the desirable products (ethylene and propylene) with minimal CO and CO_2 was optimized over $K_2Ti_{5.9}Ni_{0.1}O_{13}$. NiO is present in $K_2Ti_{5.8}Ni_{0.2}O_{13}$ and $K_2Ti_{5.5}Ni_{0.5}O_{13}$ as the impurity which gave the high yields of CO and CO_2.

The conversion and yields of all products are increased with temperature, except for CO, CO_2 which remains constant. The higher yields of light olefins containing ethylene and propylene were obtained at 625 °C, but the yield of CO and CO_2 are increased with time on stream at this temperature due to higher amount of NiO. Therefore, the reaction temperature at 600 °C is considered suitable for ethylene and propylene production. The conversion and yields of all products increased with O_2 concentration in the feed. However, the O_2 concentration in feed at 30% provided a significantly increased yield of CO, CO_2 due to further oxidation of propane and hydrocarbon products

It is proposed that the reaction pathway for oxidative dehydrogenation of propane over potassium hexatitanate-based catalysts involves the C-H activation by the reducible lattice oxygen, forming propyl radical followed by oxidative dehydrogenation to propylene. However, parallel reactions include the cracking of propyl radical to methane and ethylene, and the coupling of propyl radicals followed by cracking to ethane and higher hydrocarbons (butane, iso-butane and C_5^+).

5.2 Suggestions

5.2.1 Other synthetic methods (e.g., sol-gel and hydrothermal) or post-treatment such as ball milling to produce a catalyst with a higher surface area could be attempted.

5.2.2 High reduction potential substituted elemental which oxide form suppress the oxidation to CO and CO_2 could generate high oxygen vacancy sites.

References

[1] Szeto, K. C., Loges, B., Merle, N., Popoff, N., Quadrelli, A., Jia, H., Berrier, E.,Mallmann, A. D., Delevoye, L., Gauvin, R. M. and Taoufik, M.. 2013. "Vanadium Oxo Organometallic Species Supported on Silica for the Selective Non-oxidative Dehydrogenation of Propane." *ACS Organo.* 32 : 6452-6460.

[2] Fu, H., Liu, Z.P., Li, Z.H., Wang, W.N. and Fan, K.N. 2006 "Periodic Density Functional Theory Study of Propane Oxidative Dehydrogenation over V_2O_5(001) Surface" *Journal of American Chemical Society*. 128 : 11114-11123.

[3] Carrero, C.A., Schloegl, R., Wachs, I. E. and Schomaecker, R. 2014. "Critical Literature Review of the Kinetics for the Oxidative Dehydrogenation of Propane over Well-Defined Supported Vanadium Oxide Catalysts." *ACS Catal.* 4 : 3357–3380.

[4] Kang, K.H., Kim, T.H., Choi, W.C., Park, Y., Hong, U.G., Park, D.S., Kim, C. and Song, I.K. 2015. "Dehydrogenation of propane to propylene over CrO_y-CeO_2-K_2O/γ-Al_2O_3 catalysts: Effect of cerium content." *Catalysis Communications*. 72 : 68–72.

[5] Zaremba, T. and Witkowska, D. 2010. "Methods of manufacturing of potassium titanate fibres and whiskers. A review." *Materials Science-Poland* 28 : 25-41.

[6] Vikrama, S. V., Phase, D. M. and Chandel, V. S. 2010. "Synthesis, characterization, and electrical studies on Cu-doped $K_2Ti_6O_{13}$ lead-free ceramics: Role of defect associate dipoles." *Journal of Alloys and Compounds*. 489 : 700-707.

[7] Help save nature. 2016. Natural gas. [Online].
Available : https://helpsavenature.com/how-is-propane-fuel-made

[8] EIA. 2017. Hydrocarbon gas liquids from natural gas processing. [Online].
Available : https://www.eia.gov/energyexplained/print.php?page=hgls_where

[9] AFDC. 2018. Propane Fuel Basics. [Online].
Available : https://www.afdc.energy.gov/fuels/propane_basics.html

[10] Mater, S. and Hatch, L. F. Chemistry of petrochemical processes. 2nd ed. Houston: Gulf Publishing Company; 2000

[11] Latent Semantic Analysis at CU Boulder. 2015. Propane. [Online].
Available : http://lsa.colorado.edu/essence/texts/propane.html

[12] EMERSON. 2010. Ethylene production. [Online].
Available : http://www.emerson.com/documents/automation/chemical-sourcebook-chapter-1-2-ethylene-production-polysilicone-production-en-138242.pdf

[13] IHS Markit. 2017. Ethylene. [Online].
Available : https://ihsmarkit.com/products/ethylene-chemical-economics-handbook.html

[14] Transparency Market Research. 2017. Ethylene market. [Online].
Available : https://www.transparencymarketresearch.com/pressrelease/ethylene-market.htm

[15] ICIS. 2007. Ethylene uses and Market data. [Online].
Available : https://www.icis.com/resources/news/2007/11/05/9075777/ethylene-uses-and-market-data/

[16] TH Shubhra, Q., Alam, AKMM., Quaiyyum MA. 2013 "Mechanical properties of polypropylene composites" *Journal of Thermoplastic Composite Materials*. 26

[17] CIEC Promoting Science at the University of York. 2016. Propene. [Online].
Available : http://www.essentialchemicalindustry.org/chemicals/propene.html

[18] Maddah, H.A. 2016 "Polypropylene as a Promising Plastic: A Review" *American Journal of Polymer Science*. 6(1) : 1-11.

[19] Liu, G.,Zhao, Z.J., Wu, T.F., Zeng, L. and Gong, J. 2016. "On the Nature of Active Sites of VO_x/Al_2O_3 Catalysts for Propane Dehydrogenation" *American Chemical Society Catalysis*.

[20] Creative Mechanisms. 2016. Polypropylene. [Online].
Available : https://www.creativemechanisms.com/blog/all-about-polypropylene-pp-plastic

[21] Strumberger, N., Gospocic, A., Bratulic, C. 2005. "Polymeric Materials in Automobiles" *Traffic Engineering*. 17 : 149-160.

[22] Grishanov S. Handbook of Textile and Industrial Dyeing. 1st ed. Woodhead Publishing Series in Textiles; 2011

[23] ICIS. 2007. Acrylonitrile (ACN) Uses and Market Data. [Online].
Available : https://www.icis.com/resources/news/2007/11/01/9074882/acrylonitrile-acn-uses-and-market-data/

[24] KIMPUR. 2017. Polyurethane. [Online].
Available : http://www.kimpur.com/en/content/polyurethane-systems

[25] Pub Chem. 2018. Propylene oxide. [Online]. Available:https://pubchem.ncbi.nlm.nih.gov/compound/Propylene_oxide#section=Top

[26] ICIS. 2007. Propylene Uses and Market Data. [Online]. Available : http://www.icis.com/resources/news/2007/11/06/9076455/propylene-uses-and-market-data/

[27] Chemicals Technology. 2014. Worldwide demand for propylene to rise to 130 million tonnes by 2023. [Online]. Available : https://www.chemicals-technology.com/news/newsworldwide-demand-for-propylene-to-rise-to-130-million-tonnes-by-2023-says-ihs-4356137/

[28] Farjoo, A., Khorasheh, F., Niknaddaf, S., Soltani, M. 2011 "Kinetic modeling of side reactions in propane dehydrogenation over Pt-Sn/γ -Al_2O_3 catalyst" *Scientia Iranica.* 18 : 454-464.

[29] Virginie Marie and Therese Herauville. Catalytic Dehydrogenation of Propane. Norwegian University of Science and Technology; 2012.

[30] Siahvashi, A., Chesterfield, D. and A. Adesina, A. 2013. "Nonoxidative and Oxidative Propane Dehydrogenation over Bimetallic Mo–Ni/Al_2O_3 Catalyst." *Industrial & Engineering Chemistry Research.* 52 : 4017–4026

[31] You, H. 2005 "Kinetics of Propane Oxidative Dehydrogenation to Propylene" *Petroleum Science and Technology.* 23 : 1441-1452.

[32] Mitran, G., Ahmed, R., Irob, E., Hajimirzaee, S., Hodgson, S., Urdă, A., Olea, M., Marcu, I.C. 2018. "Propane oxidative dehydrogenation over VO_x/SBA-15 catalysts" *Catalysis Today*. 306 : 260-267.

[33] Kondratenko,E. V, Cherian, M., Baerns, M. 2005 "Mechanistic aspects of the oxidative dehydrogenation of propane over an alumina-supported $VCrMnWO_x$ mixed oxide catalyst" *Catalysis Today.* 99 : 59-67.

[34] Chen, K. Bell, A.T. and Iglesia, E. 2000. "Kinetics and Mechanism of Oxidative Dehydrogenation of Propane on Vanadium, Molybdenum, and Tungsten Oxides." *The Journal of Physical Chemistry B.* 104 : 1292-1299.

[35] K. Farhadian Azizi, M.-M. Bagheri-Mohagheghi. 2013. "Transition from anatase to rutile phase in titanium dioxide (TiO_2) nanoparticles synthesized by complexing sol–gel process effect of kind of complexing agent and calcinating temperature"*Journal of Sol-Gel Science and Technology.* 65 : 329-335.

[36] Z. Xu and John R. Kitchin. 2015. "Tuning oxide activity through modification of the crystal and electronic structure: from strain to potential polymorphs" *Physical Chemistry Chemical Physics*. 17 : 28943-28949.

[37] Shon, H. K., Phuntsho, S., Okour, Y., Cho, D. L., Kim, J. B., Na, S. and Kim, J. H. 2007 "Visible Light Responsive Titanium Dioxide (TiO_2) – a review" Faculty of Engineering, University of Technology, Sydney.

[38] Xiong,L.B., Li, J.L.,Yang, B. and Yu, Y. 2011 "Ti^{3+} in the Surface of Titanium Dioxide : Generation, Properties and Photocatalytic Application" Journal of Nanomaterials. 2012.

[39] ICIS. 2007. Titanium dioxide Uses and Market Data. [Online]. Available : http://www.icis.com/resources/news/2007/11/07/9076546/titanium-dioxide-tio2-uses-and-market-data/

[40] PROMCHANA, P. 2016 "Mechanistic study on the conversion of fatty acid to long chain olefins over titanate-based catalysts" Master's degree, Faculty of science. King Mongkut's Institute Technology of Ladkrabang.

[41] Liu, C.,He, M.,Lu, X.,Zhang, Q. and Xu, Z. 2005 "Reaction and Crystallization Mechanism of Potassium Dititanate Fibers Synthesized by Low-Temperature Calcination" *Crystal Growth & Design*. 5 : 1395-1404.

[42] Zaremba, 2012. T. "Molten salt synthesis of potassium hexatitanate" Materials Science-Poland. 30 : 180-188.

[43] Yahya, R., Hassan, A. and Aiyub, Z. 2006 "Structural studies of Potassium Hexatitanates prepared under Hydrothermal and Solid State conditions" *Materials Science Forum*. 517 : 222-226.

[44] Transparency market research. Potassium Hexatitanate Market. [Online]. Available : https://www.transparencymarketresearch.com/potassium-hexatitanate-market.html

[45] Wang, B.L., Chen, Q., Wang, R.H., Peng, L.M. 2005 "Synthesis and Characterization of Single-Crystalline Alkali Titanate Nanowires" *Journal of American Chemical Society*. 127 : 11584-11585.

[46] Wang, B.L., Chen, Q., Wang, R.H., Peng, L.M. 2003. "Synthesis and characterization of $K_2Ti_6O_{13}$ nanowires" *Chemical Physics Letters*. 376 : 726-731.

[47] Kapusuz, D., Kalay Y. E., Park, J. and Ozturk, A. 2015. "Synthesis and characterization of hydrothermally grown potassium titanate nanowires" *Journal of Ceramic Processing Research.* 16 : 291-297.

[48] Maneenun, S., Aiemlaor, S., Koomtongdee, S. 2015 "Oxidative dehydrogenation of propane over potassium hexatitanate-based catalysts" Bachelor's degree, Faculty of science. King Mongkut's Institute Technology of Ladkrabang.

[49] Siddiqui, M.A. Chandel, V.S. and Azam, A. 2012. "Comparative study of potassium hexatitanate ($K_2Ti_6O_{13}$) whiskers prepared by sol–gel and solid state reaction routes." *Applied Surface Science.* 258 : 7354–7358.

[50] Jua, W., Chuna, L., Bina, L. and Xiaoqing W. 2009 "Synthesis of potassium hexatitanate whiskers using hydrothermal method" *RARE METALS.* 28 : 24-32.

[51] Li, J., Zhang, Y. C. and Zhang, M. 2012. "Low temperature preparation and optical properties of $K_2Ti_6O_{13}$" *Materials Letters.* 79 : 136–138.

[52] Xu, L. and Cheng, L. 2010. "Environmentally friendly growth of single-crystalline $K_2Ti_6O_{13}$ nanoribbons from KCl flux." *Materials characterization.* 61 : 245–248.

[53] Chaar, M.A.Patel, D. and Kung, H.H. 1988. "Selective oxidative dehydrogenation of propane over V-Mg-O catalysts." *Journal of catalysis.* 109 : 463-267.

[54] Lin, X. Li, G. Huang, C. Weng, W. and Wan, H. 2013. "P-modified cobalt oxide: A novel and effective catalyst for oxidative dehydrogenation of propane." *Chinese Chemical Letters.* 24 : 789–792.

[55] Jibril, B.Y. 2004. "Propane oxidative dehydrogenation over chromium oxide-based catalysts." *Applied Catalysis A: General.* 264 : 193–202.

[56] Stelzer, J.B. Caro, J. and Fait, M. 2005. "Oxidative dehydrogenation of propane on TiO_2 supported antimony oxide/vanadia catalysts." *Catalysis Communications.* 6 : 1–5.

[57] Damien M. Murphy. EPR (Electron Paramagnetic Resonance) Spectroscopy of Polycrystalline Oxide Systems. WILEY-VCH; 2009

[58] Carabineiro, S. AC., Bogdanchikova, N., Pestryakov, A.,Tavares, P. B.,Fernandes, L. SG. and Figueiredo, J. L. 2011 "Gold nanoparticles supported on magnesium oxide for CO oxidation" *Nanoscale Research Letters.* 6:435 : 1-6.

[59] Materials project. CrO_3. [Online].
Available : https://materialsproject.org/materials/mp-510421/#xrd-panel

[60] Zhao, X., Zhuang, Q. C., Xu, S. D., Xu, Y. X. Shi, Y. L. and Zhang, X. X. 2015 "Investigation of Cr_2O_3 as Anode Materials for Lithium-Ion Batteries by Electrochemical Impedance Spectroscopy" *Journal of The Electrochemical Society*. 162 : 1156-1162.

[61] Suresh, S., Karthikeyan, S., Jayamoorthy, K. 2015 "Effect of bulk and nano-Fe_2O_3 particles on peanut plant leaves studied by Fourier transform infrared spectral studies" *Journal of Advanced Research*. 7.

[62] R. D. Shannon. 1976. "Revised Effective Ionic Radii and Systematic Studies of Interatomie Distances in Halides and Chaleogenides" *Acta Crystallographica Section A*. 32 : 751-767.

[63] Wang, Y., Liang, Y., He, Y., Zhang, W. X., Luo, J. W., Lu, J. Q., Luo, M. F. 2016 "Catalysis Behaviors of Cr_2O_3 and CrO_x/Cr_2O_3 Catalysts for Gas Phase Fluorination of 2-Chloro-1,1,1-trtifluoroethane : Active Species and Catalyst Deactivation" Chinese Journal of Inorganic Chemistry. 32 : 1-11.

[64] Yan,H., Zhang, D., Xu, J., Lu, Y., Liu, Y., Qiu, K., Zhang, Y. and Luo, Y. 2014 "Solution growth of NiO nanosheets supported on Ni foam as high-performance electrodes for supercapacitors" *Nanoscale Research Letters*. 9:424.

[65] Kappers, L.A., Gilliam, O.R., Evans, S.M., Halliburton, L.E., Giles, N.C. 2008 "EPR optical study of oxygen and zinc vacancies in electron-irradiated ZnO" Nuclear Instruments and Methods in Physics Research B. 266 : 2953-2957.

[66] Avdeev, V. I., Bedilo, A. F. 2016 "Molecular mechanism of propane oxidative dehydrogenation on surface oxygen radical sites of VO_x/TiO_2 catalysts" *Research on Chemical Intermediates*. 42 : 5237-5252.

[67] Jeneres. 2010. Reduction potential table. [Online].
Available : http://jeneres.blogspot.com/2010/08/reduction-potential-table.html

APPENDICES

APPENDIX A

CHARACTERIZATION

Energy dispersive X-ray spectroscopy (EDX)

Table A1 Elemental analysis of all catalysts

Catalysts	Elemental composition (wt.%) by EDX				Theoretical composition (wt.%)			
	K	Ti	Metal	O	K	Ti	Metal	O
$K_2Ti_6O_{13}$	13.10	44.84	-	42.07	13.63	49.27	-	36.26
$K_2Ti_{5.9}Mg_{0.1}O_{13}$	12.50	46.10	0.28	41.12	13.69	49.47	0.43	36.41
$K_2Ti_{5.9}Al_{0.1}O_{13}$	11.74	42.13	N/A	46.14	13.68	49.45	0.47	36.40
$K_2Ti_{5.9}Cr_{0.1}O_{13}$	12.13	44.82	0.27	42.78	13.62	49.23	0.91	36.24
$K_2Ti_{5.9}Co_{0.1}O_{13}$	12.40	39.34	0.72	47.55	13.61	49.18	1.03	36.19
$K_2Ti_{5.9}Ni_{0.1}O_{13}$	12.73	42.81	0.41	44.05	13.61	49.18	1.02	36.19
$K_2Ti_{5.9}Fe_{0.1}O_{13}$	12.61	46.13	1.02	40.24	13.61	49.20	0.97	36.21
$K_2Ti_{5.9}Mn_{0.1}O_{13}$	12.32	42.72	0.49	41.47	13.62	49.21	0.96	36.22

Temperature-programmed reduction (H_2-TPR)

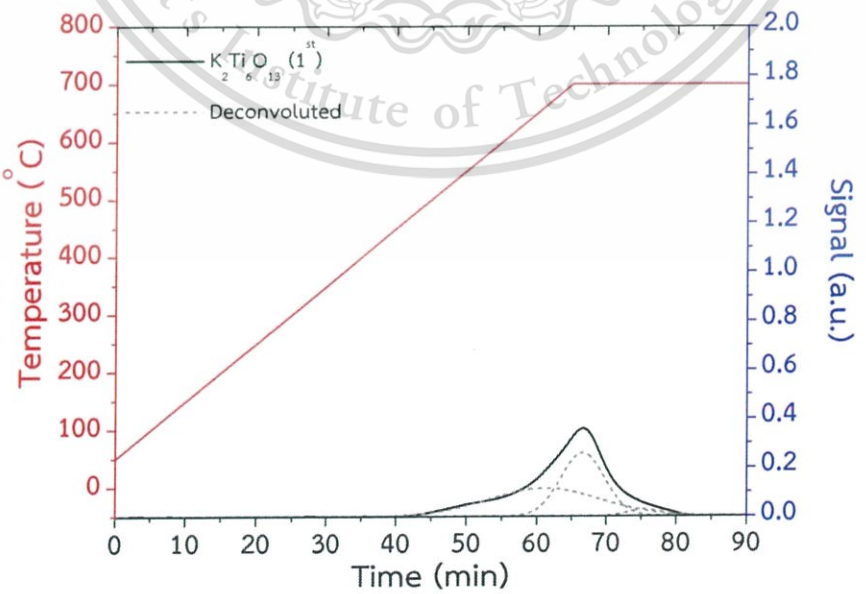

Figure A1 H_2-TPR profile of $K_2Ti_6O_{13}$.

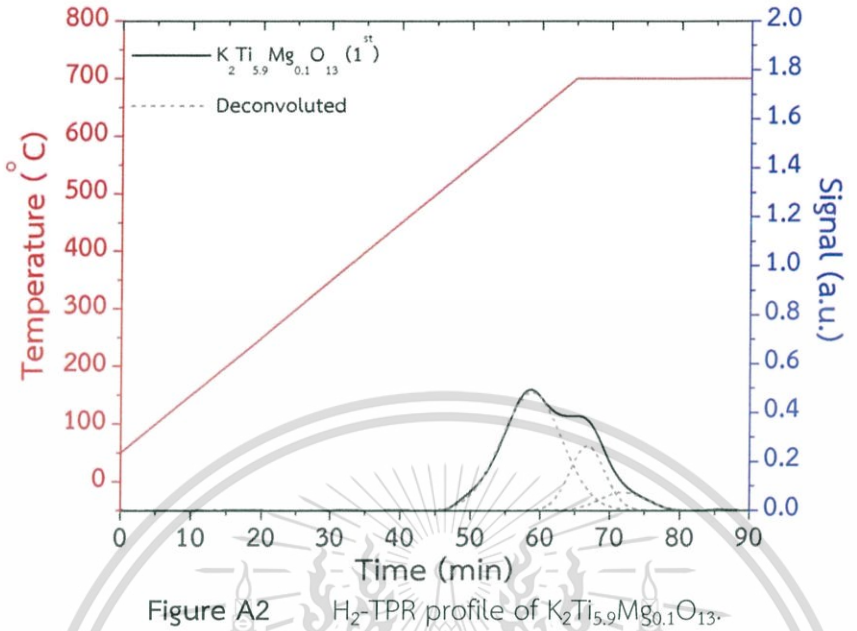

Figure A2 H_2-TPR profile of $K_2Ti_{5.9}Mg_{0.1}O_{13}$.

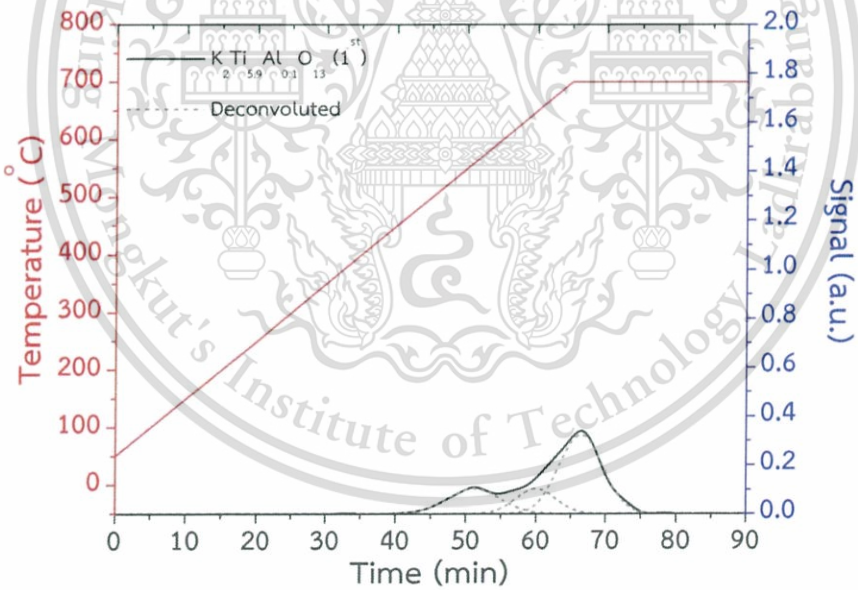

Figure A3 H_2-TPR profile of $K_2Ti_{5.9}Al_{0.1}O_{13}$.

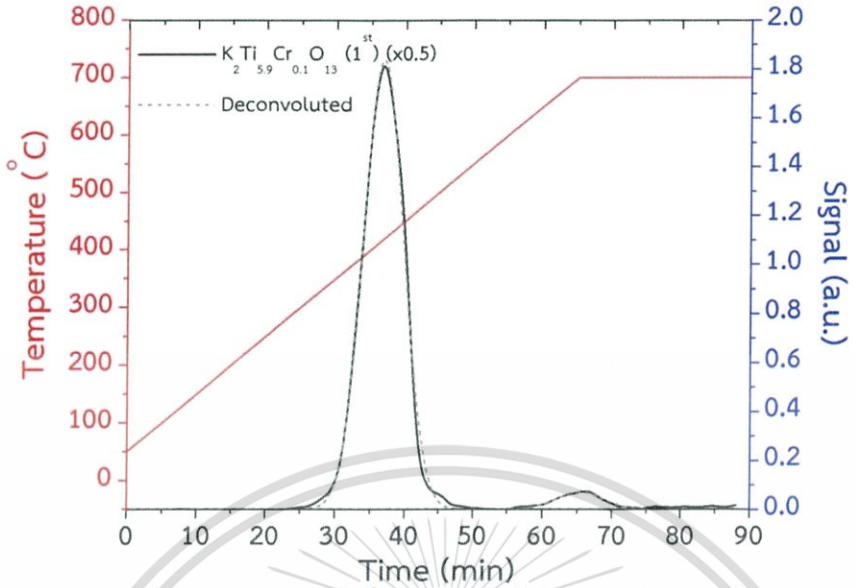

Figure A4 H_2-TPR profile of $K_2Ti_{5.9}Cr_{0.1}O_{13}$.

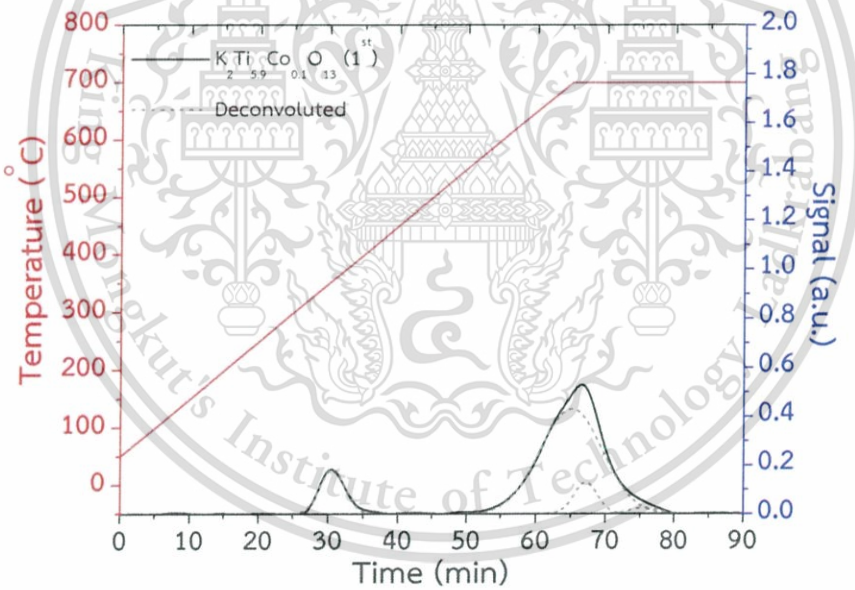

Figure A5 H_2-TPR profile of $K_2Ti_{5.9}Co_{0.1}O_{13}$.

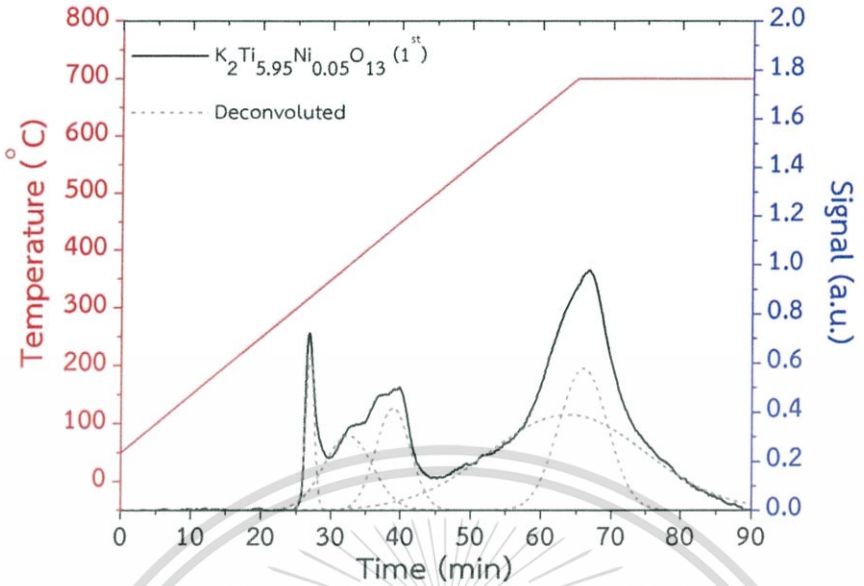

Figure A6 H_2-TPR profile of $K_2Ti_{5.95}Ni_{0.05}O_{13}$.

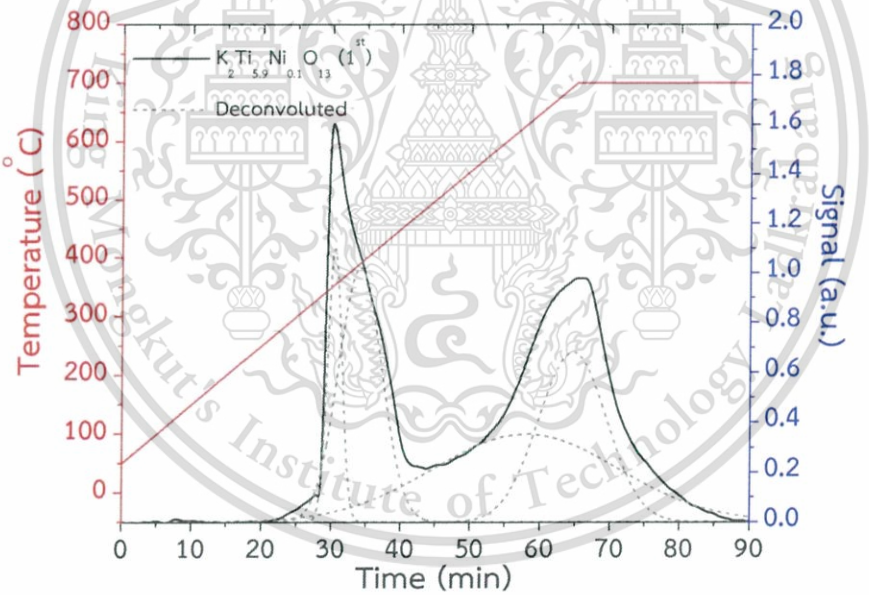

Figure A7 H_2-TPR profile of $K_2Ti_{5.9}Ni_{0.1}O_{13}$.

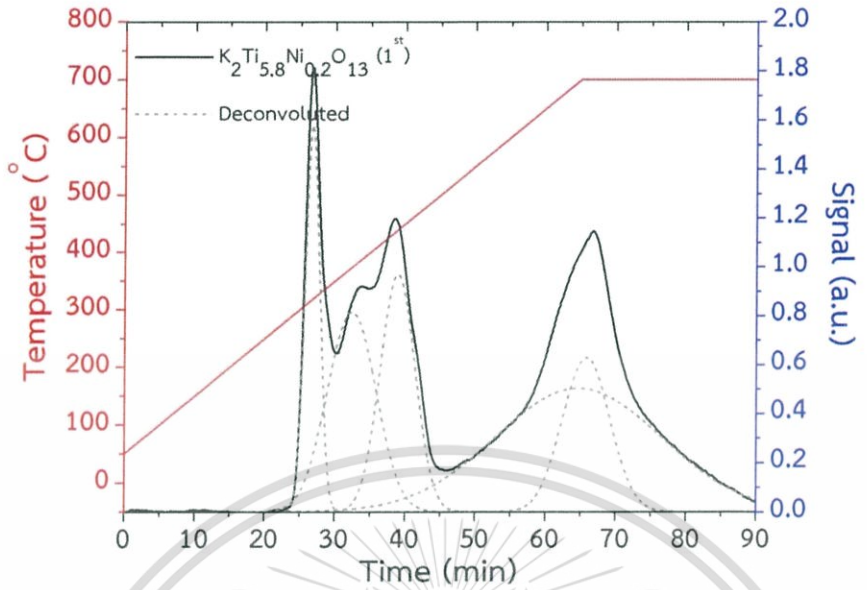

Figure A8 H_2-TPR profile of $K_2Ti_{5.8}Ni_{0.2}O_{13}$.

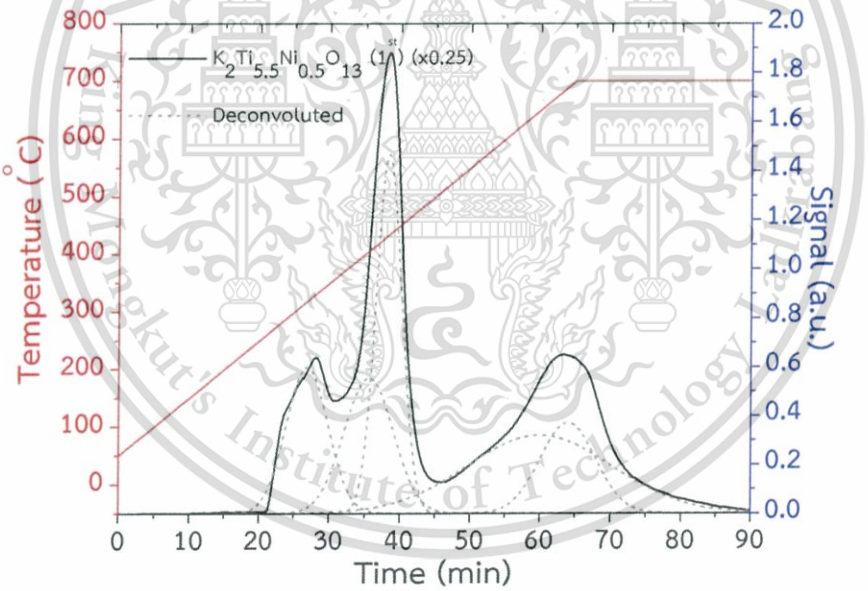

Figure A9 H_2-TPR profile of $K_2Ti_{5.5}Ni_{0.5}O_{13}$.

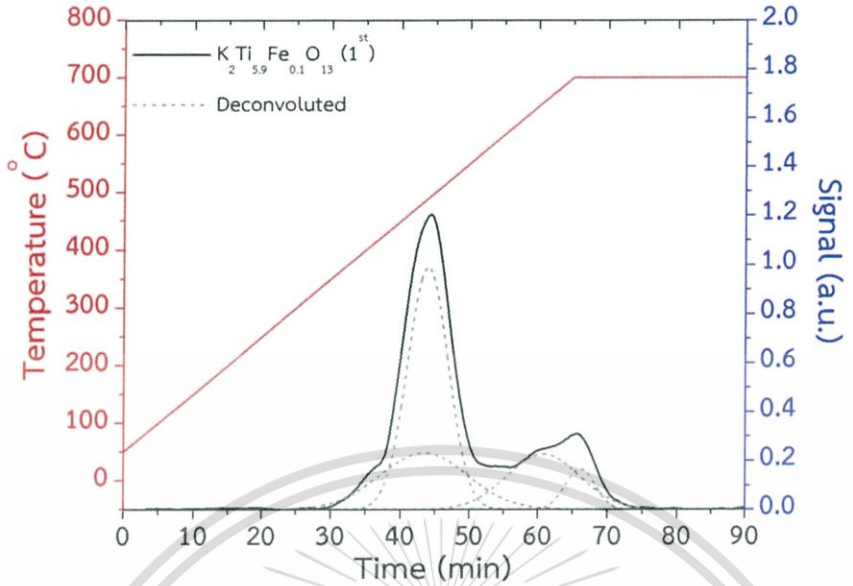

Figure A10 H_2-TPR profile of $K_2Ti_{5.9}Fe_{0.1}O_{13}$.

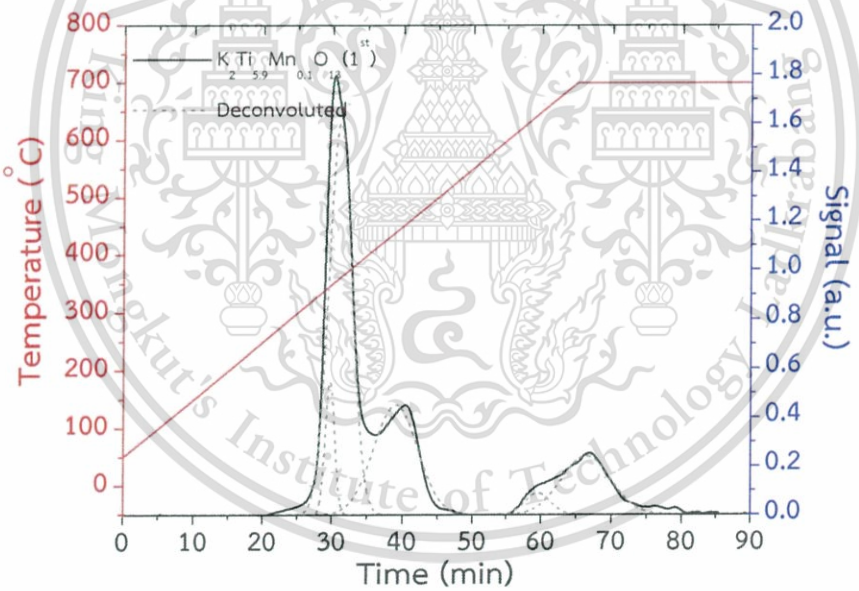

Figure A11 H_2-TPR profile of $K_2Ti_{5.9}Mn_{0.1}O_{13}$.

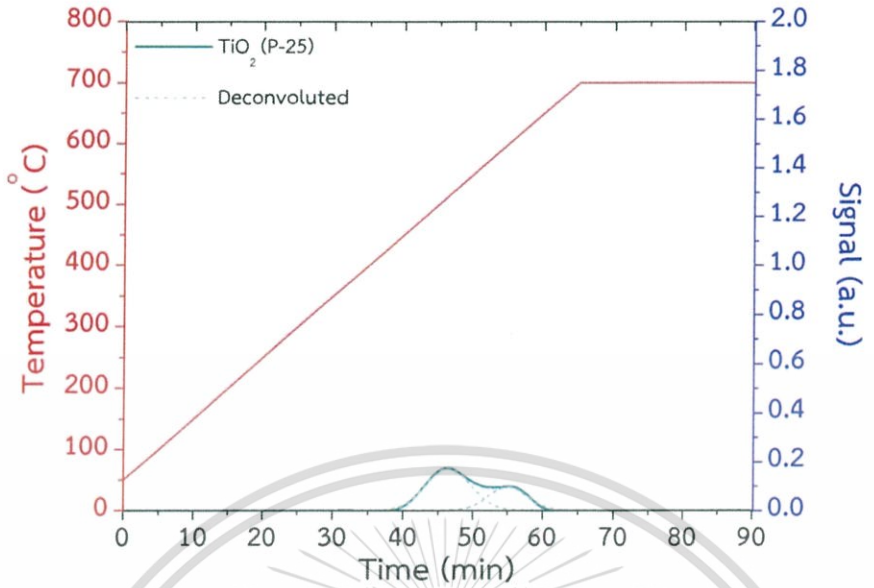

Figure A12 H_2-TPR profile of TiO_2 (P-25).

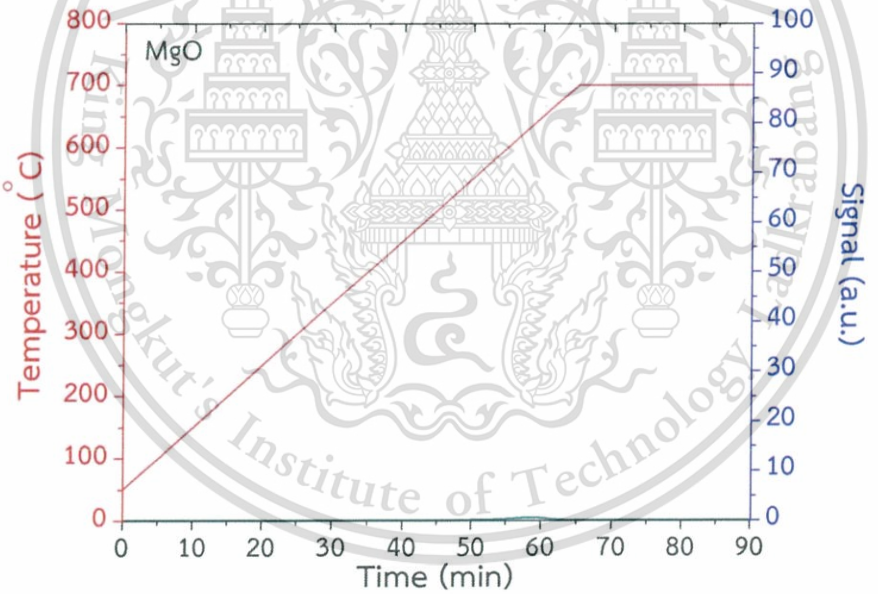

Figure A13 H_2-TPR profile of MgO.

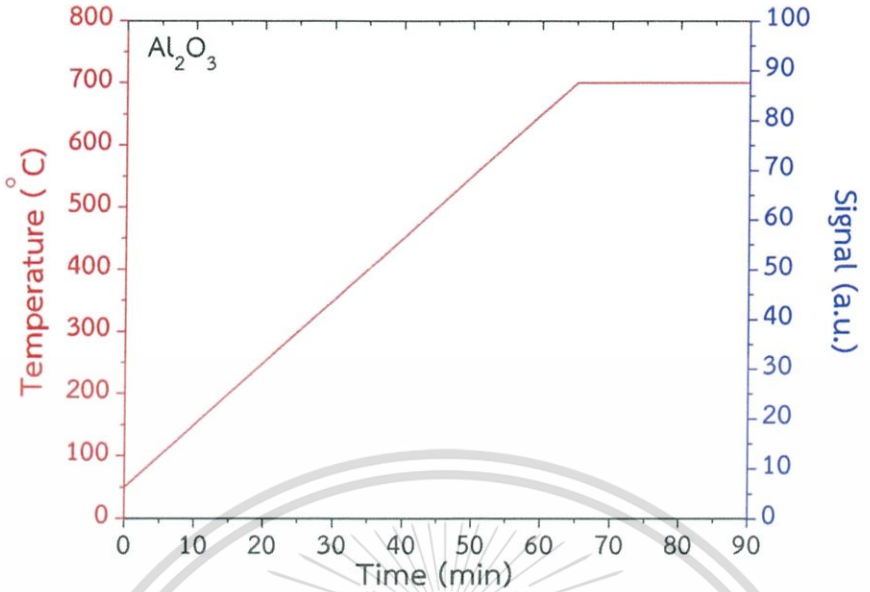

Figure A14 H_2-TPR profile of Al_2O_3.

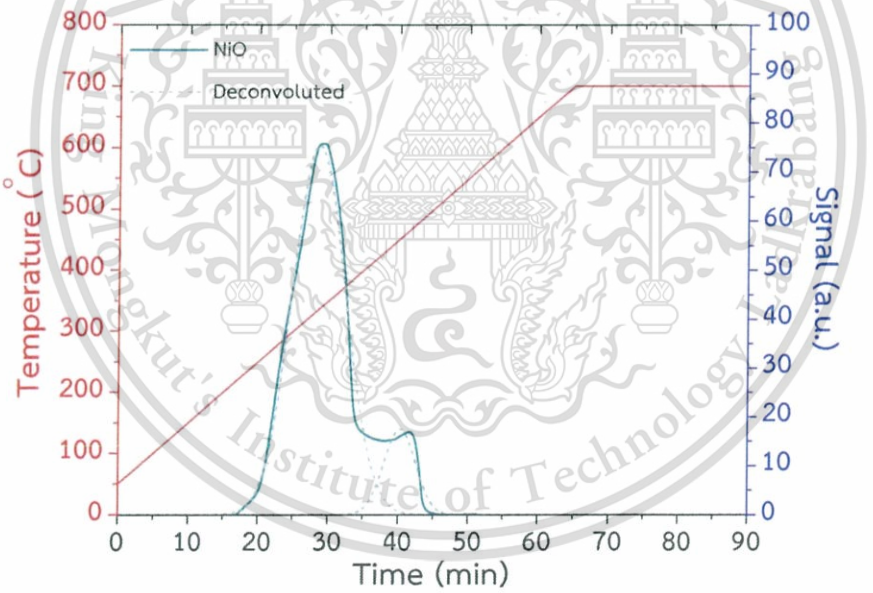

Figure A15 H_2-TPR profile of NiO.

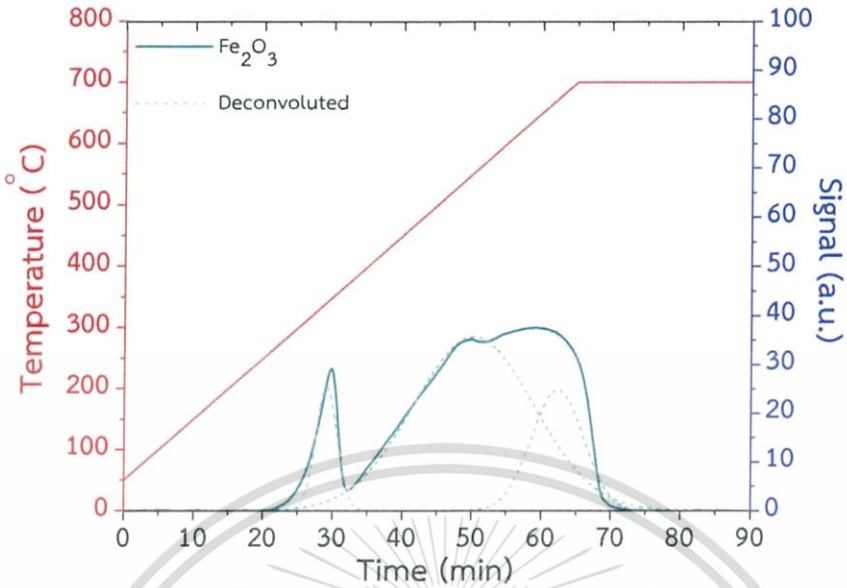

Figure A16 H_2-TPR profile of Fe_2O_3.

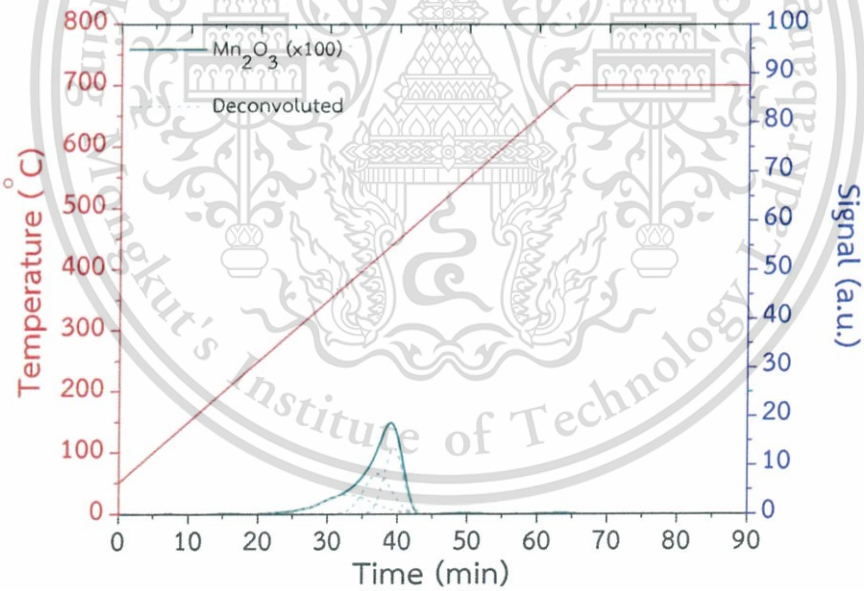

Figure A17 H_2-TPR profile of Mn_2O_3.

Gas adsorption-desorption isotherm

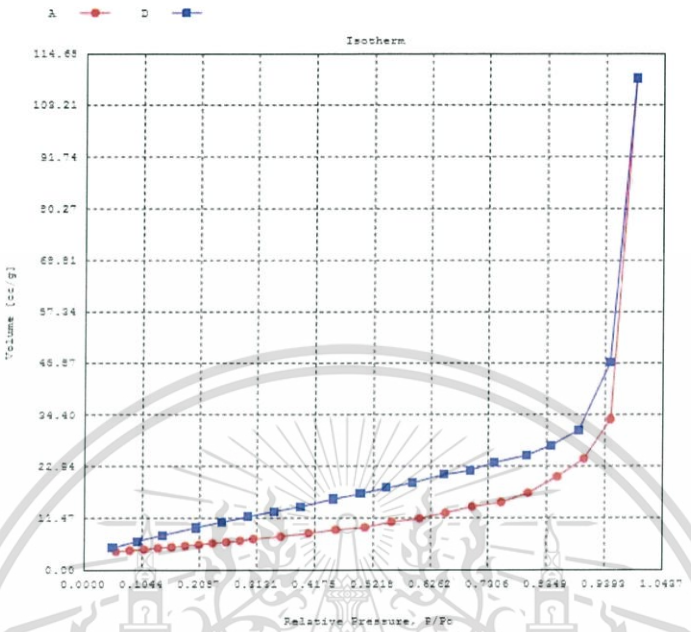

Figure A18 Adsorption-Desorption isotherm of $K_2Ti_6O_{13}$

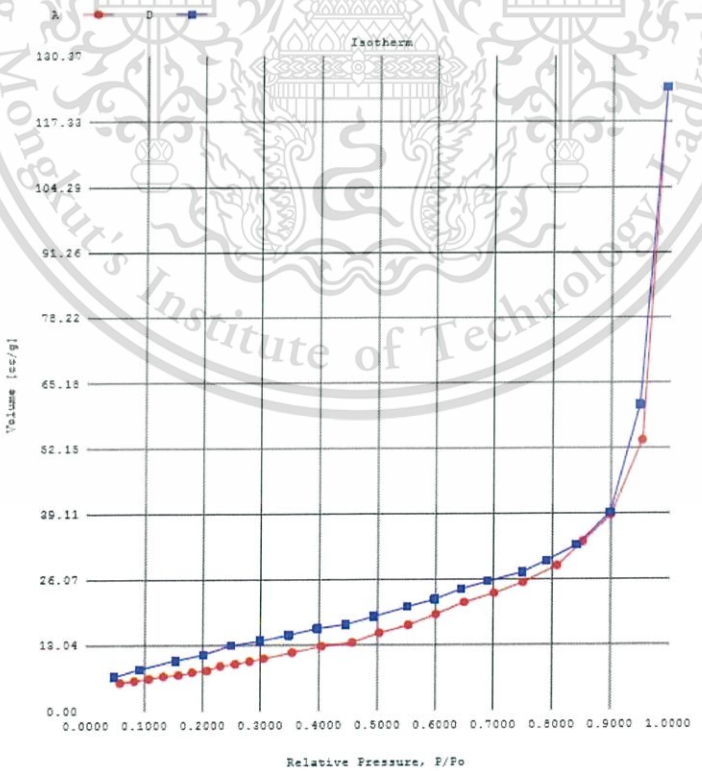

Figure A19 Adsorption-Desorption isotherm of $K_2Ti_{5.9}Mg_{0.1}O_{13}$

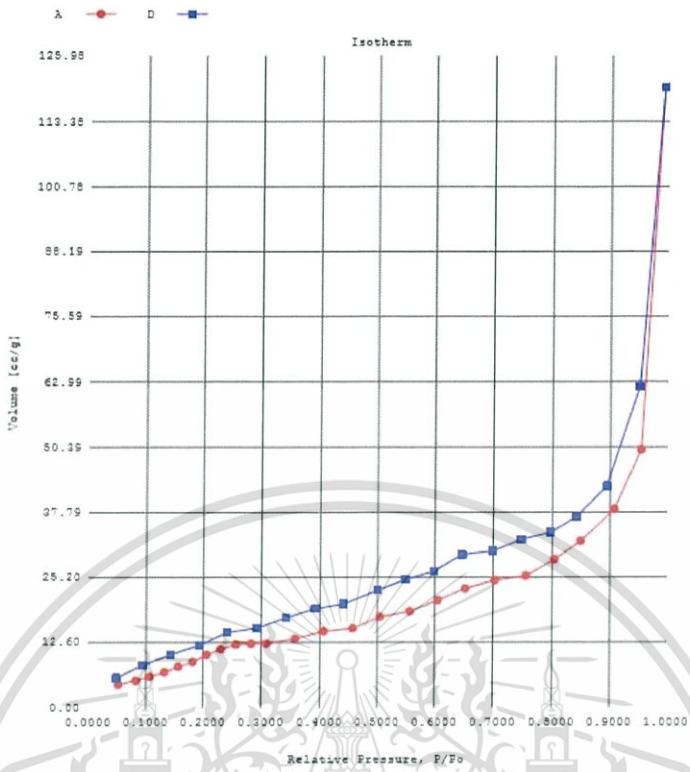

Figure A20 Adsorption-Desorption isotherm of $K_2Ti_{5.9}Al_{0.1}O_{13}$

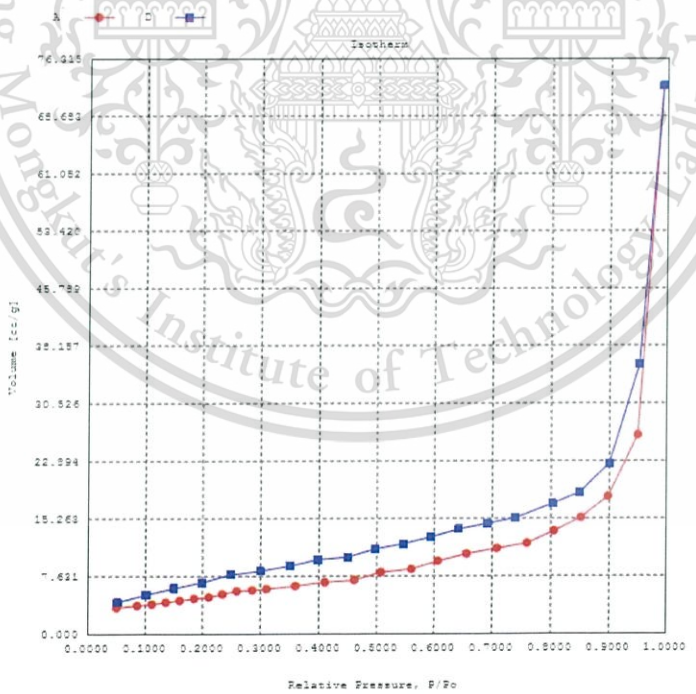

Figure A21 Adsorption-Desorption isotherm of $K_2Ti_{5.9}Cr_{0.1}O_{13}$

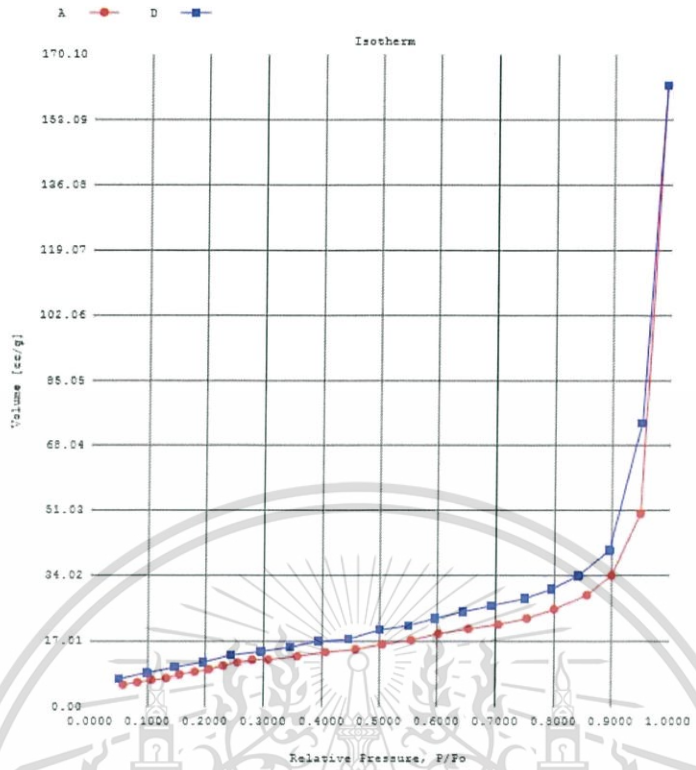

Figure A22 Adsorption-Desorption isotherm of $K_2Ti_{5.9}Co_{0.1}O_{13}$

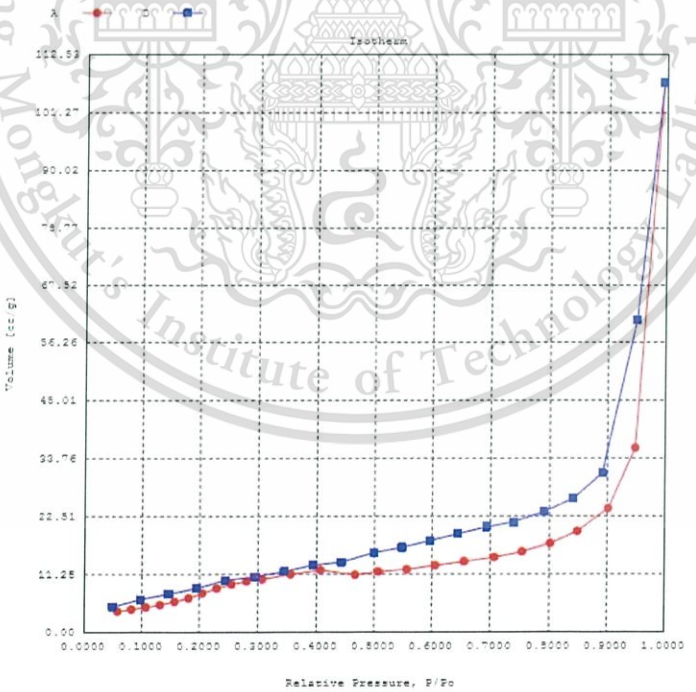

Figure A23 Adsorption-Desorption isotherm of $K_2Ti_{5.95}Ni_{0.05}O_{13}$

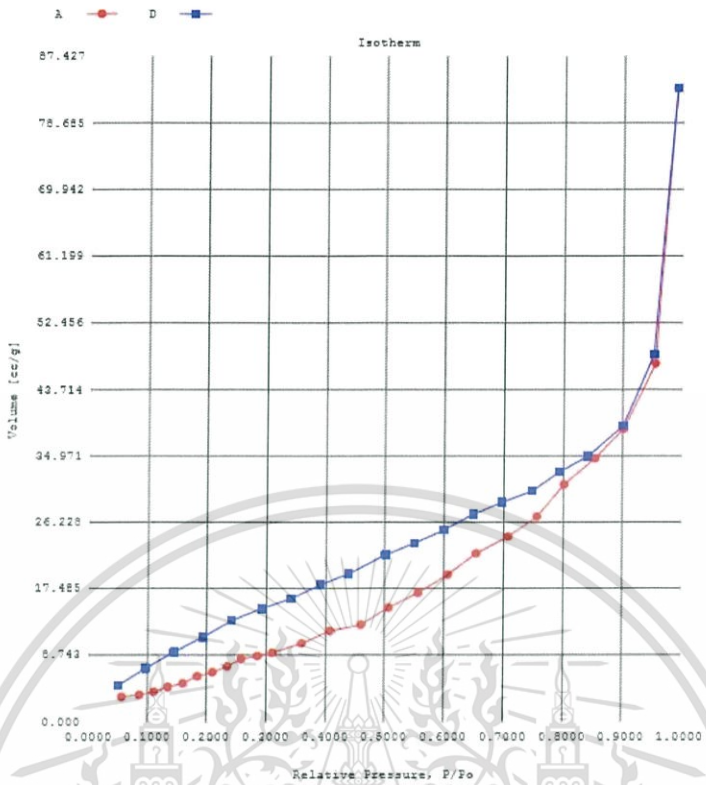

Figure A24 Adsorption-Desorption isotherm of $K_2Ti_{5.9}Ni_{0.1}O_{13}$

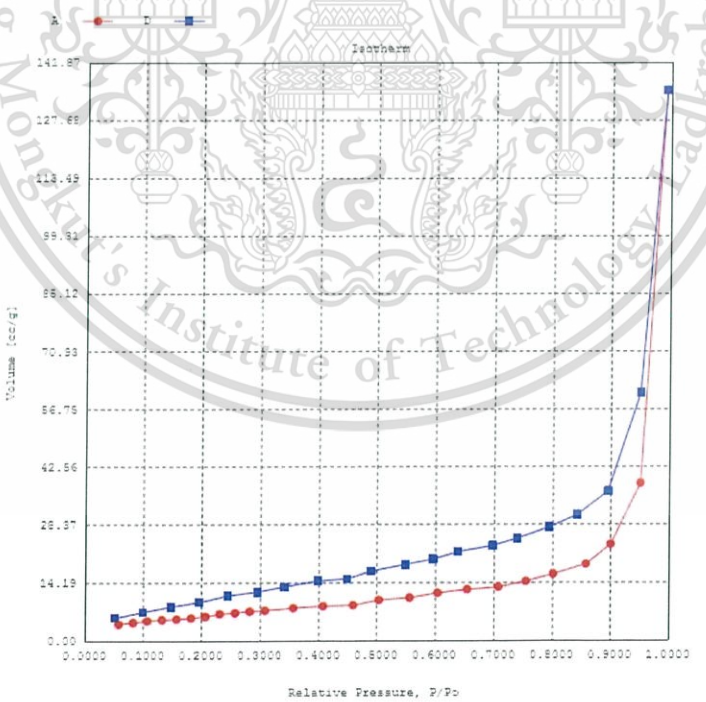

Figure A25 Adsorption-Desorption isotherm of $K_2Ti_{5.8}Ni_{0.2}O_{13}$

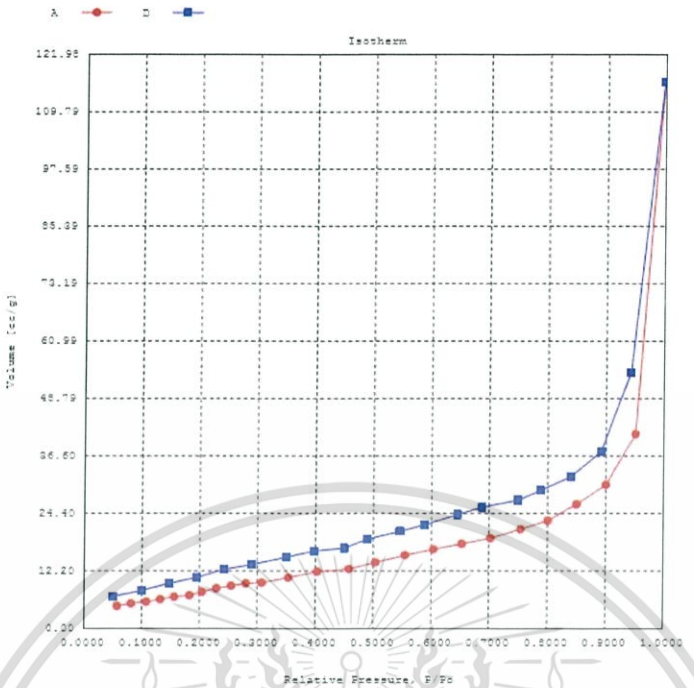

Figure A26 Adsorption-Desorption isotherm of $K_2Ti_{5.5}Ni_{0.5}O_{13}$

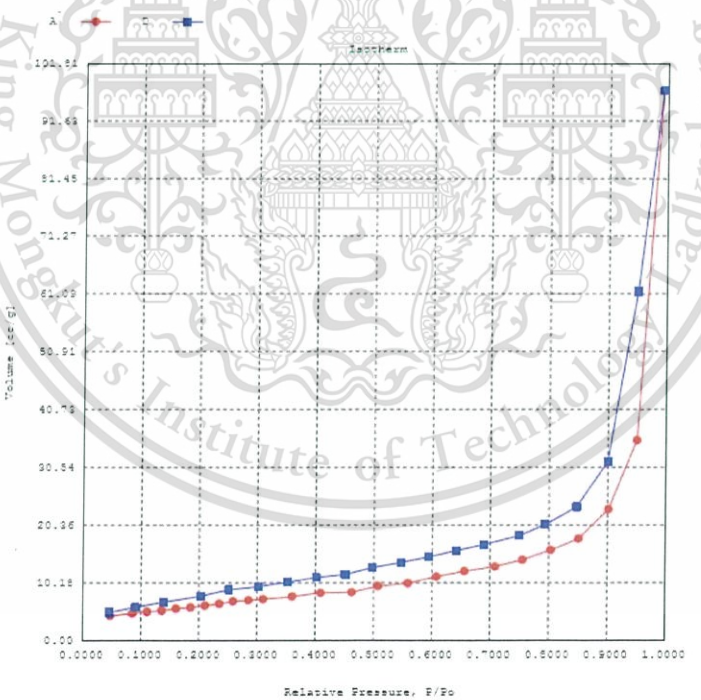

Figure A27 Adsorption-Desorption isotherm of $K_2Ti_{5.9}Fe_{0.1}O_{13}$

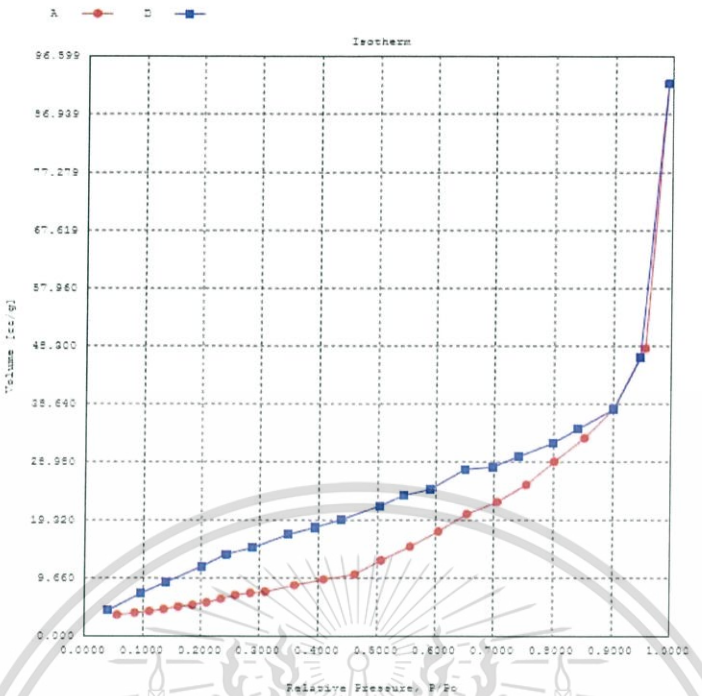

Figure A28 Adsorption-Desorption isotherm of $K_2Ti_{5.9}Mn_{0.1}O_{13}$

X-ray fluorescence (XRF)

Table A2 Elemental analysis of 1% Ni/P-25 catalysts

Ti	Ni	Sum
58.1 %	0.899 %	59 %

Powder X-ray diffraction (XRD)

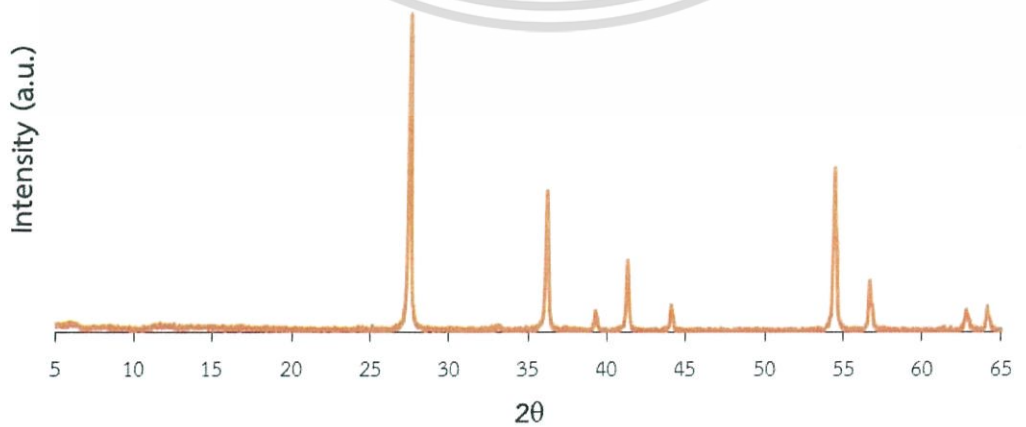

Figure A29 The XRD pattern of 1%Ni/P-25.

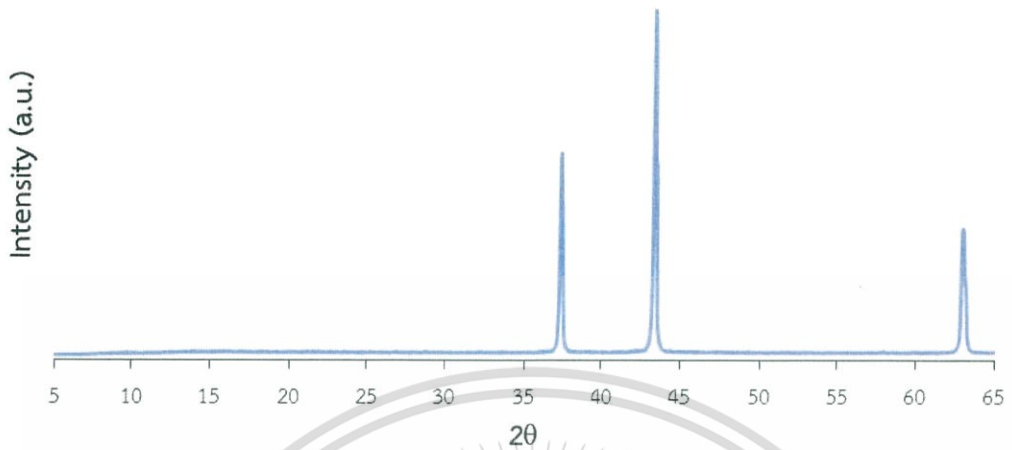

Figure A30 The XRD pattern of NiO.

APPENDIX B

CALCULATION

d-spacing

d-spacing can be determined by Bragg's law equation.

$$n\lambda = 2d \sin\theta$$

$$d = \frac{\lambda}{2 \sin\left(\left(\frac{\pi}{180}\right) \times \frac{2\theta}{2}\right)}$$

Contact time, W/F

$$W/F = \frac{\text{Weight of catalyst (g)}}{\text{Molar feed rate (mol/h)}}$$

In the reaction using 0.0258 mol/h of propane in feed and using 0.6 grams of catalyst, the W/F is calculated as follow:

$$W/F = \frac{0.6\ (g)}{0.0258\ (mol/h)}$$

$$= 23.2558\ g.h/mol$$

In similar manner; W/F of catalysts with different catalyst weight and different feed rate are calculated.

%Metal loading by weight, wt.%

$$wt.\% = \frac{(\text{Molecular weight of metal (g/mol)} \times \text{mol of metal loading (mol)}) \times 100\%}{\text{Molecular weight of catalyst (g/mol)}}$$

For example;

% Metal loading by mol of $K_2Ti_{5.9}Ni_{0.1}O_{13}$ is 0.1 mol loading/unit cell, wt.% is calculated as follow:

$$wt.\% = \frac{(58.69(g/mol) \times 0.1\ (mol)) \times 100\%}{[(39.1 \times 2)g + (47.87 \times 5.9)g + (58.69 \times 0.1)g + (16.00 \times 13)g]}$$

$$= 1.02\ wt.\%$$

Table A1 The summation of the peak area for products

Product	Peak area
Methane	1328.2
Ethane	36.8
Ethylene	4510.1
Propylene	10389.2
Butane	109.5
iso-butane	181.7
C_5^+	80.1
CO, CO_2	11912.3
(Area of propane inlet feed – Total)	
Propane outlet feed	172044.6
Total	188680.2
Propane inlet feed (Blank)	200592.5

* Average data obtained over $K_2Ti_{5.9}Ni_{0.1}O_{13}$, Contact time = 23.2558 g.h/mol, time on stream = 300 minutes, Flow rate of carrier gas: N_2 at 40 mL/min

Calculation of % Conversion

%Conversion can be calculated from the following equation:

$$\%\text{Conversion} = \frac{\text{Area of propane (inlet)} - \text{Area of propane (outlet)}}{\text{Area of propane (inlet)}} \times 100\%$$

For example;

$$\%\text{Conversion} = \frac{(200592.5 - 172044.6)}{200592.5} \times 100\%$$

$$= 14.23\ \%$$

Calculation of the percent yield of each component in a sample can be done as follows:

$$\%\text{Yield in each product} = \frac{\text{Peak area of A}}{\text{Area of propane (inlet)}} \times 100\%$$

For example;

$$\%\text{Yield of Methane} = \frac{1328.2}{200592.5} \times 100\%$$

$$= 0.66\ \%$$

The %yield of each product obtained from above calculation is shown in **Table A2.**

Table A2 Yield of product derived by normalization method

Product	Yield (%)
Methane	0.66
Ethane	0.02
Ethylene	2.25
Propylene	5.18
Butane	0.05
iso-butane	0.09
C_5^+	0.04
CO, CO_2	5.94
Total	14.23

Calculation of %Selectivity

%Selectivity can be obtained from the following equation:

$$\%\text{Selectivity in each product} = \frac{\%\text{Yield of each product}}{\%\text{Conversion}} \times 100\%$$

For example;

$$\%\text{Selectivity of Methane} = \frac{0.66}{14.23} \times 100\%$$

$$= 4.64\ \%$$

APPENDIX C

GAS CHROMATOGRAM

Analysis of gas product from gas chromatography

Prior to analysis, the structure of each products in the sample is identified. Then the quantitative analysis of each product was carried out by GC-FID with the condition in Table C1

Table C1 The GC condition for quantitative analysis

GC-FID	Agilent (6890)
Column	HP-PLOT, 30 m x 0.53 mm x 15 μm
Temperature program	80 °C (3 min hold) to 150 °C (10 min hold) at 10 °C /min
Carrier gas	Nitrogen at 2.8 mL/min (25 cm/sec)
Injection	100 °C
Detector	200 °C

The chromatogram of gas products were identified by comparing the retention time with reference standard as shown in Table C2.

Table C2 Chromatogram data of the product distributions in the standard and also in the feed

Feed or Products	Retention time (min)
Methane	2.58
Ethane	2.78
Ethylene	2.99
Propane	3.56
Propylene	4.84
Butane	5.36
iso-butane	6.82–7.60
C_5^+	> 8.00

APPENDIX D

REACTION DATA

1. Effect of metal oxides

Table D1 Oxidative dehydrogenation of propane over TiO_2 (P-25) catalysts

Time on stream (min)	Conversion (%)	Yield (%)							
		Methane	Ethane	Ethylene	Propylene	Butane	iso-butane	C_5^+	CO, CO_2
30	8.38	0.20	0.01	0.56	1.55	0.01	0.00	0.00	6.05
60	9.35	0.22	0.01	0.62	1.69	0.00	0.00	0.00	6.81
90	8.46	0.21	0.00	0.61	1.68	0.00	0.00	0.00	5.94
120	10.46	0.21	0.00	0.60	1.63	0.00	0.00	0.00	8.01
150	8.03	0.21	0.00	0.58	1.62	0.00	0.00	0.00	5.61
180	9.07	0.23	0.00	0.65	1.79	0.00	0.00	0.00	6.38

(Reaction condition: T_{react} = 600 °C, T_{red} = 700 °C, F = 10:10:40 mL/min (C_3H_8:Air:N_2), W/F = 23 g·h/mol, atmospheric pressure)

Table D2 Oxidative dehydrogenation of propane over CeO_2 catalysts

Time on stream (min)	Conversion (%)	Yield (%)							
		Methane	Ethane	Ethylene	Propylene	Butane	iso-butane	C_5^+	CO, CO_2
30	10.81	0.29	0.01	1.08	1.76	0.01	0.00	0.00	7.66
60	12.58	0.27	0.01	1.06	1.63	0.01	0.00	0.00	9.61
90	9.66	0.27	0.01	1.08	1.61	0.00	0.00	0.00	6.68
120	9.60	0.26	0.01	1.08	1.55	0.00	0.00	0.00	6.69
150	8.44	0.26	0.01	1.08	1.54	0.00	0.00	0.00	5.54
180	8.23	0.27	0.01	1.09	1.53	0.00	0.00	0.00	5.34

(Reaction condition: T_{react} = 600 °C, T_{red} = 700 °C, F = 10:10:40 mL/min (C_3H_8:Air:N_2), W/F = 23 g·h/mol, atmospheric pressure)

Table D3 Oxidative dehydrogenation of propane over NiO catalysts

Time on stream (min)	Conversion (%)	Yield (%)							
		Methane	Ethane	Ethylene	Propylene	Butane	iso-butane	C_5^+	CO, CO_2
30	11.78	0.53	0.02	0.68	1.99	0.00	0.01	0.00	8.54
60	13.02	0.55	0.02	0.58	1.77	0.00	0.01	0.00	10.07
90	14.19	0.56	0.02	0.46	1.52	0.00	0.01	0.00	11.61
120	13.07	0.50	0.01	0.17	0.68	0.00	0.00	0.00	11.68
150	12.80	0.51	0.02	0.12	0.58	0.00	0.00	0.00	11.54
180	12.27	0.51	0.02	0.06	0.42	0.00	0.00	0.00	11.22

(Reaction condition: T_{react} = 600 °C, T_{red} = 700 °C, F = 10:10:40 mL/min (C_3H_8:Air:N_2), W/F = 23 g·h/mol, atmospheric pressure)

Table D4 Oxidative dehydrogenation of propane over $K_2Ti_6O_{13}$ catalysts

Time on stream (min)	Conversion (%)	Yield (%)							
		Methane	Ethane	Ethylene	Propylene	Butane	iso-butane	C_5^+	CO, CO_2
30	13.02	0.54	0.03	3.44	2.49	0.03	0.07	0.01	6.40
60	13.20	0.48	0.02	3.27	2.55	0.02	0.06	0.01	6.76
90	13.37	0.50	0.02	3.48	2.78	0.02	0.07	0.01	6.47
120	14.10	0.48	0.02	3.30	2.67	0.01	0.06	0.01	7.51
150	13.72	0.48	0.02	3.29	2.68	0.01	0.06	0.01	7.12
180	13.53	0.50	0.02	3.46	2.82	0.01	0.06	0.01	6.59

(Reaction condition: T_{react} = 600 °C, T_{red} = 700 °C, F = 10:10:40 mL/min (C_3H_8:Air:N_2), W/F = 23 g·h/mol, atmospheric pressure)

2. Effect of metal cations substituted to Ti(IV)

Table D5 Oxidative dehydrogenation of propane over $K_2Ti_{5.9}Al_{0.1}O_{13}$ catalysts

Time on stream (min)	Conversion (%)	Yield (%)							
		Methane	Ethane	Ethylene	Propylene	Butane	iso-butane	C_5^+	CO, CO_2
30	12.85	0.33	0.01	2.47	2.15	0.05	0.03	0.01	7.81
90	11.27	0.36	0.01	2.59	2.36	0.04	0.03	0.01	5.87
120	13.42	0.34	0.01	2.55	2.32	0.04	0.03	0.01	8.12
150	12.78	0.37	0.01	2.61	2.41	0.01	0.03	0.01	7.30
180	12.27	0.38	0.01	2.66	2.47	0.01	0.03	0.01	6.66

(Reaction condition: T_{react} = 600 °C, T_{red} = 600 °C, F = 10:10:40 mL/min (C_3H_8:Air:N_2), W/F = 23 g·h/mol, atmospheric pressure)

Table D6 Oxidative dehydrogenation of propane over $K_2Ti_{5.9}Ni_{0.1}O_{13}$ catalysts

Time on stream (min)	Conversion (%)	Yield (%)							
		Methane	Ethane	Ethylene	Propylene	Butane	iso-butane	C_5^+	CO, CO_2
30	12.97	0.60	0.02	2.10	4.69	0.04	0.08	0.03	5.42
60	14.46	0.66	0.02	2.26	5.29	0.05	0.09	0.03	6.05
90	14.63	0.66	0.02	2.23	5.25	0.06	0.09	0.03	6.27
120	14.66	0.69	0.02	2.30	5.30	0.05	0.09	0.04	6.15
150	14.37	0.68	0.02	2.29	5.26	0.07	0.09	0.07	5.87
180	14.31	0.69	0.02	2.31	5.29	0.06	0.09	0.05	5.80

(Reaction condition: T_{react} = 600 °C, T_{red} = 400 °C, F = 10:10:40 mL/min (C_3H_8:Air:N_2), W/F = 23 g·h/mol, atmospheric pressure)

Table D7 Oxidative dehydrogenation of propane over $K_2Ti_{5.9}Co_{0.1}O_{13}$ catalysts

Time on stream (min)	Conversion (%)	Yield (%)							
		Methane	Ethane	Ethylene	Propylene	Butane	iso-butane	C_5^+	CO, CO_2
30	16.30	0.45	0.02	2.97	2.07	0.02	0.05	0.02	10.70
60	14.78	0.44	0.02	2.98	2.06	0.01	0.04	0.02	9.20
90	14.20	0.48	0.02	3.14	2.20	0.01	0.05	0.02	8.27
120	15.41	0.46	0.02	3.02	2.12	0.01	0.04	0.02	9.71
150	14.68	0.47	0.02	3.11	2.17	0.01	0.04	0.01	8.84
180	16.33	0.44	0.02	3.10	2.13	0.01	0.04	0.01	10.57

(Reaction condition: T_{react} = 600 °C, T_{red} = 400 °C, F = 10:10:40 mL/min (C_3H_8:Air:N_2), W/F = 23 g·h/mol, atmospheric pressure)

Table D8 Oxidative dehydrogenation of propane over $K_2Ti_{5.9}Mn_{0.1}O_{13}$ catalysts

Time on stream (min)	Conversion (%)	Yield (%)							
		Methane	Ethane	Ethylene	Propylene	Butane	iso-butane	C_5^+	CO, CO_2
30	16.16	0.56	0.11	3.11	2.71	0.06	0.17	0.08	9.34
60	16.67	0.57	0.11	3.12	2.73	0.06	0.14	0.06	9.86
90	16.55	0.60	0.11	3.28	2.86	0.06	0.15	0.06	9.41
120	15.25	0.59	0.10	3.23	2.80	0.05	0.14	0.06	8.26
150	15.90	0.56	0.09	3.20	2.71	0.05	0.14	0.06	9.07
180	15.23	0.61	0.10	3.35	2.88	0.05	0.15	0.06	8.02

(Reaction condition: T_{react} = 600 °C, T_{red} = 500 °C, F = 10:10:40 mL/min (C_3H_8:Air:N_2), W/F = 23 g·h/mol, atmospheric pressure)

Table D9 Oxidative dehydrogenation of propane over 1Ni%/P-25 catalysts

Time on stream (min)	Conversion (%)	Yield (%)							
		Methane	Ethane	Ethylene	Propylene	Butane	iso-butane	C_5^+	CO, CO_2
30	17.05	0.16	0.03	0.09	1.51	0.03	0.01	0.00	15.22
60	14.33	0.17	0.02	0.11	1.54	0.04	0.01	0.00	12.45
90	13.09	0.17	0.02	0.13	1.44	0.04	0.01	0.00	11.28
120	10.69	0.17	0.02	0.13	1.34	0.04	0.01	0.00	8.99
150	10.45	0.17	0.02	0.12	1.22	0.03	0.01	0.00	8.88
180	10.02	0.16	0.01	0.08	1.30	0.03	0.01	0.00	8.42

(Reaction condition: T_{react} = 600 °C, T_{red} = 400 °C, F = 10:10:40 mL/min (C_3H_8:Air:N_2), W/F = 23 g·h/mol, atmospheric pressure)

3. Effect of reaction temperature

Table D10 Oxidative dehydrogenation of propane over $K_2Ti_{5.9}Ni_{0.1}O_{13}$ catalysts at 550 °C

Time on stream (min)	Conversion (%)	Yield (%)							
		Methane	Ethane	Ethylene	Propylene	Butane	iso-butane	C_5^+	CO, CO_2
30	12.20	0.14	0.00	0.87	3.00	0.01	0.02	0.01	8.13
60	11.62	0.13	0.00	0.83	2.98	0.01	0.01	0.00	7.65
90	10.75	0.12	0.00	0.80	2.98	0.01	0.01	0.00	6.82
120	10.23	0.12	0.00	0.79	3.02	0.02	0.01	0.00	6.26
150	11.55	0.11	0.00	0.77	2.98	0.02	0.01	0.00	7.64
180	10.13	0.10	0.00	0.75	2.95	0.02	0.01	0.00	6.27

(Reaction condition: T_{react} = 550 °C, T_{red} = 400 °C, F = 10:10:40 mL/min (C_3H_8:Air:N_2), W/F = 23 g·h/mol, atmospheric pressure)

Table D11 Oxidative dehydrogenation of propane over $K_2Ti_{5.9}Ni_{0.1}O_{13}$ catalysts at 575 °C

Time on stream (min)	Conversion (%)	Yield (%)							
		Methane	Ethane	Ethylene	Propylene	Butane	iso-butane	C_5^+	CO, CO_2
30	10.85	0.24	0.01	1.31	3.81	0.02	0.04	0.02	5.40
60	12.45	0.23	0.01	1.27	3.75	0.02	0.04	0.02	7.12
90	12.71	0.23	0.01	1.28	3.81	0.02	0.04	0.02	7.31
120	12.21	0.23	0.01	1.32	3.80	0.02	0.04	0.02	6.77
150	11.97	0.23	0.01	1.32	3.73	0.02	0.04	0.02	6.60
180	11.61	0.22	0.01	1.29	3.74	0.02	0.04	0.02	6.27

(Reaction condition: T_{react} = 575 °C, T_{red} = 400 °C, F = 10:10:40 mL/min (C_3H_8:Air:N_2), W/F = 23 g·h/mol, atmospheric pressure)

Table D12 Oxidative dehydrogenation of propane over $K_2Ti_{5.9}Ni_{0.1}O_{13}$ catalysts at 625 °C

Time on stream (min)	Conversion (%)	Yield (%)							
		Methane	Ethane	Ethylene	Propylene	Butane	iso-butane	C_5^+	CO, CO_2
30	18.48	1.46	0.08	3.74	5.98	0.05	0.16	0.06	6.96
60	20.06	1.49	0.07	3.80	6.05	0.05	0.16	0.17	8.27
90	19.85	1.60	0.08	4.02	6.28	0.06	0.17	0.12	7.51
120	20.43	1.64	0.08	3.90	6.00	0.07	0.16	0.16	8.41
150	20.77	1.68	0.08	3.53	5.40	0.07	0.13	0.14	9.72
180	21.67	1.67	0.08	3.34	5.13	0.07	0.13	0.14	11.08

(Reaction condition: T_{react} = 625 °C, T_{red} = 400 °C, F = 10:10:40 mL/min (C_3H_8:Air:N_2), W/F = 23 g·h/mol, atmospheric pressure)

4. Effect of O_2 concentration in feed

Table D13 Oxidative dehydrogenation of propane over $K_2Ti_{5.9}Ni_{0.1}O_{13}$ catalysts at 13% O_2 concentration in feed

Time on stream (min)	Conversion (%)	Yield (%)							
		Methane	Ethane	Ethylene	Propylene	Butane	iso-butane	C_5^+	CO, CO_2
30	12.05	0.37	0.02	1.83	3.57	0.03	0.07	0.02	6.14
60	10.72	0.35	0.02	1.88	3.64	0.03	0.07	0.02	4.70
90	10.89	0.31	0.02	1.80	3.53	0.03	0.06	0.02	5.11
120	12.06	0.39	0.02	1.98	3.72	0.04	0.07	0.02	5.81
150	10.83	0.35	0.02	1.91	3.60	0.05	0.06	0.02	4.81
180	11.64	0.42	0.02	2.10	3.74	0.07	0.07	0.02	5.18

(Reaction condition: T_{react} = 600 °C, T_{red} = 400 °C, F = 10:6.5:43.5 mL/min (C_3H_8:Air:N_2), W/F = 23 g·h/mol, atmospheric pressure)

Table D14 Oxidative dehydrogenation of propane over $K_2Ti_{5.9}Ni_{0.1}O_{13}$ catalysts at 30% O_2 concentration in feed

Time on stream (min)	Conversion (%)	Yield (%)							
		Methane	Ethane	Ethylene	Propylene	Butane	iso-butane	C_5^+	CO, CO_2
30	22.91	0.56	0.02	2.90	4.96	0.02	0.11	0.04	14.30
60	22.33	0.58	0.02	2.79	5.73	0.02	0.13	0.11	12.94
90	21.69	0.59	0.02	2.80	5.87	0.02	0.13	0.17	12.07
120	21.93	0.59	0.02	2.80	5.88	0.02	0.13	0.18	12.29
150	20.97	0.61	0.02	2.86	5.91	0.02	0.13	0.18	11.24
180	21.25	0.62	0.02	2.87	5.92	0.03	0.13	0.17	11.49

(Reaction condition: T_{react} = 600 °C, T_{red} = 400 °C, F = 10:6.5:43.5 mL/min (C_3H_8:Air:N_2), W/F = 23 g·h/mol, atmospheric pressure)

5. Effect of Ni loading

Table D15 Oxidative dehydrogenation of propane over $K_2Ti_{5.95}Ni_{0.05}O_{13}$ catalysts

Time on stream (min)	Conversion (%)	Yield (%)							
		Methane	Ethane	Ethylene	Propylene	Butane	iso-butane	C_5^+	CO, CO_2
30	13.52	0.53	0.02	2.07	4.13	0.04	0.07	0.02	6.66
60	13.44	0.54	0.02	2.12	4.27	0.04	0.07	0.02	6.35
90	14.01	0.55	0.02	2.15	4.25	0.06	0.07	0.02	6.88
120	13.86	0.61	0.02	2.31	4.42	0.06	0.08	0.02	6.32
150	13.56	0.61	0.02	2.30	4.40	0.06	0.08	0.02	6.05
180	13.76	0.66	0.02	2.42	4.48	0.06	0.08	0.03	6.01

(Reaction condition: T_{react} = 600 °C, T_{red} = 400 °C, F = 10:10:40 mL/min (C_3H_8:Air:N_2), W/F = 23 g·h/mol, atmospheric pressure)

Table D16 Oxidative dehydrogenation of propane over $K_2Ti_{5.8}Ni_{0.2}O_{13}$ catalysts

Time on stream (min)	Conversion (%)	Yield (%)							
		Methane	Ethane	Ethylene	Propylene	Butane	iso-butane	C_5^+	CO, CO_2
30	28.41	0.37	0.01	1.46	4.35	0.03	0.07	0.02	22.08
60	14.24	0.51	0.02	1.74	4.86	0.04	0.10	0.01	6.96
90	13.81	0.53	0.02	1.80	5.05	0.04	0.10	0.02	6.25
120	13.41	0.59	0.02	1.92	5.24	0.05	0.12	0.02	5.44
150	13.28	0.56	0.02	1.84	5.01	0.06	0.10	0.01	5.65
180	13.21	0.56	0.02	1.87	5.07	0.07	0.10	0.02	5.49

(Reaction condition: T_{react} = 600 °C, T_{red} = 400 °C, F = 10:10:40 mL/min (C_3H_8:Air:N_2), W/F = 23 g·h/mol, atmospheric pressure)

Table D17 Oxidative dehydrogenation of propane over $K_2Ti_{5.5}Ni_{0.5}O_{13}$ catalysts

Time on stream (min)	Conversion (%)	Yield (%)							
		Methane	Ethane	Ethylene	Propylene	Butane	iso-butane	C_5^+	CO, CO_2
30	29.78	0.41	0.01	0.01	0.38	0.02	0.00	0.00	28.95
60	22.55	0.45	0.01	0.02	0.37	0.04	0.00	0.00	21.66
90	19.67	0.52	0.02	0.02	0.33	0.04	0.00	0.00	18.74
120	19.55	0.53	0.02	0.02	0.31	0.03	0.00	0.00	18.63
150	18.86	0.52	0.01	0.02	0.29	0.02	0.00	0.00	18.00
180	18.33	0.55	0.01	0.02	0.29	0.05	0.00	0.00	17.41

(Reaction condition: T_{react} = 600 °C, T_{red} = 400 °C, F = 10:10:40 mL/min (C_3H_8:Air:N_2), W/F = 23 g·h/mol, atmospheric pressure)

6. Effect of reduction temperature

Table D18 Oxidative dehydrogenation of propane over non-reduced $K_2Ti_{5.9}Ni_{0.1}O_{13}$ catalysts

Time on stream (min)	Conversion (%)	Yield (%)							
		Methane	Ethane	Ethylene	Propylene	Butane	iso-butane	C_5^+	CO, CO_2
30	14.03	0.59	0.01	2.56	3.68	0.05	0.06	0.02	7.05
60	13.88	0.65	0.02	2.65	3.97	0.05	0.07	0.02	6.45
90	14.06	0.64	0.02	2.57	4.00	0.05	0.06	0.02	6.68
120	13.96	0.70	0.02	2.73	4.22	0.05	0.07	0.02	6.14
150	14.12	0.69	0.02	2.71	4.24	0.05	0.07	0.02	6.30
180	13.35	0.70	0.02	2.71	4.29	0.05	0.07	0.02	5.49

(Reaction condition: T_{react} = 600 °C, T_{red} = - °C, F = 10:10:40 mL/min (C_3H_8:Air:N_2), W/F = 23 g·h/mol, atmospheric pressure)

Table D19 Oxidative dehydrogenation of propane over reduced (700 °C) $K_2Ti_{5.9}Ni_{0.1}O_{13}$ catalysts

Time on stream (min)	Conversion (%)	Yield (%)							
		Methane	Ethane	Ethylene	Propylene	Butane	iso-butane	C_5^+	CO, CO_2
30	17.58	0.82	0.03	1.58	2.73	0.04	0.05	0.00	12.32
60	16.19	0.85	0.03	1.85	3.44	0.04	0.06	0.06	9.85
90	15.36	0.89	0.03	2.13	3.98	0.04	0.08	0.10	8.11
120	15.18	0.86	0.03	2.19	4.17	0.04	0.08	0.10	7.71
150	14.64	0.86	0.03	2.31	4.44	0.04	0.09	0.10	6.77
180	15.30	0.88	0.03	2.43	4.65	0.04	0.09	0.12	7.05

(Reaction condition: T_{react} = 600 °C, T_{red} = 700 °C, F = 10:10:40 mL/min (C_3H_8:Air:N_2), W/F = 23 g·h/mol, atmospheric pressure)

7. Effect of contact time

Table D20 Oxidative dehydrogenation of propane over $K_2Ti_{5.9}Ni_{0.1}O_{13}$ catalysts at contact time 3.1 g.h/mol

Time on stream (min)	Conversion (%)	Yield (%)							
		Methane	Ethane	Ethylene	Propylene	Butane	iso-butane	C_5^+	CO, CO_2
30	10.21	0.40	0.01	1.26	3.22	0.02	0.02	0.00	5.28
60	9.10	0.50	0.01	1.47	3.44	0.05	0.03	0.00	3.59
90	8.71	0.48	0.01	1.41	3.27	0.04	0.03	0.00	3.46
120	9.29	0.48	0.01	1.38	3.15	0.05	0.03	0.00	4.19
150	8.53	0.52	0.01	1.48	3.28	0.05	0.03	0.00	3.13
180	8.74	0.51	0.01	1.45	3.22	0.05	0.03	0.00	3.47

(Reaction condition: T_{react} = 600 °C, T_{red} = 400 °C, F = 10:10:40 mL/min (C_3H_8:Air:N_2), W/F = 23 g·h/mol, atmospheric pressure)

Table D21 Oxidative dehydrogenation of propane over $K_2Ti_{5.9}Ni_{0.1}O_{13}$ catalysts at contact time 5.8 g.h/mol

Time on stream (min)	Conversion (%)	Yield (%)							
		Methane	Ethane	Ethylene	Propylene	Butane	iso-butane	C_5^+	CO, CO_2
30	7.06	0.48	0.01	1.66	3.92	0.04	0.04	0.01	0.88
60	12.33	0.46	0.01	1.63	4.09	0.07	0.05	0.01	6.00
90	12.39	0.51	0.01	1.75	4.24	0.05	0.05	0.01	5.75
120	11.84	0.51	0.01	1.71	4.10	0.05	0.05	0.00	5.40
150	16.64	0.43	0.01	1.52	3.74	0.04	0.04	0.00	10.87
180	10.16	0.54	0.01	1.76	4.03	0.06	0.05	0.01	3.70

(Reaction condition: T_{react} = 600 °C, T_{red} = 400 °C, F = 10:10:40 mL/min (C_3H_8:Air:N_2), W/F = 23 g·h/mol, atmospheric pressure)

Table D22 Oxidative dehydrogenation of propane over $K_2Ti_{5.9}Ni_{0.1}O_{13}$ catalysts at contact time 7.8 g.h/mol

Time on stream (min)	Conversion (%)	Yield (%)							
		Methane	Ethane	Ethylene	Propylene	Butane	iso-butane	C_5^+	CO, CO_2
30	12.21	0.53	0.01	1.93	4.45	0.04	0.06	0.02	5.16
60	12.43	0.58	0.02	2.04	4.87	0.04	0.07	0.04	4.76
90	11.87	0.59	0.02	2.03	4.81	0.04	0.07	0.04	4.27
120	12.27	0.59	0.02	2.03	4.84	0.04	0.07	0.05	4.63
150	12.37	0.58	0.02	1.99	4.70	0.04	0.06	0.04	4.93
180	11.99	0.52	0.01	1.88	4.50	0.04	0.06	0.04	4.93

(Reaction condition: T_{react} = 600 °C, T_{red} = 400 °C, F = 10:10:40 mL/min (C_3H_8:Air:N_2), W/F = 23 g·h/mol, atmospheric pressure)

Table D23 Oxidative dehydrogenation of propane over $K_2Ti_{5.9}Ni_{0.1}O_{13}$ catalysts at contact time 11.7 g.h/mol

Time on stream (min)	Conversion (%)	Yield (%)							
		Methane	Ethane	Ethylene	Propylene	Butane	iso-butane	C_5^+	CO, CO_2
30	14.27	0.51	0.01	1.93	4.56	0.05	0.07	0.02	7.09
60	12.66	0.56	0.02	2.08	5.17	0.05	0.09	0.06	4.62
90	13.05	0.57	0.02	2.09	5.22	0.05	0.09	0.06	4.94
120	13.19	0.60	0.02	2.16	5.32	0.06	0.09	0.06	4.87
150	13.17	0.64	0.02	2.25	5.35	0.05	0.09	0.09	4.68
180	13.78	0.60	0.02	2.16	5.22	0.03	0.08	0.09	5.55

(Reaction condition: T_{react} = 600 °C, T_{red} = 400 °C, F = 10:10:40 mL/min (C_3H_8:Air:N_2), W/F = 23 g·h/mol, atmospheric pressure)

Table D24 Oxidative dehydrogenation of propane over $K_2Ti_{5.9}Ni_{0.1}O_{13}$ catalysts at contact time 46 g.h/mol

Time on stream (min)	Conversion (%)	Yield (%)							
		Methane	Ethane	Ethylene	Propylene	Butane	iso-butane	C_5^+	CO, CO_2
30	13.06	0.48	0.02	2.02	4.42	0.02	0.08	0.03	5.99
60	13.95	0.50	0.02	2.04	4.74	0.02	0.08	0.03	6.51
90	14.47	0.52	0.02	2.05	4.84	0.03	0.08	0.03	6.89
120	14.20	0.54	0.02	2.10	4.88	0.03	0.08	0.03	6.51
150	14.82	0.57	0.02	2.18	4.99	0.03	0.09	0.04	6.90
180	15.07	0.55	0.02	2.16	4.96	0.03	0.09	0.03	7.22

(Reaction condition: T_{react} = 600 °C, T_{red} = 400 °C, F = 10:10:40 mL/min (C_3H_8:Air:N_2), W/F = 23 g·h/mol, atmospheric pressure)